CHALMERS

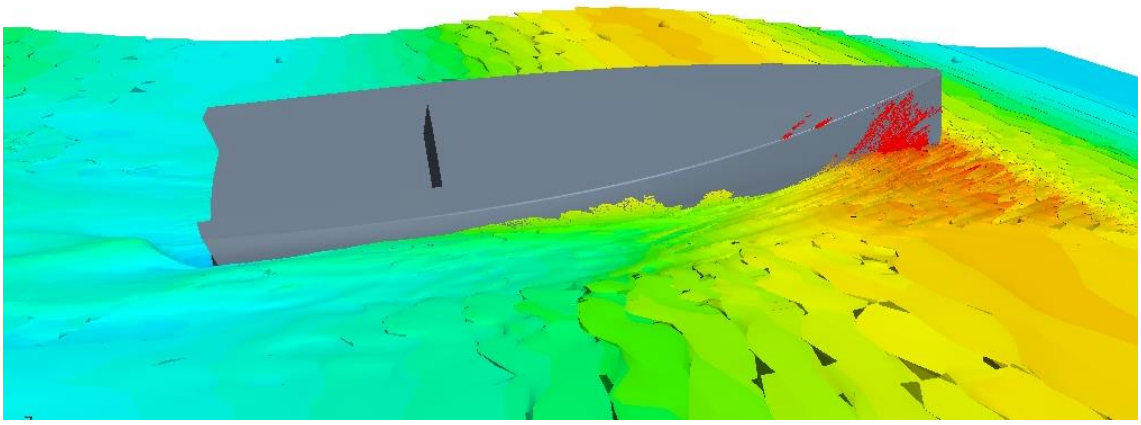

A CFD Investigation of SailingYacht Forebodies in Head Seas

Master's Thesis in the International Master's Programme Naval Architecture and Ocean Engineering

KONSTANTINOS KOSTALAS & ADAM PLUTO

Department of Shipping and Marine Technology
Division of Marine Technology
CHALMERS UNIVERSITY OF TECHNOLOGY
Göteborg, Sweden 2015
Master's thesis 2015:X-15/333

MASTER'S THESIS IN THE INTERNATIONAL MASTER'S PROGRAMME IN NAVAL ARCHITECTURE AND OCEAN ENGINEERING

A CFD Investigation of SailingYacht Forebodies in Head Seas

KONSTANTINOS KOSTALAS & ADAM PLUTO

Department of Shipping and Marine Technology
Division of Marine Technology
CHALMERS UNIVERSITY OF TECHNOLOGY
Göteborg, Sweden 2015

A CFD Investigation of Sailing Yacht Forebodies in Head Seas
KONSTANTINOS KOSTALAS & ADAM PLUTO

Master's Thesis 2015:X-15/333
ISSN 1652-8557
Department of Shipping and Marine Technology
Division of Marine Technology
Chalmers University of Technology
SE-412 96 Göteborg
Sweden
Telephone: + 46 (0)31-772 1000

Cover:
Hull A at 20 degrees of heel running in a 25 m long wave at a speed of 7.5 knots.

Department of Shipping and Marine Technology
Göteborg, Sweden 2015

A CFD Investigation of Sailing Yacht Forebodies in Head Seas
Master's Thesis in the International Master's Programme in Naval Architecture and Ocean Engineering

KONSTANTINOS KOSTALAS & ADAM PLUTO
Department of Shipping and Marine Technology
Division of Marine Technology
Chalmers University of Technology

ABSTRACT

The objective of this thesis is to investigate the hydrodynamic performance of a modern 41 feet sailing yacht by comparing the performance values acquired from simulations for different forebody geometry designs on the yacht. The particulars such as length, beam, displacement and prismatic coefficient are kept as similar as possible for all hulls. The resistance of the different designs are tested in flat water and in tests with waves. The set up for the waves is made with data taken from Svenska Björn; which is a caisson lighthouse in the Baltic Sea. The wave lengths tested in this study includes lengths of 12.5m, 25m and 34.5m and the yachts are run in straight head sea. The encounter frequency for the 25m wave matches the natural pitch frequency of the yachts. To evaluate realistic upwind condition, for cruising and racing, tests with a heel angle of 20^{o} are additionally performed. All hulls are tested at Froude number 0.35 in the conditions described in the previous paragraph.

This investigation is made with the aid of CFD using Unsteady Reynolds Averaged Navier-Stokes (U-RANS) equations integrated in the solvers provided in Star CCM+ software. Also, Volume of Fluids method for surface capturing is used. At the start of the study a verification of the software is made with the use of Least Square Root method. Then, a validation of the CFD results from the software is done by a comparison with data from towing tank tests from Delft Systematic Yachts Hull Series hull. In total three hulls are tested with a systematic forebody geometry variation of shape.

The main result of this study is a better understanding of how the forebody design of a sailing yacht affects the performance. The study is done at high Froude number, where the gain from having a sharp and pointed entry angle and then diving into the water is larger than having volumes in the lower part of the bow. Having a tumblehome design that prevents the yacht from diving into waves gives calmer motions but higher resistance. However it is important to conclude that the drag, pitch and heave for all yachts are close and a definite winner hull is difficult to name because some of the three yachts are better than the other in certain conditions. Nevertheless, the best design overall is the hull with sharp entry angle and flare.

Key words: CFD, LSR method, Sailing yachts, Seakeeping, V&V, VOF, U-RANS, Yacht Design,

En undersökning i CFD av segelbåtsförar i motsjö
Examensarbete inom Naval Architecture and Ocean Engineering
KONSTANTINOS KOSTALAS & ADAM PLUTO
Institutionen för sjöfart och marin teknik
Avdelningen för Marine Technology
Chalmers tekniska högskola

SAMMANFATTNING

I detta examensarbete analyseras olika former av förskepp på segelbåtar i platt vatten och i vågor. Samtliga segelbåtar är 41 fot långa och har gemensamma värden på bland annat bredd, deplacement och prismatisk koefficient. Båtarna simuleras i rak motsjö i CFD-programmet STAR CCM+ och testas i tre våglängder: 12.5m, 25m och 34.5m. Mötandefrekvensen när båten körs i vågländen 25m matchar båtens egenfrekvens för stampning och hävning. Båtarna simuleras i 7.5 knop i upprätt läge samt med en fast krängningsvinkel för att ett realistiskt motvindsscenario ska testas. I studien ingår även verifikation och validering av beräkningarna för att se vilken noggrannhet som nås.

De tre segelbåtarna är moderna, anpassade för hög prestanda och är gjorda med systematisk ändring av förskeppet. Resultat från studien visar att det är fördelaktigt att ha en för med lite volym i vattenlinjen för att motståndet i platt vatten ska bli så litet som möjligt. Den typen av för är även fördelaktig i vågscenarion även om det skapar stora rörelser på båten då den lätt dyker in i vågor. Den för som har större volym i vattenlinjen är dock bättre i vissa förhållanden och har generellt lite lugnare rörelser än fören med mindre volym. Dock är det inte någon större skillnad på de olika skroven i något av de testade fallen.

Nyckelord: (CFD, Förskepp, Segelbåt, Sjöegenskaper)

Contents

Preface

This thesis is a part of the requirements for the master's degree in Naval Architecture and Ocean Engineering at Chalmers University of Technology, Göteborg. It has been carried out at the Division of Marine Design, Department of Shipping and Marine Technology, Chalmers University of Technology between January and June of 2015.

We would like to acknowledge and thank our examiner, Full Professor Lars Larsson, and supervisor PhD student Rickard Lindstrand, at the Department of Shipping and Marine Technology, for their excellence, enthusiasm, guidance and support throughout the work with this thesis.

We would also like to give our sincerest thank you to the person with the restless spirit that had the idea of this project, Yacht Designer Gabriel Heyman. Without his beautiful yachts and visionary attitude this would never have been done.

Finally, we want to thank our family and friends for putting up with the endless talk of yacht motion and CFD.

Göteborg, June 2015

Konstantinos Kostalas & Adam Pluto

Notations

Roman upper case letters

B_s	*Main boom height [m]*
CAD	*Computer aided design*
CFD	*Computational fluid dynamics*
COE	*Centre of effort [m]*
COG	*Centre of Gravity [m]*
Cp	*Prismatic Coefficient [-]*
DSYHS	*Delf systematic yacht hull series*
Fn	*Froude's number [-]*
Iy	*Pitch moment of inertia [kgm^2]*
L	*Length of the yacht [m]*
Lcb	*Longitudinal centre of buoyancy [m]*
Lcf	*Longitudinal centre of floatation [m]*
Lwl	*Waterline Length [m]*
Raw	*Added resistance response in waves [m]*
Ra'w	*Added resistance coefficient [N/m^2]*
Re_x	*Transition Reynolds number [-]*
P	*Pressure [Pa]*
P_s	*Main Sail hoist [m]*
$\bar{P}$	*Average Pressure [Pa]*
S	*Finest grid simulation*
S_0	*Estimate of the exact solution of the extrapolation*
S_i	*Numerical solution to the i-th grid*
T	*Wave period [s]*
Tc	*Canoe draft [m]*
U-RANS	*Unsteady Reynolds-Averaged Navier-Stokes equations*

U	*Navier Stokes Velocity*	*[m/s]*
U_{SN}	*Numerical uncertainty*	
U_I	*Iterative uncertainty*	
U_G	*Grid discretization uncertainty*	
$\bar{U}$	*RANS average velocity*	*[m/s]*
$\langle \bar{U} \rangle$	*U-RANS average time velocity*	*[m/s]*
V	*Speed of the yacht*	*[m/s]*
VOF	*Volume of fluids*	
∇	*Displacement*	*[m^3]*

Roman lower case letters

h_i	*Typical Cell Size*	
g	*Gravitational acceleration*	*[m/s^2]*
l	*Length of the yacht*	*[m]*
p	*Is the observed order of accuracy of the grid convergence*	
t	*Time*	*[s]*
u_*	*Friction velocity*	
u''	*Fluctuation*	
u'	*Modelled turbulent fluctuation*	
x	*Distance*	*[m]*
y^+	*Non-dimensional wall distance*	*[m]*
u_*	*Friction velocity at the nearest wall*	*[m/s]*
k	*Turbulent kinetic energy*	
c_x	*Coefficients*	

Greek upper case letters

Ω	*Wave frequency*	*[rad/s]*

Greek lower case letters

α	*Constant*	
δ	*Boundary layer thickness*	*[m]*
δ_{RE}	*Grid discretization error*	
ε_{RE}	*Discretization error*	
λ	*Wavelength*	*[m]*
μ_t	*Eddy viscosity*	*[m^2/s]*
ν	*Kinematic Viscosity of the fluid*	*[m^2/s]*
ξ	*Amplitude*	*[m]*
ρ	*Sea water density*	*[kg/m^3]*
ε	*Rate of dissipation of turbulent kinetic energy*	
σ_x	*Constants*	

1 Introduction

Since the era of primitive boatbuilding there have been people working on improving the designs. Their thoughts of improvement and the willingness to implement new concepts have led to the hulls of today. Throughout the centuries; observations and thoughts of how a yacht can be improved have made serious impact in reducing the resistance of a hull and increase the performance.

Sail yacht designers have always been in pursuit of the ultimate yacht. Research is made to evaluate and optimize the shape of the hulls to make them more efficient. Model testing, empirical formulas and more recent CFD techniques are used in the process to find a design that is slightly better than anything out there. Flat water testing is most commonly used as the benchmark for the design; the best performing yacht in calm water is deemed the best overall. A yacht is however most often not sailed in dead calm seas, where there is wind there are waves and having a fast upwind leg in mirror like water is more a dream than reality.

There are many parameters that are affecting the performance of a yacht. Waterline length, beam, draft, wetted surface area, centre of buoyancy and prismatic coefficient are the typical indicators of a sailing yacht hull. These parameters are often used to predict the performance of a sailing yacht but none of them take the shape above the water or shape differences into consideration. When yachts are not run in dead calm seas the yacht is constantly moving and rotating slightly and the change in pitch and heave cause the shape beneath the waterline to change. Pitch and heave motions are explained in *Figure 1-1*.

The bow is a particularly interesting part of the yacht as it has a large effect on the waves formed around the hull. In head seas, as is considered in this thesis, the bow is also the part of the yacht that hits the waves first and by doing so it has a large impact on the reaction of the boat. It is of interest how the shape of the bow affects the performance of the yacht if all the main dimensions and coefficients of the different hulls are the same.

In *Figure 1-1* the coordinate system and the degrees of freedom are shown. Rotational movements roll, pitch and yaw are indicated around each respective axis. In this thesis movement in x-direction (surge) and y-direction (sway) is restrained and so is the roll and yaw. This simulates the case when the boat is running in head sea (see *Figure 3-4*) without any heel angle and without a leeway angle. Further heave is defined as motion in z-direction and heel angle is a fixed roll angle. In the flat water pitch angle is also referred to as trim.

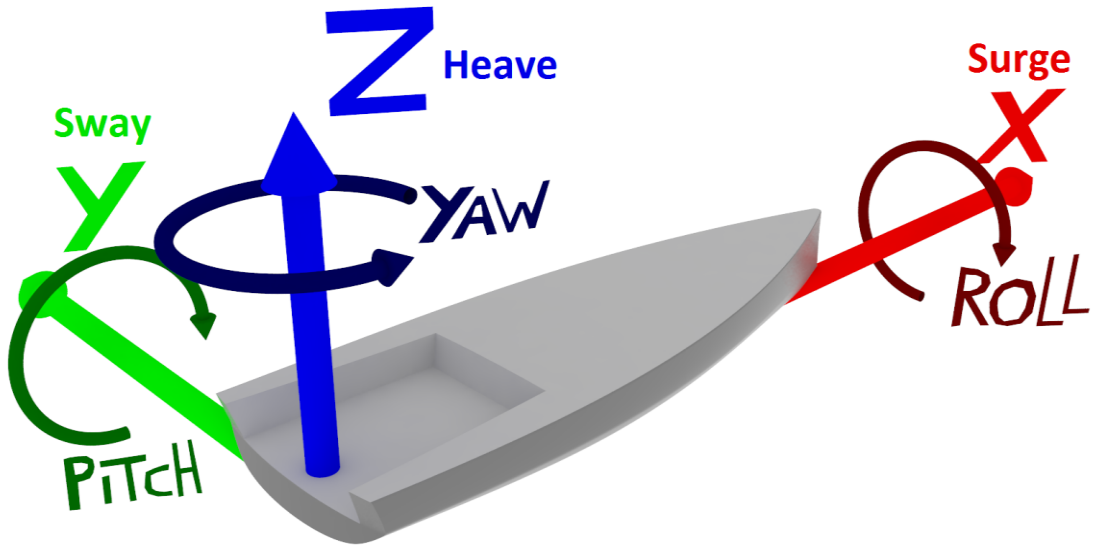

Figure 1-1 The used coordinate system. The origin is the intersection between the design waterline and the aft perpendicular. X-axis is pointing forward, y-axis to port and z-axis upwards.

1.1 Background

Following the thesis "Comparison Between a State-of-the-Art Sailing Yacht and a New Concept Design" by Nicolas Bathfield (Chalmers, 2014:X-04/151) more questions arose on the subject of motions and resistance of a sailboat. Yacht designer Gabriel Heyman had thoughts of how a yacht reacts when running into a wave; it will slow down and it will lift the bow. To what extent the boat will slow down and how the movements of the hull affect the increased drag will be influenced by the shape of the hull and the shape of the bow. A very sharply pointed bow that has narrow entry angles may be able to pierce the wave without a high increase in resistance. To what extent the bow will lift out of the water will depend on the volume forward; a flared top of the bow will lift the bow out of the water and this may reduce the resistance. If the volume near the deck is not sufficient to lift the bow then the effect may be opposite. Does in that case a bow with volume lower in its sections, which provides sufficient lift, have an advantage when running into waves? Furthermore, does the volume near the deck affect how well the yacht recovers from a deep dive into a wave; is a reversed tumble-home design, as seen on many modern catamarans, advantageous also for a mono-hull sailing yacht? These questions are among those that Gabriel Heyman had and introduced as the idea for this thesis. The effect of a heel angle was also introduced as the change in geometry, from the upright condition, can possibly make a great difference in performance of differently shaped bows. The effects of heel are of great importance since sailing yachts are not in upright condition when sailing to windward at speed. Worth mentioning is the fact that when a sailing yacht is designed; the effect of waves and the shape above water is not usually taken into account for the resistance calculations.

1.2 Objective of the investigation

The question of this thesis is whether different hull forebody geometries will affect the resistance and the performance of a sailing yacht in upright and heeled conditions, in flat water and wave scenarios. What forebody shape is the most beneficial, while keeping the particulars of the hull the same, and are certain shapes better in certain wave cases?

The aim of this thesis is to answer the following three questions:

- What is the best shape of a yacht forebody to reduce resistance when going against waves?
- How does the shape influence pitch and heave and how does this in turn affect resistance?
- What are the effects of heel on the resistance, pitch and heave and what shape is best in the heeling condition?

1.3 Limitations

The main limitations of this study are that the yachts are run in straight head seas in a well-defined number of wave cases as are explained in Section 4.5. The study is limited to evaluating pitch, heave and resistance. For all cases the yacht is restricted in surge, sway, roll and yaw. Even in the non-symmetric case that is created when the yacht is subjected to a heel angle; sway and surge motions and roll, yaw rotations are fixed and are thus not examined.

No appendages such as keel, rudders and rigging are included in the simulations. Only the hull with transom and deck is simulated. The yachts are also run without leeway angle.

The chosen heel angle is 20^{o}, which is a typical heel angle when sailing upwind at the chosen speed. This study is limited to only evaluate one forward speed. The boat is fixed in the domain while the air and water moves past it. Subsequently, instead of measuring the speed and accelerations, the resistance and motions over time are measured. The speed that is used for the simulation is a Froude number of 0.35 which means that the speed is 7.5 knots which is a typical speed for upwind sailing for this type of yacht [Larsson, Eliasson, Orych, 2014].

The available computer power sets restrictions on the coarseness of the mesh which as a result limits the accuracy of the calculations. A grid independency study is done, in order to estimate the numerical errors, see Sections 3.2.4, 4.1 and 4.2.

2 Description of the yachts

The hulls are modern performance-cruiser type sailboat hulls intended for a lightweight performance oriented cruiser that can be used for occasional racing. As stated in Section 1.2 the aim of the thesis is to evaluate which bow shape is best for flat water and head sea condition, thus the stern design of the hulls and the hull characteristic coefficients are kept as similar as possible.

The hulls have a wide modern stern, and it is intended for them to be equipped with a deep keel to minimize the weight. As a result; all of the hulls have a low canoe body draft, Tc, and are very flat-bottomed at the stern. There is a rounded chine running along the hull that smoothens out near the bow.

All hull versions were designed by yacht designer Gabriel Heyman and Lars Hedberg, while design inputs to hull B and C were given by the authors. The main particulars of the three hulls are presented in *Table 2-1*.

Table 2-1 Hull particulars

Yacht version	**A**	B	**C**
LWL [*m*]	11.97	11.97	11.97
Tc [m]	0.442	0.442	0.467
Displacement $[m^3]$	5.985	5.979	5.989
LCB fwd. of AP [*m*], ([%])	5.293, (44.173)	5.285, (44.157)	5.252, (43.868)
LCF fwd. of AP [*m*], ([%])	4.952, (41.173)	5.035, (42.067)	4.816, (40.224)
Cp [-]	0.527	0.527	0.515

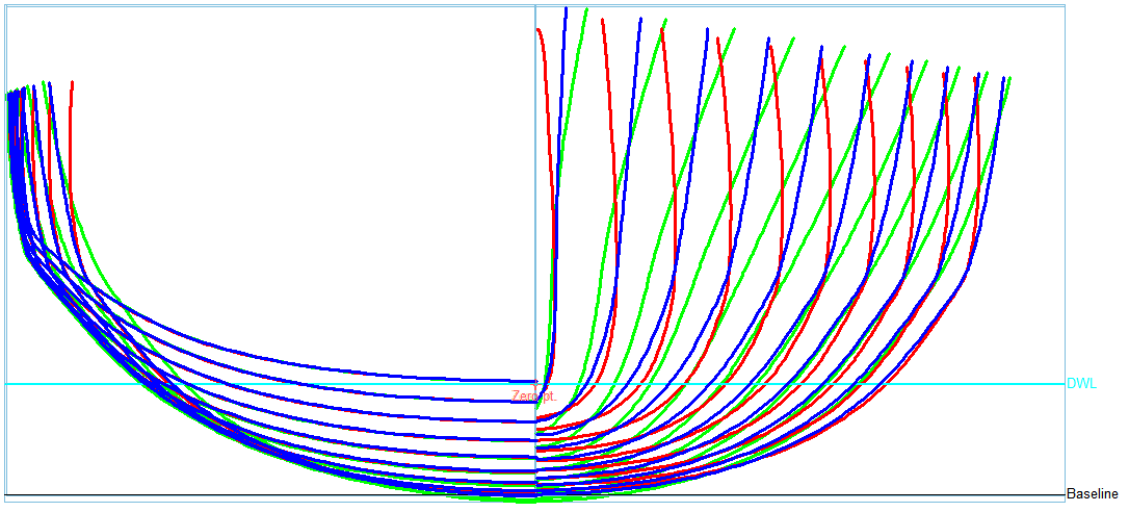

Figure 2-1, Illustration of 20 stations with spacing 0.63m starting from -0.12 m. Blue sections are for hull A, red for hull B and green for hull C

In all figures blue lines represent hull A, hull B is represented with red lines and hull C have green lines. In *Figure 2-1* the stations of the yachts are presented and for the different designs, a separate color was used for each one of them.

The gradual progression of the bow shape can clearly be seen with hull A being the middle design. The same progression of the bow shape can be seen in *Figure 2-2* where the buttocks bend backwards for hull B and forwards for C while the buttocks for A are almost vertical.

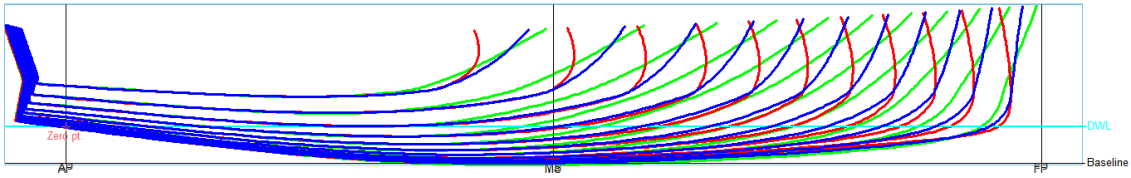

Figure 2-2, Illustration of 11 buttocks with spacing 0.175m starting from 0.175

In *Figure 2-3* the waterlines for each hull are displayed. The wider flare of hull C can be seen where the waterlines stretch outwards in the bow region. The deeper bottom line of hull C and the sharper bow can be seen as the lowest two waterlines are sharper at the bow than it is for hull B and A. The lowest bow draft of hull B can be seen as the two lowest red waterlines stretch the least forward.

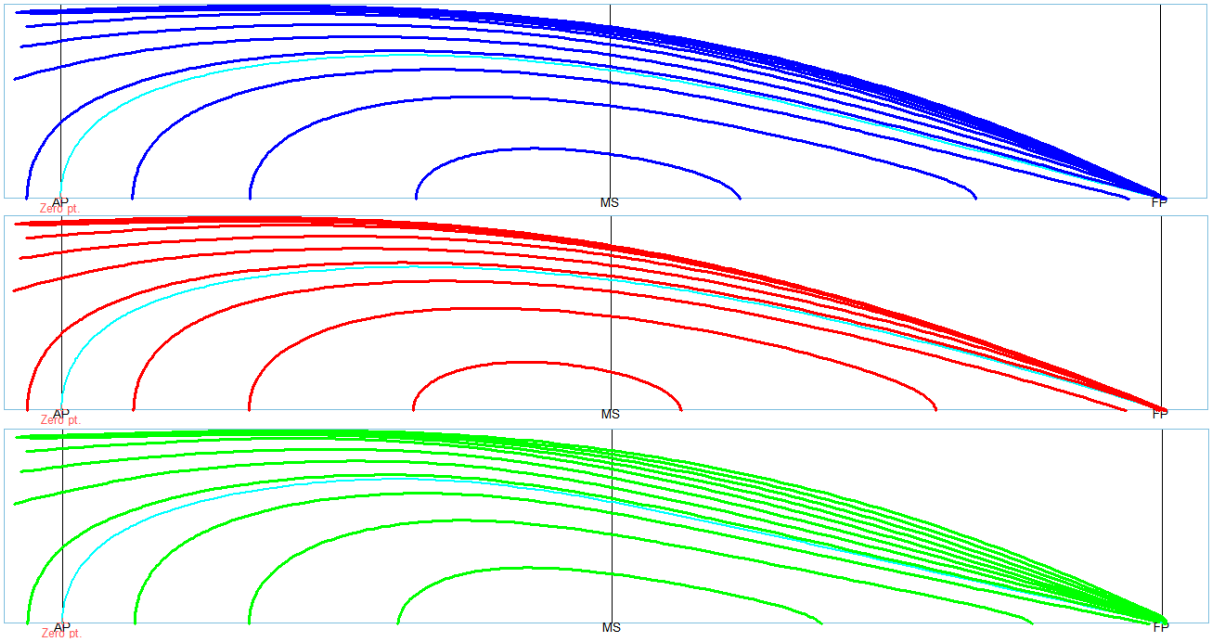

Figure 2-3, Illustration of 11 waterlines in steps of 0.15 m starting from -0.4 m

As the yachts are still concepts the pitch moment of inertia, I_y was estimated by using the group weights and their locations on the example yacht used in [Larsson, Eliasson, Orych, 2014]. I_y was calculated to 31346 [kgm^2] resulting in a pitch radius of gyration of 18.8% of LWL which is reasonable for a lightweight performance cruiser.

2.1 Heyman A

Hull A was designed first. It has a slight inversed bow and more or less vertical stations in the topsides. This can be seen in *Figure 2-1* where the blue lines are for hull A. Main characteristic of hull A is that it has a harmonic shape forwards and is a good reference design as an intermediate design between the two other. In *Figure 2-4* and *Figure 2-5* hull A can be seen in perspective view.

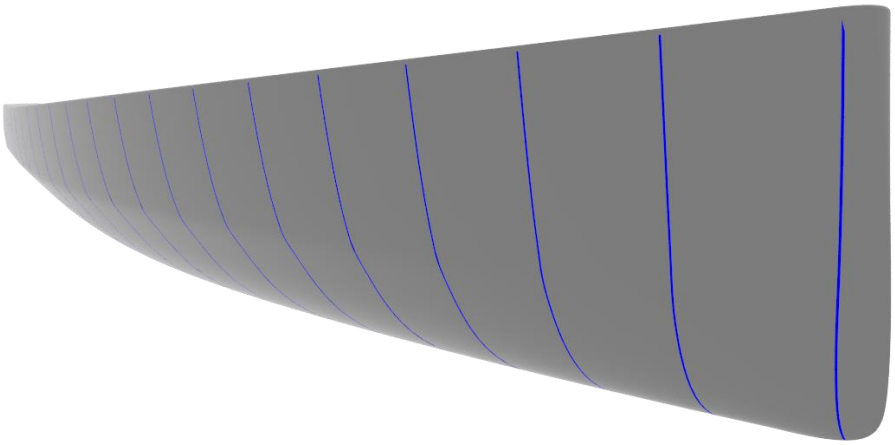

Figure 2-4 Hull A, perspective view with stations

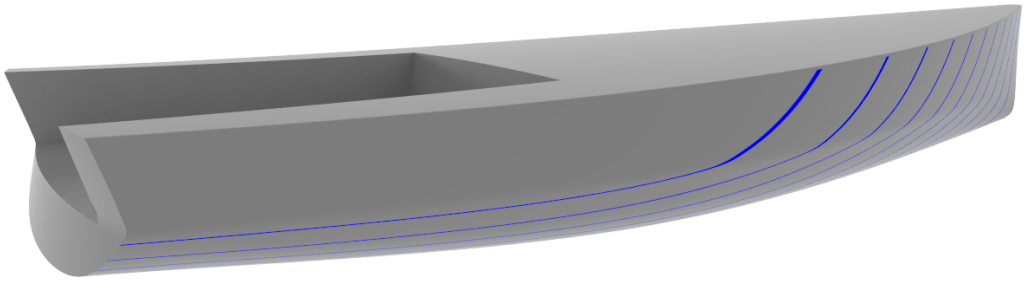

Figure 2-5 Hull A, stern perspective view with buttocks

2.2 Heyman B

Hull B, the second design, has a more inverted bow which can be noticed by the narrower deck near the bow area. Hull B is fuller further down around the design waterline. In order to keep the LCB, Cp and displacement similar, the bottom, has instead been pulled slighly upwards near the bow. This can be seen in *Figure* 2-1 where the stations for hull B are red. The fuller shape, in and around the water level, as well as the narrower tumble home topsides that stretch back to midship, make the design harmonic. The fuller bow shape in the lower area is intended to stop the yacht

from diving deep into waves while the narrow top design is intented to decreace the frontal area if this should happen. In *Figure 2-6 and Figure 2-7* hull B can be seen in perspective view, the narrower top compared to hull A and C can be clearly distinguished.

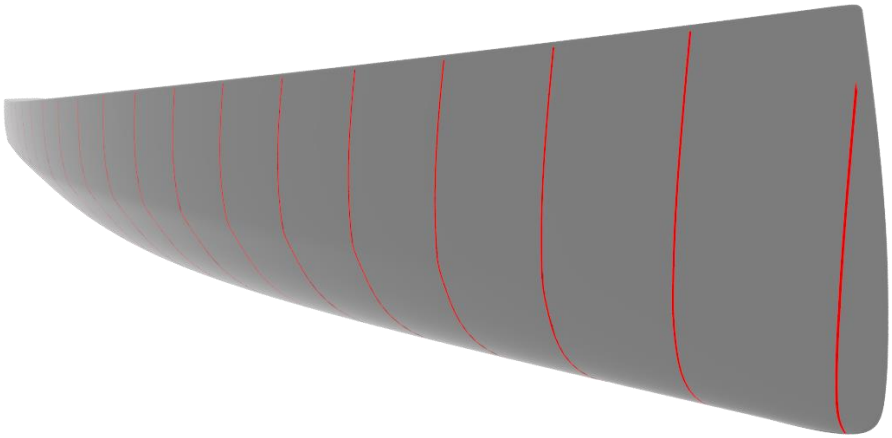

Figure 2-6 Hull B, perspective view with stations

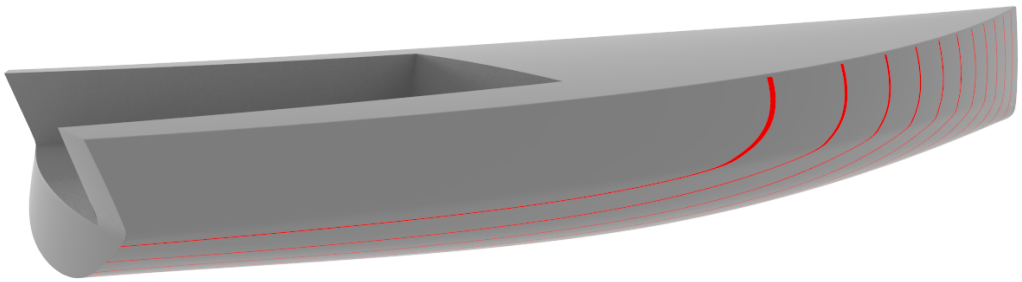

Figure 2-7 Hull B, stern perspective view with buttocks

2.3 Heyman C

Hull C is the third design and the intention when making it was to move in the opposite direction from hull A compared to B. Hull C was made as narrow as possible around the design waterline and as a result of this the bottom has been pulled slightly downwards at the bow to keep the characteristic coefficients the same. Hull C has a rather big flare and a wider deck compared to the straight or tumble home sections of A and B, see *Figure 2-1*. As with hull B the changes from hull A are visible back to midship. Hull C is intended to easily cut through waves while the flared top insures that the deck does not get submerged in extreme dives. Hull C is represented in perspective view in *Figure 2-8 and Figure 2-9.*

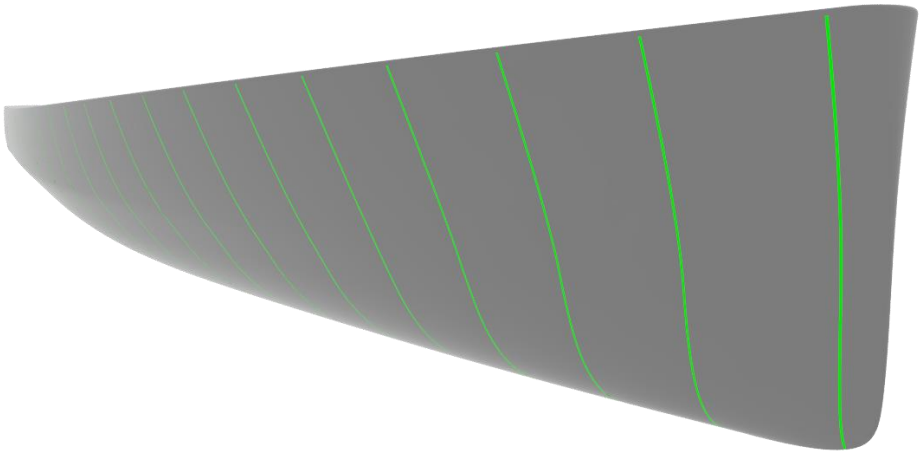

Figure 2-8 Hull C, Bow perspective view with stations

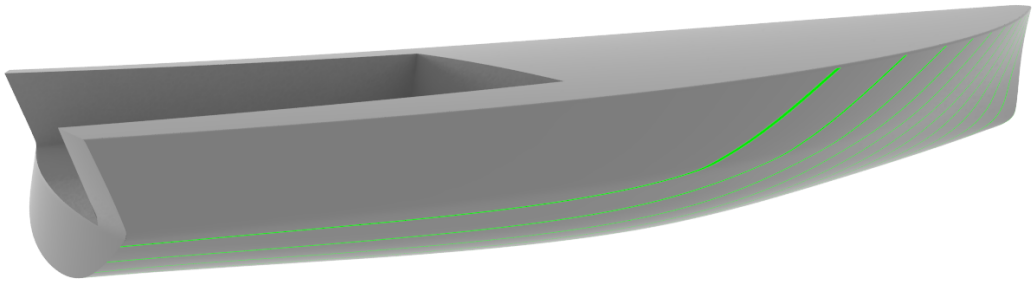

Figure 2-9 Hull C, Stern perspective view with buttocks

3 Theory

In this chapter the concepts of yacht resistance, CFD and seakeeping are explained. The theory in this chapter was used for the calculations in Chapter 4.

3.1 Resistance of a vessel

When a hull moves through water; different phenomena in the flow which affect one another, can be identified, as shown in *Figure 3-1*. Each one of these different components contributes differently to the total resistance since they are dependent on various factors. Some that can be named are the hull geometry as studied in this project, the velocity of the vessel and the sea state the vessel is in. In order to be able to follow the content of this study, a level of knowledge about these resistance contributors and flow regions around the hull is needed.

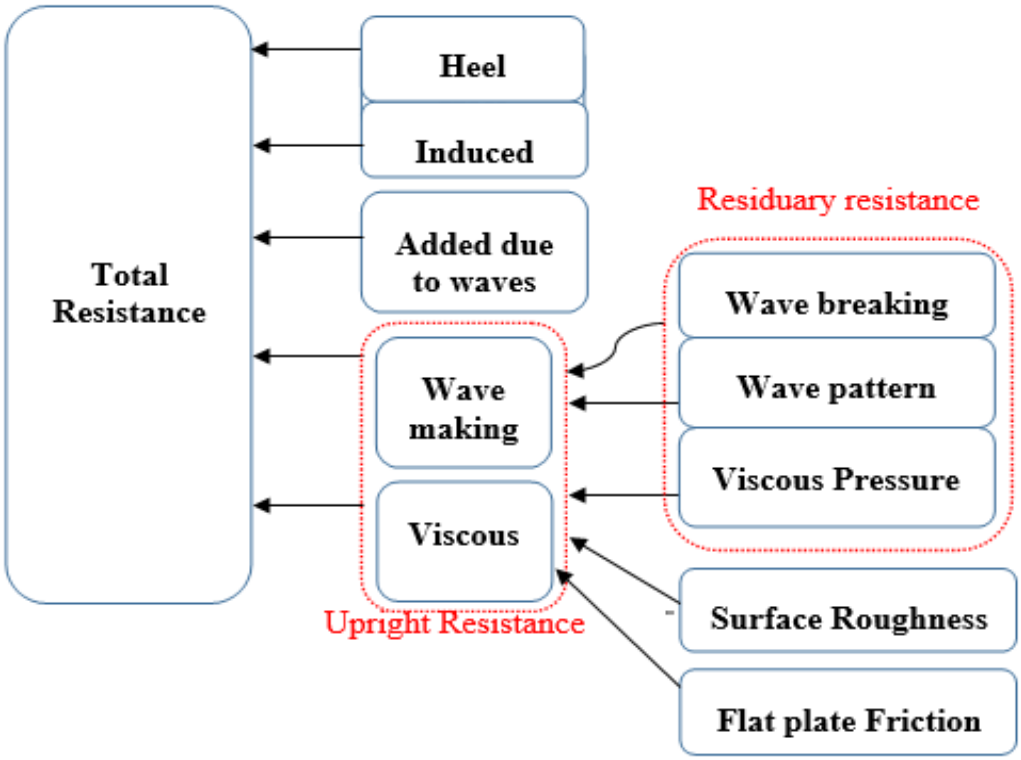

Figure 3-1 Total resistance of a sailing yacht, broken down to its different resistance components

In upright resistance of a hull in calm water, there are two main contributors to shape the final resistance and these are the wave making resistance and the viscous resistance [Larsson, Eliasson, Orych, 2014]. Wave resistance is created by pressure variations acting alongside the hull surface. This is the reason for the creation of waves containing energy to be transmitted from the hull motion to the water. The wave resistance is split into wave pattern resistance and wave breaking resistance see Section 3.1.2. Viscous resistance is the result of friction between the hull and the water. The viscous resistance is subdivided into flat plate friction, roughness effects, friction and form effect on pressure, see Section 3.1.1. The sum of the wave resistance and the viscous resistance if often referred to as upright resistance. For the case where

a yacht is having a leeway angle, is heeled or is encountering waves more components can be identified.

Induced resistance is a result of energy added to the wake by the hull and appendages when there is a leeway angle. This is creating different pressure regions on the leeward and the windward side of the foils [Larsson, Eliasson, Orych, 2014]. Since simulations of appendages are not included in this thesis and no leeway angle introduced; this resistance component is not of interest.

Resistance due to heel is caused by changes to the underwater body when the yacht is heeled. The change in the resistance is caused by a change in the wet area of the hull and a change in the wave making resistance [Larsson, Eliasson, Orych, 2014]. See Section 3.1.3.

The added resistance component originates from encountering waves that increase the resistance by moving the yacht. These movements cause radiated waves that increase the wave making and thus the resistance. See Section 3.1.4.

The different resistance components, such as wave making resistance, are not identified by the software instead the resistance of the yachts is evaluated from the simulation result by the integrated pressure and shear force on the hull. The computations are automatically made by the models formulas used in the physics definition of the settings of the simulations, see Section 3.2.

3.1.1 Viscous Resistance

This resistance component is created due to interaction of viscosity of the water with various parts of the hull of the yacht; or simpler by friction between the wet surface of the hull and the water. The molecular forces between the hull and the water cause the water layer closest to the hull to stick to the surface. Thus, meaning that these forces are strong enough to cause the water to have no speed or motion in the innermost water layer, a fact resulting in the no-slip condition. This layer works as a solid boundary, the water will have zero velocity relative to it. Moving away from the hull, layer by layer the velocity increases. Further away from the hull, the velocity will have the same velocity as the undisturbed flow.

The boundary layer created around the hull, where the flow is disturbed by the yacht, has a thickness in order of 0.1m [Larsson, Eliasson, Orych, 2014]. The boundary layer thickness, δ, for the Heyman yachts at the speed in this study is estimated to 0.1386 m at the stern, using *Eq1* and *Eq. 2* [Schlichting, 1979].

$$Re_x = u_0 * \frac{l}{v} \qquad \textit{Eq. 1}$$

$$\delta = 0.382 * \frac{l}{Re_x^{0.2}} \qquad \textit{Eq. 2}$$

The flow in the boundary layer transitions from laminar flow in the bow area, to turbulent flow as can be seen in *Figure 3-2.* Additionally there is the separation phenomenon in the stern area where the geometry rapidly bends inwards and forms

larger turbulent eddies. This can be visualised as varying size eddies containing energy in the wake of the yacht; as seen in *Figure 3-2*.

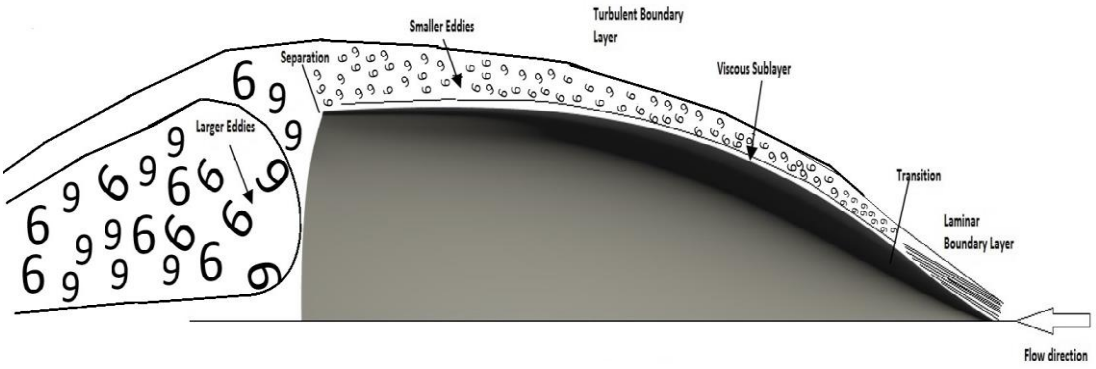

Figure 3-2 Schematic representation of different flow regions that are formed around a hull shaped geometry. Representation of the boundary layer might seem exaggerated and blunt but this is done on purpose, just to indicate the formations.

Another important contributor in viscous resistance is the component of surface roughness. Since the thickness of the boundary layer is dependent on the velocity of the flow and increases downstream of the hull, roughness component can be neglected if it is less than the viscous sub layer thickness. This is called hydrodynamically smooth [Larsson, Eliasson, Orych, 2014].

Last component but not least important is the viscous pressure resistance. As the yacht moves through the water, the phenomenon will initiate with a pressure increase in the bow area as the water particles are decelerated. As flow moves alongside the hull moving away from the bow area, the water particles will be accelerated and experience lower pressure as explained by Bernoulli's principle [White, 2015]. When progressively approaching the stern area, the flow will slow down again and there will be a pressure increase. In the ideal case of potential flow, meaning without friction and absence of free surfaces, there is an evening out between the pressure forces in the bow and stern. It is caused by the streamlines being equal to the bow and the stern. This cancellation means that no viscous pressure resistance occurs. In reality the existence of friction and the resulting boundary layer, with a variation of thickness from the bow to the stern, will cause a difference in pressure. This results in a pressure dropout at the stern, which creates a force acting in the opposite direction of the yachts velocity. Again, in this component, the thickness of the boundary layer is the major contributor and this pressure imbalance between the fore and the aft part is referred to as viscous pressure resistance.

3.1.2 Wave making Resistance

Wave making resistance can also be divided into two different contributors, which are the wave breaking and the wave pattern. Pressure differences alongside the hull are the reason for the existence of this component. However for sailing yachts only the waves created by the high pressure areas, the bow and stern, are to be considered even if theoretically waves from low pressure points such as the shoulders of the hull contribute to the wave system [Larsson, Eliasson, Orych, 2014]. The wave system

generated at the bow and the system generated at the stern inevitably interact and that is greatly dependent on the yachts speed, see *Eq. 3* [Larsson, Raven, 2010].

$$\lambda = 2\pi * Fn^2 * L \qquad \textit{Eq. 3}$$

When wave making resistance is calculated; both waves systems have to be considered since there will always be interference between them. If the bow wave, while progressing, meets the stern as a crest it will add to the stern wave. This will result in a larger wave and subsequently increased wave resistance; this is called positive interference. On the other hand, if the speed of the yacht is such that the bow wave has at trough when it reaches the stern, it will somewhat cancel the stern wave, leaving a smaller wave pattern and result in a reduced wave resistance; this is called negative interference.

The wave making resistance is largely dependent on a dimensionless speed quantity that is called the Froude number defined in *Eq. 4*.

$$Fn = \frac{V}{\sqrt{g * L}} \qquad \textit{Eq. 4}$$

Ships generally experience a number of crests and troughs in the wave making resistance curve that is due to positive or negative interference between the bow and stern wave systems, as speed varies. A typical crest in the resistance is for a hull speed of Froude number of 0.4 where positive interference occurs [Larsson, Eliasson, Orych, 2014].

3.1.3 Heel Resistance

Heel resistance is the sum of the changes to viscous, wave and added resistance caused by introducing a heel angle. Subsequently, as the submerged shape of the hull changes with heel, all resistance components change. Most often the change in underwater geometry causes the resistance to increase; a phenomenon called added resistance due to heel which must be added while calculating the total resistance. The heel resistance generally has a small effect on the total resistance [Larsson, Eliasson, Orych, 2014] and is mostly due to changes in the wet area. The heel resistance is calculated in this report as the difference in resistance for the yachts in flat water; heeled and upright.

3.1.4 Added Resistance due to waves

Added resistance in waves is the part of a vessel's total resistance, which is created by encountering waves. These waves activate motions of the hull which in term creates radiated waves around the hull. The most important motions at ship in head seas, which are affecting the resistance, are hydrodynamic damping of the heave motion and pitch rotation, which are usually coupled [Larsson, Eliasson, Orych, 2014]. While the vessel oscillates, it transmits energy by the waves radiated from it; this is creating a resistance force in the same way the still water pattern does. The problematic state occurs, when the frequency of the encounter waves is resonant with the natural frequency and these motions get larger.

The added resistance can be added to the calm water resistance to sum up to the total resistance while in seaway. The formula used to non dimensionalize the added resistance is shown in *Eq. 5* [Keuning, Vermeulen, Have, 2006]

$$Ra'w = \frac{Raw}{\rho * g * \xi^2 * L} \qquad \textit{Eq. 5}$$

3.2 CFD

The definition of computational fluid dynamics is the setting up of a model that describes the physical phenomenon and resolving equations that describes the model. The use of it in Naval Architecture can be present in areas such as hull and propeller design, vibration analysis and heat flow. Data retrieved from these analyses, are used in order to estimate engine power, reducing the noise levels and eliminating cavitation in propellers. In this study, it was used in order to examine how different hull forebody shapes affect the yachts performance, by computing and comparing the resistance of them.

An alternative way to the use of CFD calculations, which is the most widespread and common way of computing resistance, is the model testing and hand calculations with the use of empirical formulas. The use of CFD though saves a lot of time and expenses compared to model testing and is more flexible than empirical formulas. However, model towing tests are very accurate compared to CFD which has areas where its accuracy is on debate. Nowadays, it is observed that the results from model testing are used to validate the CFD results. As far as hand calculations are concerned, they are mostly used as a starter point or guidance line to a more thorough detailed design process, since CFD is more flexible and efficient to use.

3.2.1 About Star CCM+

The chosen CFD software is STAR CCM+ because it used unsteady RANS and integrated models for water surfaces and waves. Star CCM+ is a computational continuum mechanics software that performs engineering physics simulations for problems considering both viscid an inviscid flow and heat transfer. Star CCM+ uses a polyhedral mesh with problem adaptive hybrid cell convergence so that the user does not need to spend excessive time on meshing. It gives the opportunities to simulate almost any kind of physics problem, with its integrated CAD Modeller, Physics models, Meshing technology, turbulence modelling, post processing ability, libraries and up to date solvers, enable the user to set the simulation according to his will and the predicted outcome.

3.2.2 URANS

This CFD study is based on the numerical solution of U-RANS equations for the dynamic flow field and the pressure fields. U-RANS gives the advantage of solving the equations with a global time step in every cell and with a small time step you can capture unsteady behaviour in these calculated mean values. This means that it renders the solution time accurate in comparison with RANS that marches the solution just with local optimized time step for each cell and not a global time step.

Down to a more mathematical model description, in U-RANS, Reynolds decomposition is employed, as seen in *Eq. 6*.

$$\bar{U} = \frac{1}{2T}\int_{-T}^{T} U(t)dt, \qquad U = \bar{U} + u^{"} \qquad \textit{Eq. 6}$$

For the U-RANS equations, the normal RANS equations are used. However the unsteady (transient) term is kept, *Eq. 7* and *Eq. 8*.

$$\frac{\partial \bar{U}_i}{\partial t} + \frac{\partial}{\partial x_j}(\bar{U}_i\bar{U}_j) = -\frac{1}{\rho}\frac{\partial \bar{P}}{\partial x_i} + \nu\frac{\partial^2 \bar{U}_i}{\partial x_i \partial x_j} - \frac{\partial \overline{u_i^{"}u_j^{"}}}{\partial x_j} \text{ with } \frac{\partial \bar{U}_i}{\partial x_i} = 0 \qquad \textit{Eq. 7}$$

$$\bar{U}_i = \bar{U}_i(x,y,z,t), \bar{P} = \bar{P}(x,y,z,t) \text{ and } \overline{u_i^{"}u_j^{"}} = \overline{u_i^{"}u_j^{"}}(x,y,z,t) \qquad \textit{Eq. 8}$$

The results from U-RANS are unsteady, still the time averaged flow is of interest. The Reynolds averaging is done in order to achieve shorter time–scales. Time averaged velocity is denoted as a $\langle\bar{U}\rangle$, which means a decomposition of the U-RANS results as a time averaged part, $\langle\bar{U}\rangle$, a fluctuation u' and the modeled, turbulent fluctuation $u^{"}$. Still the resolved fluctuations in the mean field can be averaged. *Eq.* 9, [Davidson, 2015], gives that:

$$U = \bar{U} + u^{"} = \langle\bar{U}\rangle + u' + u^{"} \qquad \textit{Eq. 9}$$

3.2.3 K-ε Turbulence Model

This turbulence model is a two equation model which solves a transport equation for a turbulent kinetic energy. Usually this turbulence model is used when there is strong vortex shedding. The equations embedded in the U-RANS model follow; *Eq. 10*, *Eq. 11* and *Eq. 12* [Davidson, 2015].

$$\frac{\partial \rho k}{\partial t} + \frac{\partial \rho \bar{U}_j k}{\partial x_j} = -\frac{\partial}{\partial x_j}\left[\left(\mu + \frac{\mu_t}{\sigma_k}\right)\frac{\partial k}{\partial x_j}\right] + P_k + \rho\varepsilon \qquad \textit{Eq. 10}$$

$$\frac{\partial \rho \varepsilon}{\partial t} + \frac{\partial \rho \bar{U}_j \varepsilon}{\partial x_j} = -\frac{\partial}{\partial x_j}\left[\left(\mu + \frac{\mu_t}{\sigma_\varepsilon}\right)\frac{\partial \varepsilon}{\partial x_j}\right] + \frac{\varepsilon}{k}(c_{1\varepsilon}P_k - c_{\varepsilon 2}\rho\varepsilon) \qquad \textit{Eq. 11}$$

$$\mu_t = c_\mu \rho \frac{k^2}{\varepsilon} \qquad \textit{Eq. 12}$$

In addition, this model was adjusted with the implementation of the two-layer approach. This gives the flexibility of y+ wall treatment, which means that near-wall cells are found within the logarithmic region of the boundary layer. Specifically, wall y+ is a non-dimensional wall distance, for a wall-bounded flow. Wall y+ distribution for the finest mesh, can be seen at *Figure 4-4*.

Wall y+ can be defined as *Eq. 13*.

$$y^+ \equiv \frac{u_* y}{\nu} \qquad \textit{Eq.13}$$

3.2.4 Verification and Validation

When an attempt is made to model a physical phenomenon with differential equations a discretization of these equations must be done in order to reduce them to algebraic equations. This raises the question of purely numerical errors of the equations solution since it creates uncertainties in the results. For that reason verification and validation must be performed in order to estimate how accurate the computations are.

The verification method is used to estimate the numerical uncertainty in a CFD computation. The sources that cause the numerical error are the round-off, iteration and grid discretization errors. Following the procedure as suggested from [Larsson, Zou, 2014]; it is assumed in this study that the round-off error is negligible and that the numerical error would be caused only by iteration, grid discretization and diffusive discretization scheme. The formula for the numerical uncertainty will be *Eq. 14*.

$$U_{SN} = \sqrt{U_I^2 + U_G^2} \qquad \textit{Eq.14}$$

As shown from most procedures for numerical error estimation, the discretization error is assumed to be dominant. As suggested [Eça, Hoekstra, 2014], it is important for the iterative error to be at least two or more orders smaller than the discretization error. With that taken into consideration, the numerical uncertainty estimation will not be disturbed and then it can be approximated to the grid discretisation certainty, see *Eq. 15*.

$$U_{SN}=U_G \qquad \textit{Eq.15}$$

For the grid convergence study further explained in Section 4.1, all the used grids, which must exceed the number of three to avoid data perturbations, must be compared to the finest grid case. In this thesis, four grids are used for the study and the Least Square Root method is used in order to estimate the exact solution. The estimated exact solution should be allocated in the interval that bounds the uncertainty with 95% probability. In *Eq. 16*, the S_0 is the estimate of the exact solution and S is the finest grid simulation.

$$S-U_{SN} \leq S_0 \leq S+U_{SN} \qquad \textit{Eq.16}$$

Using the least square error estimation gives the ability to determine the order of accuracy and the numerical error for the scatter of the numerical solutions taken into

consideration. After the fitting is performed, so there is less scatter in the data and a monotonic convergence with the order of the grid convergence would be desirable result. This method is designed in order to perform computations which have theoretical second order of accuracy, assuming the theoretical order of accuracy $p_{th}=2$ [Larsson, Zou, 2014]

As used in the LSR method, ε_{RE} indicates the discretization error and is determined by the general Richardson Extrapolation, *Eq. 17*, from [Roache, 1998].

$$\varepsilon_{RE} \backsimeq \delta_{RE} = S_i - S_0 = \alpha\, h_i^P \qquad (i = 1,2 \ldots n_g > 3 \text{ , grid number}) \qquad \text{Eq.17}$$

The next step, is to determine the three values unknown in the above equation (S_0, a, p). In order to do that three or more solutions are needed and the order of accuracy p can be estimated from the curve fit. After the three solutions one should aim for monotonic convergence i.e. $p>0$. At this part of the description further explanation of the procedure that [Larsson, Zou, 2014] proposed would deviate from the purpose of this thesis, as verification and validation were not the main concerns.

As far Validation is concerned; this procedure controls the estimated error and uncertainty of both numerical and CFD computations in more thorough way. By comparing the numerical solution to the experimental data, it determines the level of accuracy of the numerical model. For this thesis the same procedure that was used by [Larsson, Zou, 2014]was used so further explanations, equations and input parameters about uncertainty and data uncertainty are described more thoroughly there.

3.3 Seakeeping

The performance of a ship in waves is largely dependent on the encountered wave's frequency, type and heading. The waves in this study are sinusoidal first order waves. Both the peak and through are rounded, compared to ocean waves that have more pointy peaks, the wave is specified with only wave length and amplitude as inputs. Here follows a brief explanation of the mechanics of waves. In *Figure 3-3* a simple sinusoidal wave is illustrated, the wave length is represented by the blue line and the wave amplitude is represented by the green line.

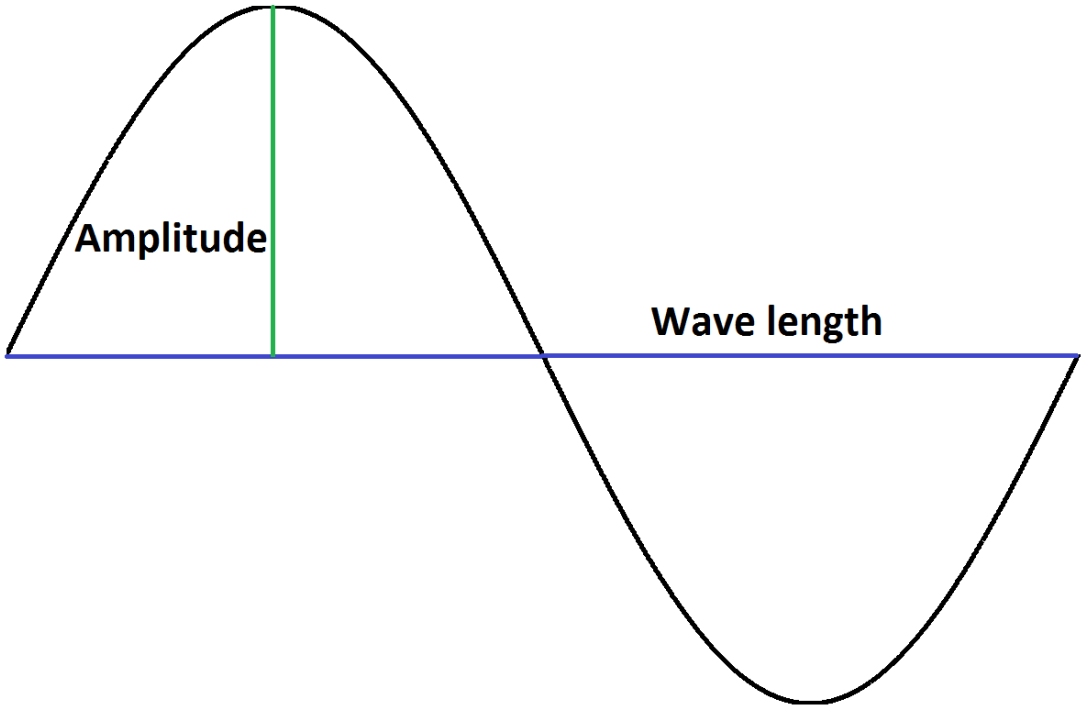

Figure 3-3 Wave specifications

From the inputs of wave length the wave phase speed, the speed of which the peak moves, the frequency and wave period can be calculated using *Eq. 18*, *Eq. 19* and *Eq. 20* where λ is the wavelength, Ω is the wave frequency and T is the wave period.

$$\Omega = \sqrt{\frac{2 * \pi * g}{\lambda}} \qquad \textit{Eq. 18}$$

$$T = \frac{2 * \pi}{\Omega} \qquad \textit{Eq. 19}$$

$$v_{phase} = \frac{\lambda}{T} \qquad \textit{Eq. 20}$$

The speed of the waves relative to the boat is calculated by adding the speed of the boat to the phase speed of the waves. The specifications of the waves used in this study are explained in Section 4.5.

Because ships have a forward speed the frequency that the ship encounters the waves will differ from the frequency of the waves themselves. The encounter frequency is thus dependent on the frequency of the waves, the speed of the ship and relative the angle between the ship velocity and wave phase velocity; the relative heading angle β. This angle is illustrated in *Figure 3-4*, [Lewis, 1989] and as mentioned in Section 1.3; only straight head sea is considered in this report.

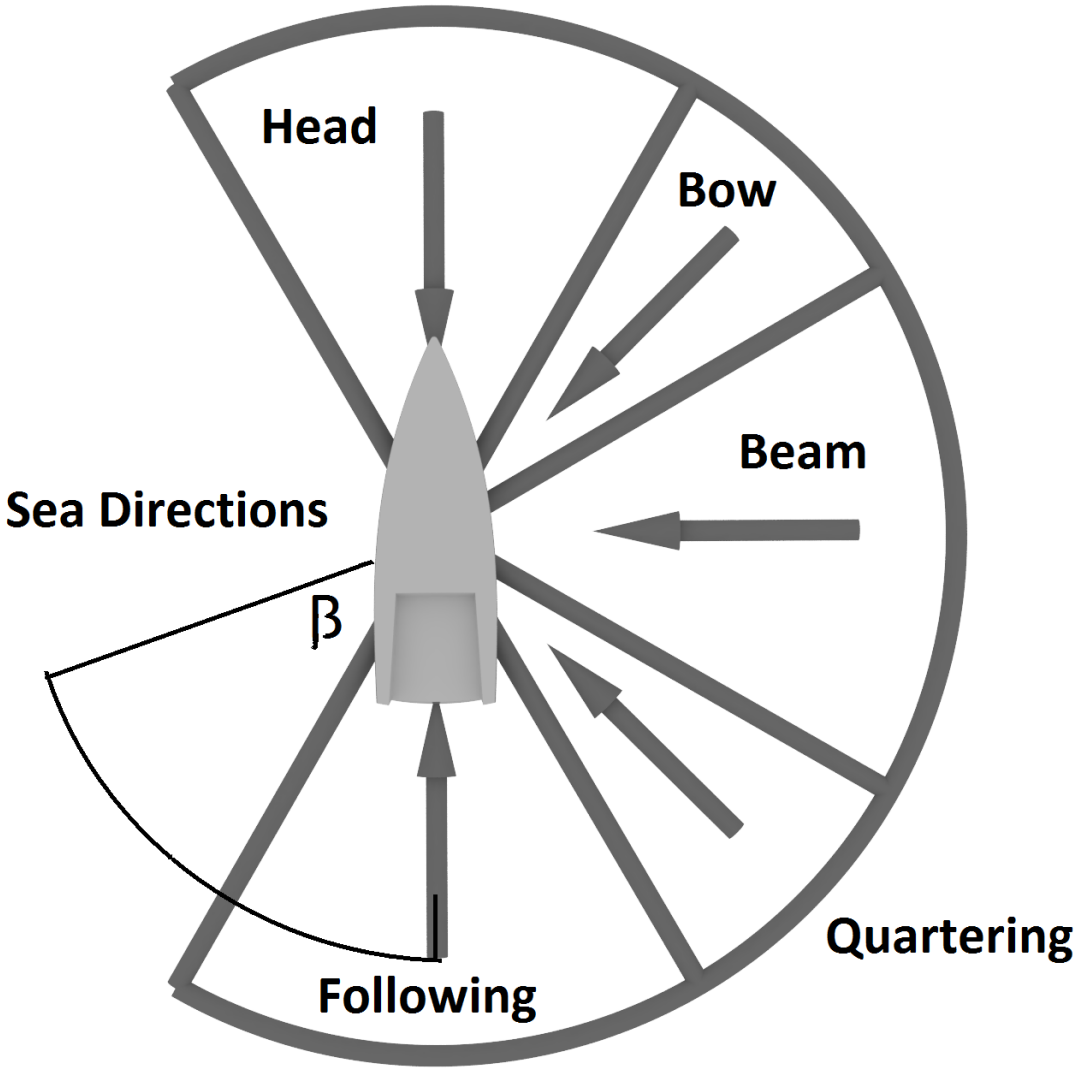

Figure 3-4 Sea directions definition

The encounter frequency, the frequency of which a ship hits a new wave can be calculated using *Eq. 21*, [Lloyd, 1998]. Here V is the speed of the ship and $cos(\beta) = -1$ because the yacht is going straight against the waves.

$$\Omega_e = -V * \frac{\Omega^2}{g} * \cos(\beta) + \Omega \qquad \textit{Eq. 21}$$

The performance of a ship generally is believed to be worse when the encounter frequency matches the natural frequency of the ship. More on the natural frequency of the of the yacht are in Section 4.5.

4 Method

The choice of the software where the CFD simulations is performed is STAR CCM+. The setup is an Unsteady Reynolds averaged Navier-Stokes (U-RANS) k-ε solver with (Volume of Fluid) VOF treatment of free surface for incompressible flow at unsteady state, see Section 3.2.

Firstly verification is performed in order to make an estimation of the numerical error or uncertainty yielded while the processes of iteration and discretization in the CFD computations are performed; see Section 3.2.4. The Least Square Root method is used for the verification process.

Secondly, the stage of validation follows, which is a procedure of how to determine the accuracy of the calculation model compared to test data as experiments. For the result to be trustworthy, the configuration of the verification phase is taken into consideration when numerical calculations are run and the results are validated against experimental data. Data results from Delft Sysser 44 hull of the Delft Systematic Yacht Hull Series (DSYHS) was used in order to perform the validation see Section 4.2. In this study four different evaluations, of three different hull geometries were performed in order to predict the optimal geometry in terms of resistance and motions.

The three hulls were identically tested for resistance evaluation as can be seen from Sections 4.4 and 4.5. The cases are:

- Straight course in calm water
- Straight course in calm water while heeling 20^{o}
- Straight course, with waves.
- Straight course, with waves while heeling 20^{o}

A propulsion force was implemented in the centre of effort of the sail in order to evaluate which forebody geometry would give the most beneficial design with the correct trim; see Section 4.4.

4.1 Verification

As described in the Section 3.2.4; the verification method used in order to determine the error estimation for the numerical uncertainty to follow was the LSR method. Hull A is used in the verification simulations and is run at the same speed and with a similar mesh as described in Section 4.3. As indicated in order for this method to be valid, there should be included more than 3 grid densities and as can be seen from *Figure 4-1*; in this case four, were used to avoid scatter in the data. The calculated total resistance coefficient, as can be seen, are following the same path as the theoretical order of accuracy and the value of p suggests that there is a monotonic convergence which means that the computations are reliable according to the assumed value of $p_{th}=2$ [Larsson, Zou, 2014]

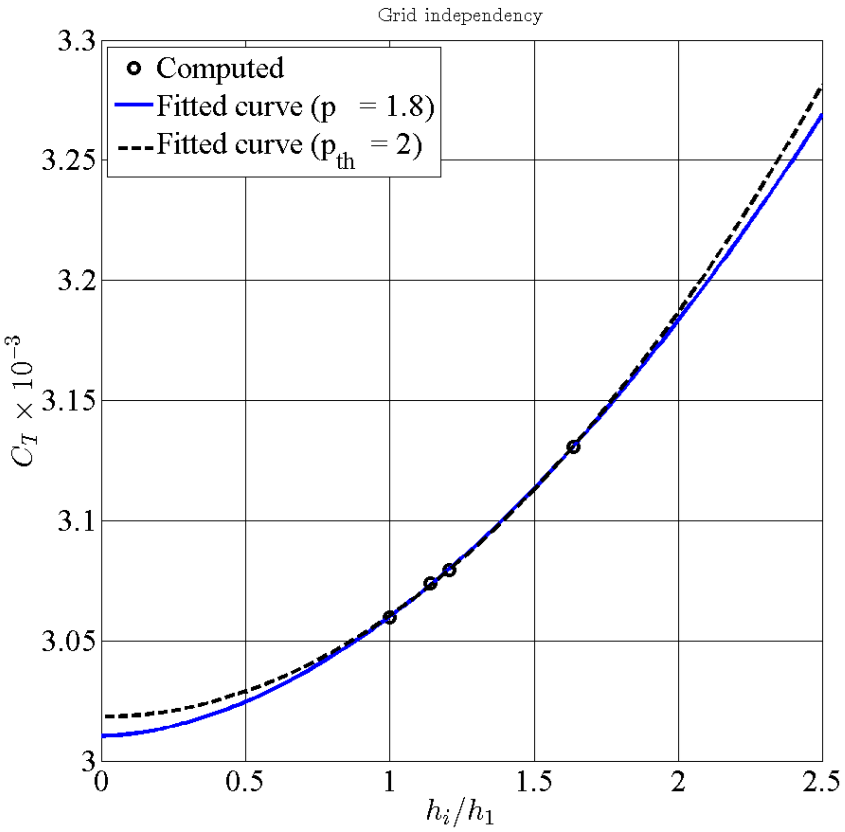

Figure 4-1 Grid independency study

A grid density ratio corresponding to h_i/h_1=1.2 are used in all further simulations. The used grid, to h_i/h_1=1.2, has an estimated error of 3% according to *Figure 4-1*.

Table 4-1 Cell number and resistance for each of the grid rations studied.

h_i/h_1	Cell count [number of cells]	Resistance [N]
1	7696819	407.7451
1.138	5211139	409.6171
1.206	4379057	410.3595
1.634	1761791	417.1910

In *Table 4-1* , the number of cells calculated and the resistance values measured after the simulations, correspond to the each grid refinement ratio presented in *Figure 4-1*.

4.2 Validation – Delft boat

To see what accuracy the predicted absolute value of resistance from the simulations yielded, a separate test case was made with a boat of known added resistance. The yacht chosen was the Delft Sysser 44; this yacht is of similar length as the ones tested in this study. The Delft #44 has however very different hull shape. The results of the Delft #44 are found in [Keuning, Onnink, Damman, 2000]. The results in that report

are used as a benchmark in for the validation case. Some particulars of the D44 are in *Table 4-2*.

Table 4-2 Delft Yacht Particulars

Yacht	Delft Sysser 44
LOA, LWL [m]	12.31, 9.98
Displacement [m^3]	8.08
LCB from AP [*m*], ([%])	4.34, (46.834)
LCF from AP [*m*], ([%])	4.351, (43.519)
Pitch radius of gyration %LOA	20
Draft [m]	0.68

The Delft Sysser 44 was simulated in Star CCM+ using the same mesh set up as for the Heyman yachts; more about the meshing is found in Section 4.3. The Delft yacht is run in 5 different wave length at the speed of 3.219 m/s, the same as in the report. The waves do however dampen as shown in *Table 4-3*. The amplitudes are measured 15 from the inlet, which is 9 m in front AP for the Delft yacht. A flat water run is also made to be able to calculate the added resistance.

Table 4-3 Delft Case amplitudes

Wave length [m]	10	12.5	15	17.5	20
Aim amplitude [m]	0.1667	0.2083	0.2500	0.2917	0.3333
Achieved amplitude [m]	0.0921	0.1484	0.2046	0.2609	0.3171

From the added resistance in waves calculations for the 5 wave cases, with deducted flat water resistance the normalized added resistance in waves, R'_{aw}, is calculated for the Delft Sysser 44. The results from the simulations in STAR CMM+ and the results found in the Delft report are shown in Figure 4-2. Added resistance and R'_{aw} is explained in Section 3.1.4.

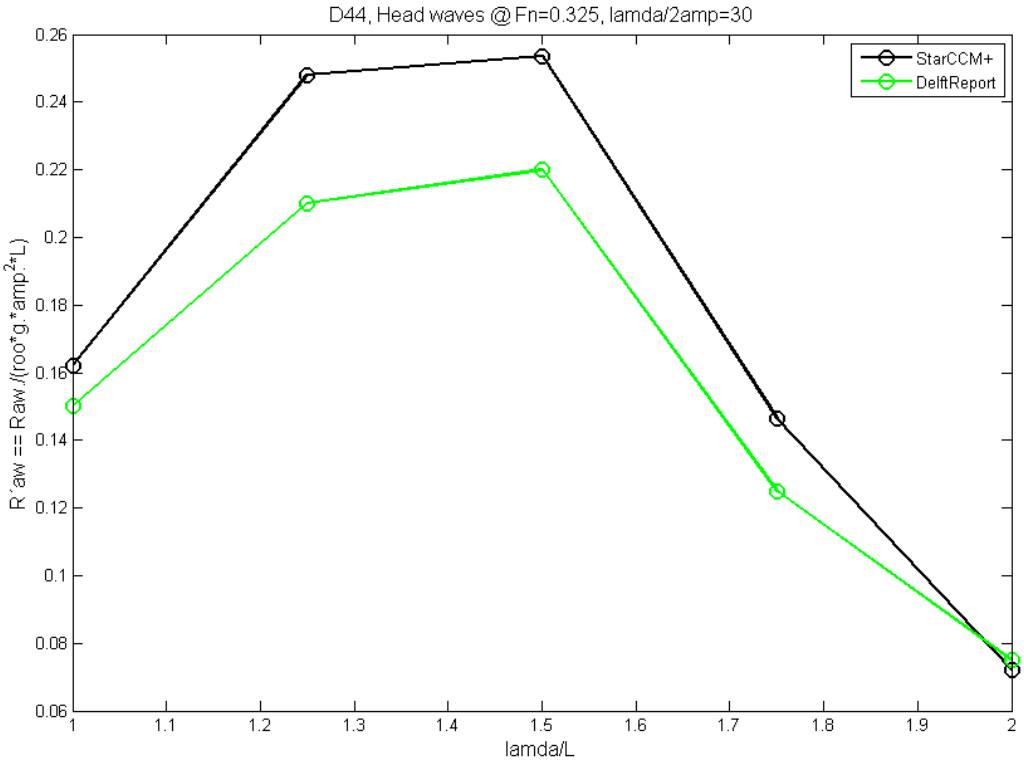

Figure 4-2 Delft #44 Case results

The error in the figure can be explained by the difference in aim amplitude and achieved amplitude even though the achieved amplitude was used in the calculation of the R'_{aw}. The point corresponding to wavelength/waterline length = 2 have the least dampened wave as shown in *Table 4-3*, this point is also where the error between the calculated added resistance and the one in the report is the smallest.

4.3 Meshing

CAD drawings of yachts A, B and C were provided by Gabriel Heyman. The geometries were imported into the software Rhinoceros where the deck and bow surface was reworked to ensure that the hulls were closed volumes, which is demanded by the meshing tool of the CFD software.

The mesh is built up of a number of volumes with different specifications in order to refine different areas around the hull and the surrounding domain. The domain in this calculation is a total of 75 meters long. Two boat length upstream from AP and four boat lengths downstream of AP. The domain is 25m and 50 m wide for the symmetry and non-symmetry case respectively. Beneath and above the waterline the domain stretches two and one boat lengths respectively. The meshing is done with an overset mesh configuration; a mesh box around the yachts that moves with the heave and pitch motions of the yacht. For every iteration of the equations the interface between the background mesh and overset is updated and interpolated. The overset mesh box initially has corners at [-3,0,-3] and [15,5,3] m x,y,z relative to AP for the symmetric case. The mesh is seen in *Figure 4-3*.

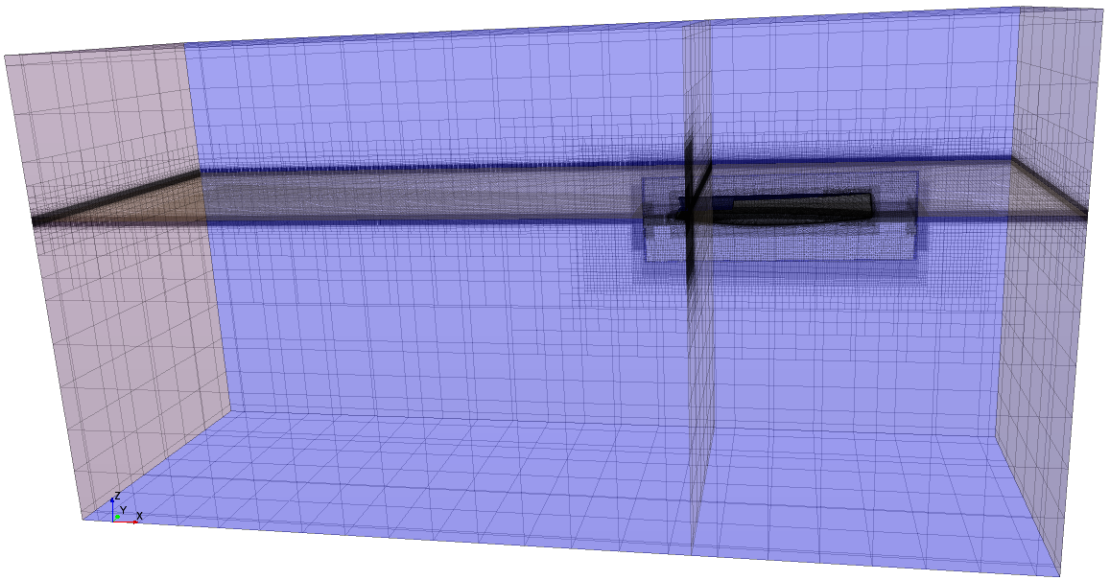

Figure 4-3 Perspective illustration of the mesh

Around the waterline the cells are sized so that there are 20 cells per wave amplitude and 50 cells per wavelength in x-direction and 25 cells per wave length in y-direction. Because of this refinement around the water level the interface region between the overset and background mesh was refined so that cells in each region can be matched when the overset mesh is moving.

Refinement around the hull was made in the overset mesh to capture the wave breaking and wave system around the boat as well as the wake from the transom. The boat hull and transom was mesh a fine surface mesh and prism layers was put on these surfaces to accurately simulate the boundary layer, see Chapter 3.

A wake box with smaller cells was made to capture the wave system that the boat creates. The Wake box stretches 3.5 boat lengths behind the boat and has a triangular shape at an angle to capture The Kelvin wedge [Larsson, Eliasson, Orych, 2014].Total Cell count for all cases for hull A is shown in *Table 4-4*.

Table 4-4 Cell count for simulations (Million cells)

Upright A	**Overset**	**Background**	**Total**	**Heel A**	**Overset**	**Background**	**Total**
Flat Water	2.638	2.305	4.944	Flat Water	5.259	4.548	9.807
λ=12.5m	4.217	3.026	7.245	λ=12.5m	8.022	6.090	14.113
λ=25m	2.507	2.079	4.577	λ=25m	4.986	4.089	9.076
λ=34.5m	2.638	2.305	4.944	λ=34.5m	5.258	2.170	7.429

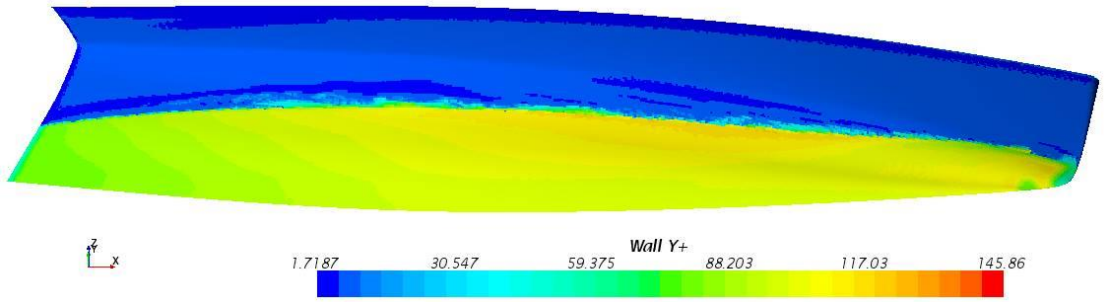

Figure 4-4 Y+ distribution over the hull A surface.

In *Figure 4-4* the wall y+ values are distributed along hull A for the mesh used in this study.

4.4 Flat water resistance

The boats are run in flat water at a speed of 3.8578 [m/s]. This speed corresponds to a Froude number of 0.35 for the length 12.5 [m]. The resistance in flat water is used both as references for the added resistance in waves and as a result. For this simulation the boats are free to pitch and heave and are run both upright and at a heel angle of 20 degrees which is regarded as a typical heel angle for upwind sailing.

The drag is measured as the integrated shear force and integrated pressure over the hull surface, with positive value in the negative x-direction in the fixed global coordinate system.

To simulate that the propulsion force is acting through the sail centre of effort a propulsion force is introduced in this point. This was done because it is only possible to lock the surge motion in the centre of gravity in the software. Because the surge motion is fixed the added force is essentially working as variable trimming moment around the COG. This force is 460 N for the upright case when only one half of the boats are simulated. That is because the starboard and port side of the yacht is symmetric. This force is the drag of hull A when pushed through the COG. The centre of effort above the waterline for the upright case is calculated with *Eq. 22*, [Larsson, Eliasson, Orych, 2014].

$$CoE = 0.39 * P_s + B_s = 9.257\ m \qquad \textit{Eq. 22}$$

Where P_s=16.3 [m] is the main sail hoist and B_s=2.90 [m] is the main boom height. The centre of effort is located at 5.695 m forward of AP. The force attachment point follows the motions of the yachts while the direction of the force is fixed forwards. For the heeling case the attachment point has been heeled with the yacht to [5.6950, -3.1661, 8.6987] m (x-y-z) relative to the zero point. For the heeling case the force is also doubled, because now in the non-symmetric case, the whole yacht is simulated.

All the yachts are run with the same COG and mass, 5.289m from the AP and 6200kg. The vertical centre of gravity is assumed to be in the design waterline.

For the heeling case the boats are rotated 20 degrees so that they have a starboard heel angle. The rotation is made around the x-axis. This causes the yachts to not be at an

initial equilibrium which causes the pitch and heave to change rapidly when the simulation is started; this also causes an offset in heave and pitch angles from the upright case.

4.5 Resistance in waves

Three wavelengths are used in the study to capture the peak in added resistance caused by the resonance encounter frequency explained in chapter 3.3.

To predict the natural pitch-frequency of the yacht the hull was put at an initial pitch angle and then released to pitch freely back to the equilibrium. The average pitch period from starting pitch angle of 5^o and 10^o to the stern was calculated; T_e=2.47 s. The yachts in this study have the same inertia and a very similar shape so the natural frequency of yacht A is used for all yachts. With these equations the wave length that matches the encounter frequency to the natural frequency is calculated to 25 m. This wavelength was therefore made the second of the three wavelengths as this should create a peak in the motions of the yachts.

In this study sinusoidal first order waves are used. The input variables to these waves are the wavelength and the wave amplitude. The wave amplitudes are derived from wave statistics of Svenska Björn [P.Söderberg, 1987], see *Figure 4-5.*

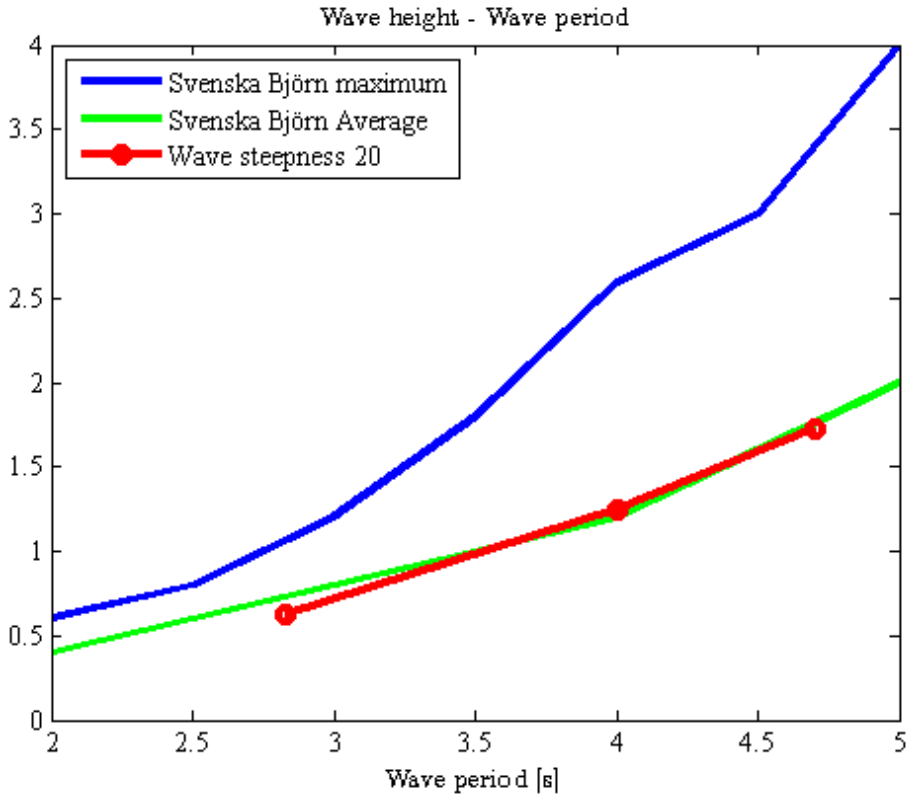

Figure 4-5 Wave statistics from Svenska Björn

The steepness of the waves, *Eq. 23,* is kept constant for all waves. Here λ is the wave length and ζ_α is the wave amplitude. With this equation the red line in *Figure 4-5* is

made, a wave steepness of 20 is clearly a realistic case. The wave period as shown in *Figure 4-5* is calculated with *Eq. 18* and *Eq. 19*.

$$\frac{\lambda}{2*\zeta_a} = 20 \qquad \textit{Eq. 23}$$

In *Table 4-5* the specifications of the waves are shown. The wave amplitude dampens in the simulations so that the aim amplitude is not achieved. A test case where the waves are simulated without the disturbance of the yacht is made to get the wave amplitude closer to the aim amplitude. The starting amplitude is then made larger and the resulting amplitude of the waves near the bow, 10m forward of AP which is 15 from the inlet in the domain, are shown in the last row of *Table 4-5*.

Table 4-5 Wave amplitudes and specifications

Case Name	**125**	**25**	**345**
Wave length	12.5 m	25 m	34.5 m
Amplitude (Aim)	0.3125 m	0.6250 m	0.8625 m
Amplitude (Start)	0.4327 m	0.6527 m	0.8625 m
Amplitude (Result)	0.2883 m	0.6047 m	0.8452 m

5 Results

In this chapter the results from the simulations are presented. The results from the flat water cases are shown in Section 5.1 and the results from the simulation in waves are presented in Chapter 5.2. The results are presented as time series and as the average, maximum and minimum values. The samples for the average, maximum and minimum values are taken from a number of periods in the drag plots. Time series results are presented with the results from all hulls in the same figures; in all plots blue lines are for hull A, red lines are for hull B and green lines are for hull C. The values for averaged resistance are shown in *Table 5-1* and *Table 5-2* and the full time series are shown for both the upright and heeled case in flat water and in wave cases. The time series are presented to be able to make a distinction between the hulls where the averaged values are very similar. The results are discussed in Chapter 6. In Appendix A a table is presented that summarises drag, pitch and heave values for the wave cases.

5.1 Flat water resistance

Even though the boats are running in flat water they all have small periodic pitch and heave, seen in *Figure 5-1*, *Figure 5-2*, *Figure 5-3* and *Figure 5-4*, this is due to numerical instabilities and should not be present in the flat water case. Yacht C is trimming more than A and B is trimming less than A. This is because the yachts have different LCF and LCB, shown in *Table 2-1*. All the yachts are trimming slightly on the bow; this is caused by the added trimming moment from the sails explained in Section 4.4.

In order to make a comparison between the different hulls; a number of values of the data provided by the tests were plotted one against the other to be able to distinguish the differences in performance between the hulls. These values were calculated over one period of drag fluctuation. For the flat water cases, i.e. without waves encounter and the yacht being either upright or in 20^{o} heel, six different plots are presented where the pitch, heave and drag of the vessels are compared.

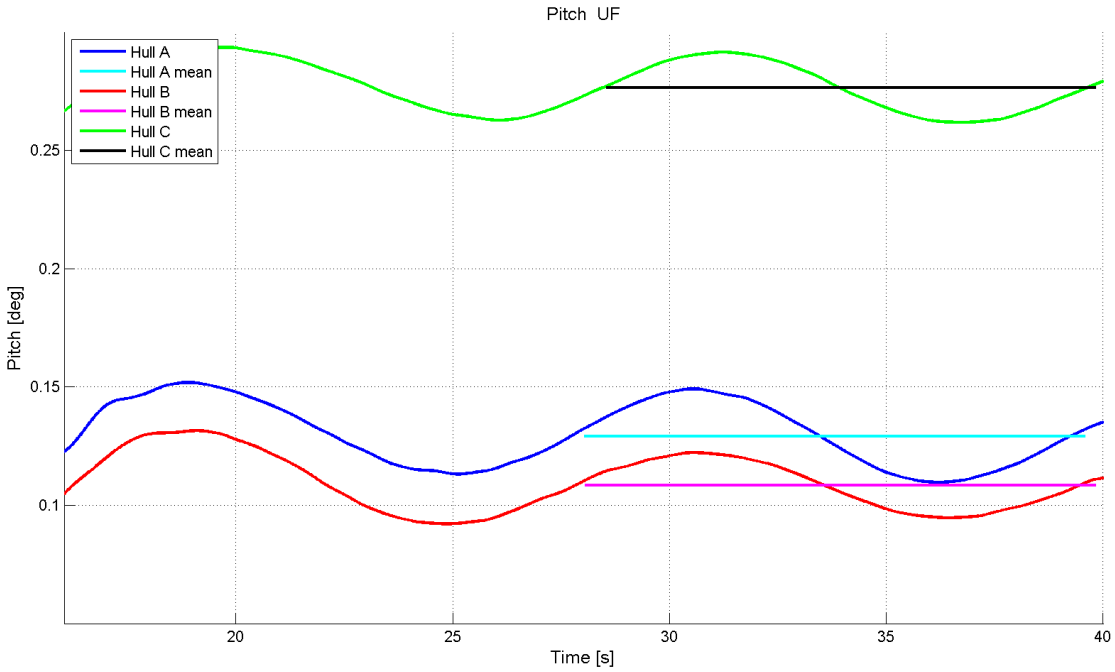

Figure 5-1 Upright Pitch in flat water

In *Figure 5-1* the comparison of the pitch motions the yachts experience for a physical time of 40 seconds is displayed. The mean values show that the hull with the highest pitch in degrees for this condition is hull C. It can also be noted that even though there are no waves; the pitch, heave and drag curves are in phase for all boats. The differences in flat water trim can be explained with the differences in LCF between the hulls as shown in *Table 2-1* where the location of the LCF of hull C is the most to the aft and thus are more prone to trim on the bow. These values will be used as the reference pitch angle for the wave cases and are found in *Table 5-1*.

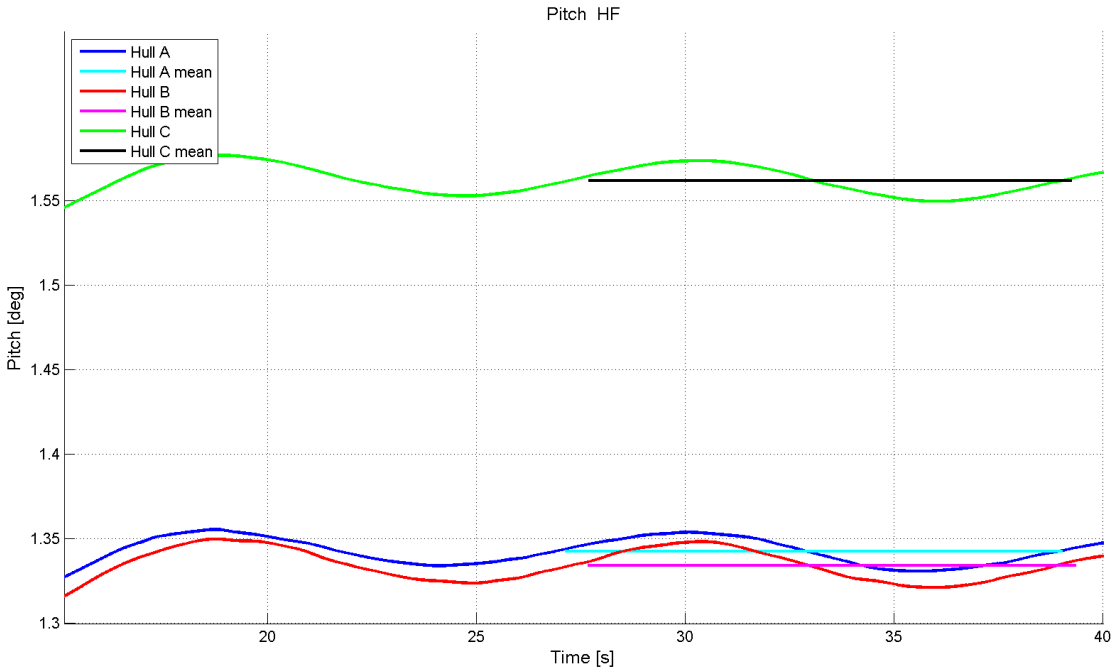

Figure 5-2 Heeled Pitch in flat water

From the measurements of pitch angles of the yachts, while they were heeled, a considerable increase, see *Figure 5-2*, is noticed. Still, the pattern is the same as the pitch in upright condition, with hull C having the highest pitch angle values, followed by hull A and finally hull B with the smallest trim. The big increase in bow trim from the upright case is partly described in Section 4.4 and is due do initial imbalance but it is also common for wide stern yachts to trim on the bow while heeled.

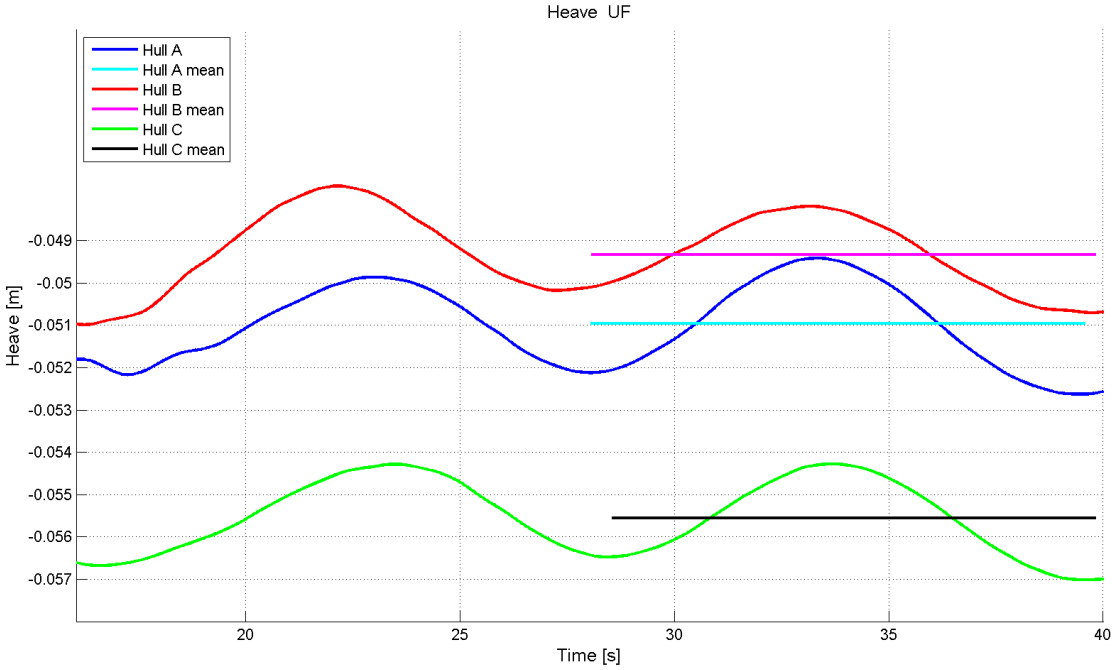

Figure 5-3 Upright Heave in flat water

All the yachts have a negative heave motion, in the upright flat water case. This is because the mass of the boats is a little more than the displacement at the design draft. Another factor affecting this also is the speed. At the Froude number that the yachts are running in, a wave through is formed mid ships that force the boat to sink a little. The same progression as before with hull A being the middle can be seen also for the heeled cases.

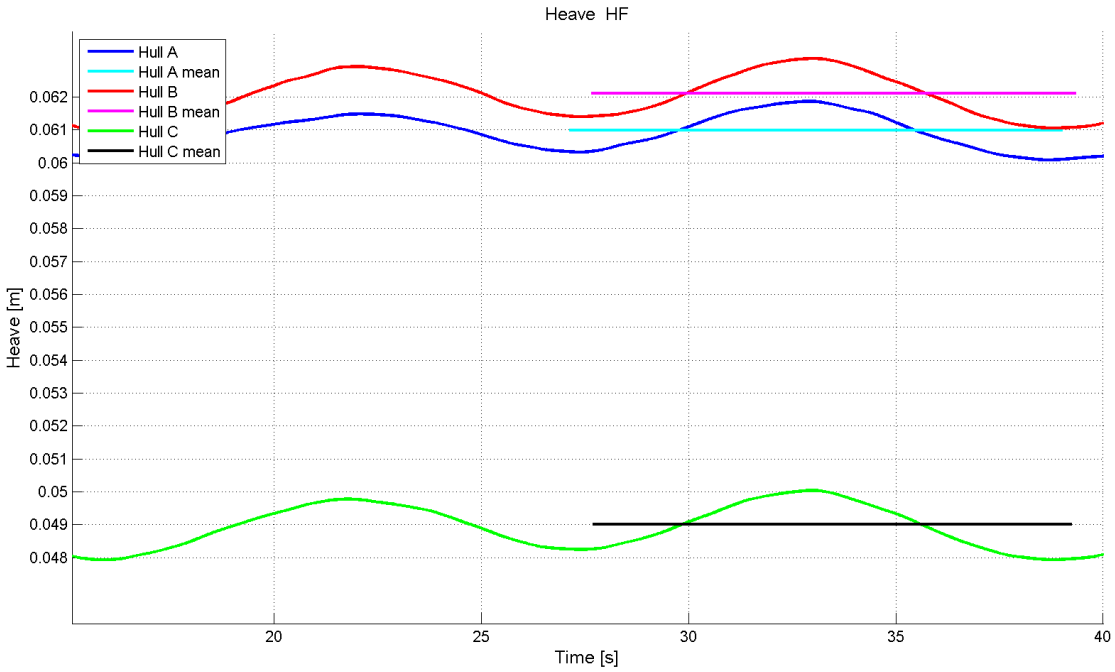

Figure 5-4 Heeled Heave in flat water

In the heeling case, the values for heave are positive and the boat is not at the equilibrium from the start so the yachts heave up to reach equilibrium, the condition at the start is explained in Section 4.4. From this plot, it can be seen that the trend of hull B having the smallest heave value, is switched with hull C in this case and hull A and B to follow.

However, in both heave measurements, the values of heave motion are quite close to each other, differing in the second and third decimal. These amounts, appearing so close in such a small scale, are not that visible when a 12.5 meter yacht is sailing, or might not even have that big of an effect overall.

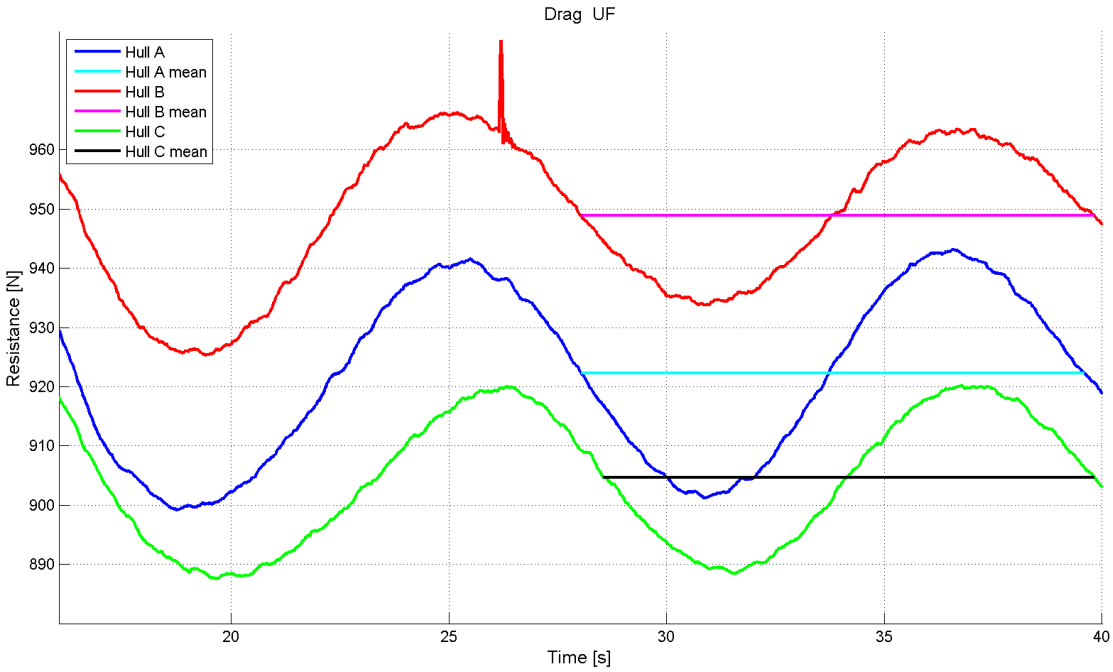

Figure 5-5 Upright Drag in flat water

As can be seen from the plots, the worst hull in terms of flat water resistance is hull B which has the tumblehome design with more volume in the lower bow area.

The heave motion and the drag values are out of phase but the pitch and drag curves are in phase, with the yachts having a drag minimum for all pitch angle maxima. Heave curve is leading the pitch and drag curves with roughly a quarter of a wavelength, see *Figure 5-1* to *Figure 5-6*. This is the case for both the heeled and the upright case and it clearly shows that hull C is the best performing in flat water.

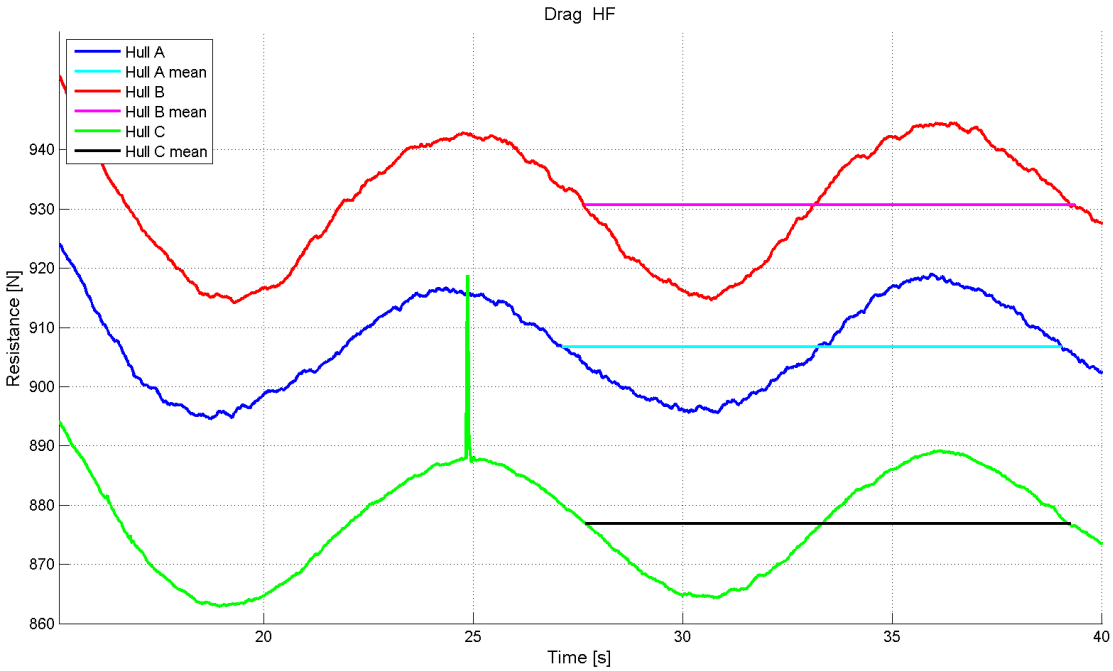

Figure 5-6 Heeled Drag in flat water

From the measurements of the drag for the yachts, while heeled, same trend is followed in *Figure 5-6* as in *Figure 5-5*. The comparison indicates that hull C is the hull with the least resistance and again this is due to the forebody design, with the narrower entry angles. In *Table 5-1* the average values for pitch, heave and drag are shown for the three yachts in flat water. It can be seen in the last two rows that C have the least resistance, almost 2% less than A in the upright case but it is also the yacht that gets the largest decrease in resistance due to heeling.

Table 5-1 Drag, heave and trim values for the hulls in flat water for the upright and heeled case.

Drag [N]	**A**	**B**	**C**
Upright	922.3	948.9	904.6
Heeled	906.7	930.7	876.8
Total resistance standard deviation from average [%]	**A**	**B**	**C**
Upright	1.567	1.083	1.213
Heeled	0.860	1.083	0.966
Pitch [deg]	**A**	**B**	**C**
Upright	0.1292	0.1083	0.2763
Heeled	1.3425	1.3343	1.5617
Heave [m]	**A**	**B**	**C**
Upright	-0.0510	-0.0493	-0.0556
Heeled	0.0610	0.0621	0.0490
Drag [%]	**A**	**B**	**C**
Upright	100 (ref)	102.88	98.08
Heeled	98.31	100.91	95.07

Hull C is clearly the best performing in flat water as can be seen in *Table 5-1* where it has 98% of the resistance of hull A in the upright case and 96.7% of the resistance of A in the heeled case. Hull C is the best even though it has the highest bow pitch angle and the most sinkage in all cases.

5.2 Resistance in waves

The resistance in waves of the yachts are made up of two components; the resistance in flat water and the added resistance in waves. The waves evaluated in this thesis are presented shown in *Table 4-5*. In the following pages, there are presented plots with comparison of the yachts in drag, heave and pitch conditions in upright and heeled scenario for the different wave cases. As in the flat water case, an average value from the data, covering four to five periods will be used to evaluate which hull has the least resistance in the different wave cases. For all time-series figures of pitch, heave and drag in Chapter 5.2 a wave contour is displayed. This wave contour has the shape of the wave that hull A encounters. It is there so that a connection, between the phase of the wave at the bow of the yacht and each quantity, easily can be made.

5.2.1 12.5 m wavelength

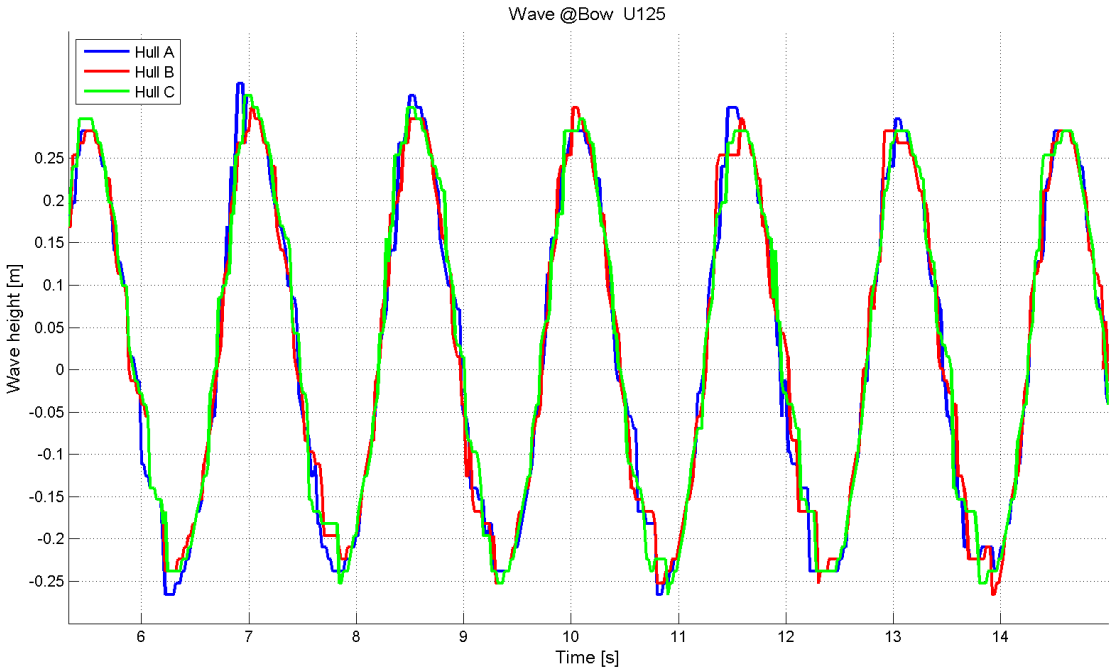

Figure 5-7 Wave of 12.5m length at bow when yacht is upright

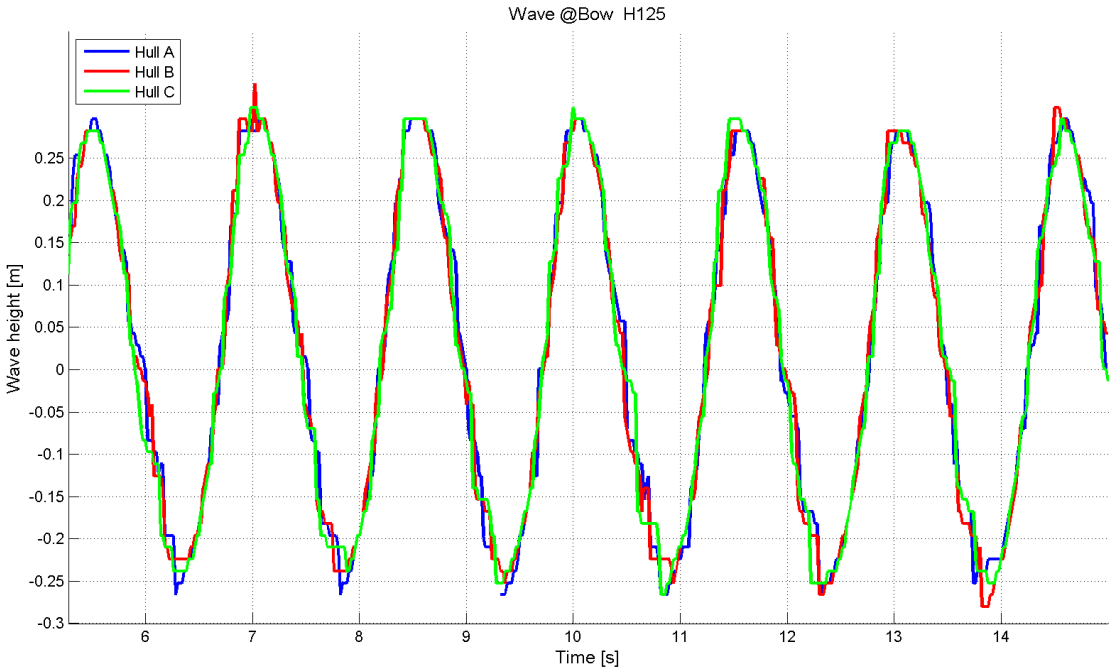

Figure 5-8 Wave of 12.5m length at bow when yacht is heeled

In *Figure 5-7* the λ=12.5 m wave is shown for the upright case. The wave height is measured 20 m port, in y-direction, of the yacht 10 m forward of AP. The wave amplitude used in the calculations of the normalized added resistance in waves is shown in *Table 4-5*. The wave height is measured on the water surface and as can be seen from the figures the wave differs little from the simulations of each boat. In *Figure 5-8* the wave is shown for the heeled case. The wave height is measured on the same locations as for *Figure 5-7* and as can be seen the wave height is very similar to the waves used in the upright case.

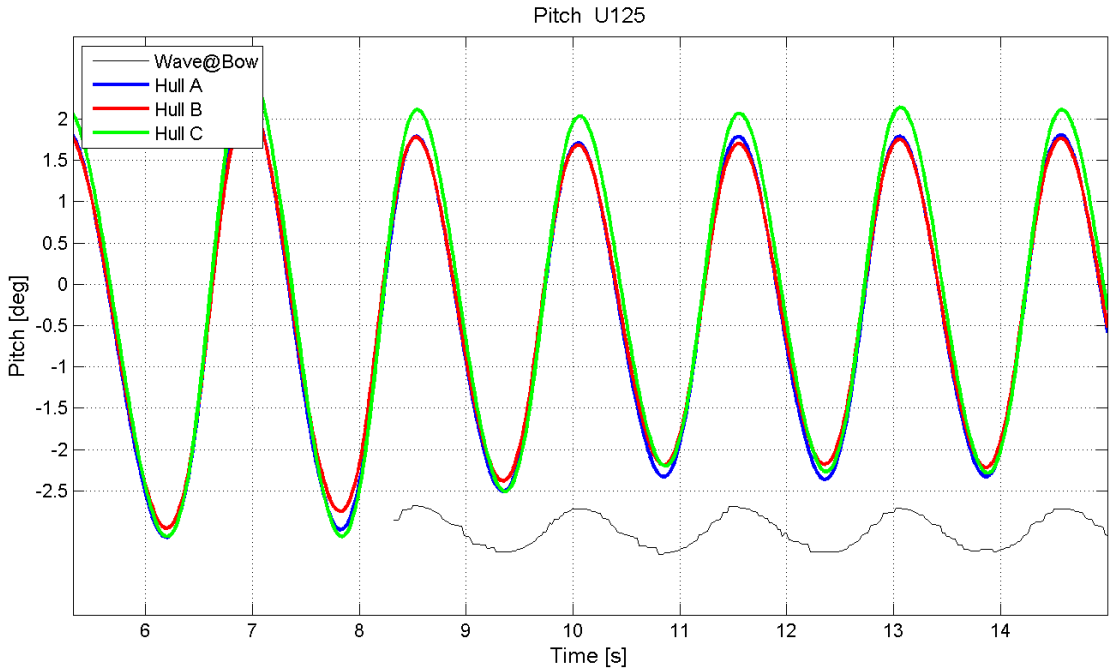

Figure 5-9 Upright Pitch 12.5 m wavelength

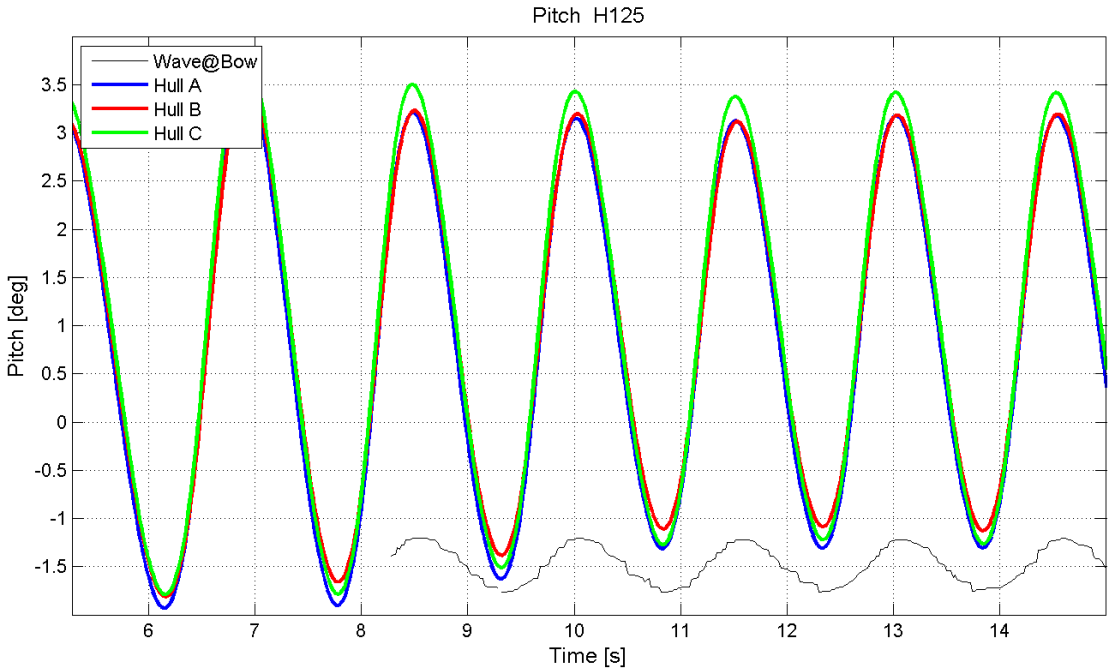

Figure 5-10 Heeled pitch 12.5m wavelength

In *Figure 5-9* and *Figure 5-10* the pitching rotation can be seen for the upright and heeled condition respectively. It can be seen in both figures that hull C experiences higher bow pitch angle and the value gap between the peak values of hull B and A, which are quite close, is in the range of 0.1 degree. For the stern pitch; hull A has the highest stern pitch with B having the smallest values. The pitching angle is half a wavelength out of phase with the wave encounters which means that the yachts are pitching bow down when there is a wave peak at the bow and are pitching bow-up when there is a wave through at the bow. The pitching angle is however larger for all yachts in the heeled case as also is seen in the flat water case, see *Table 5-1*.

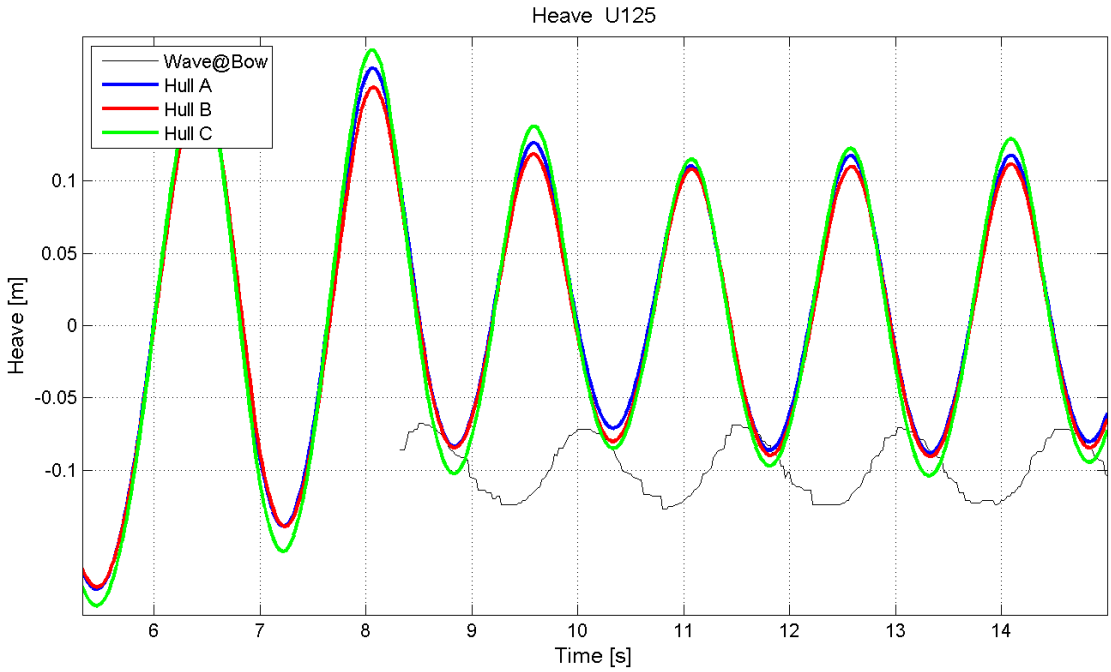

Figure 5-11 Upright Heave 12.5 m wavelength

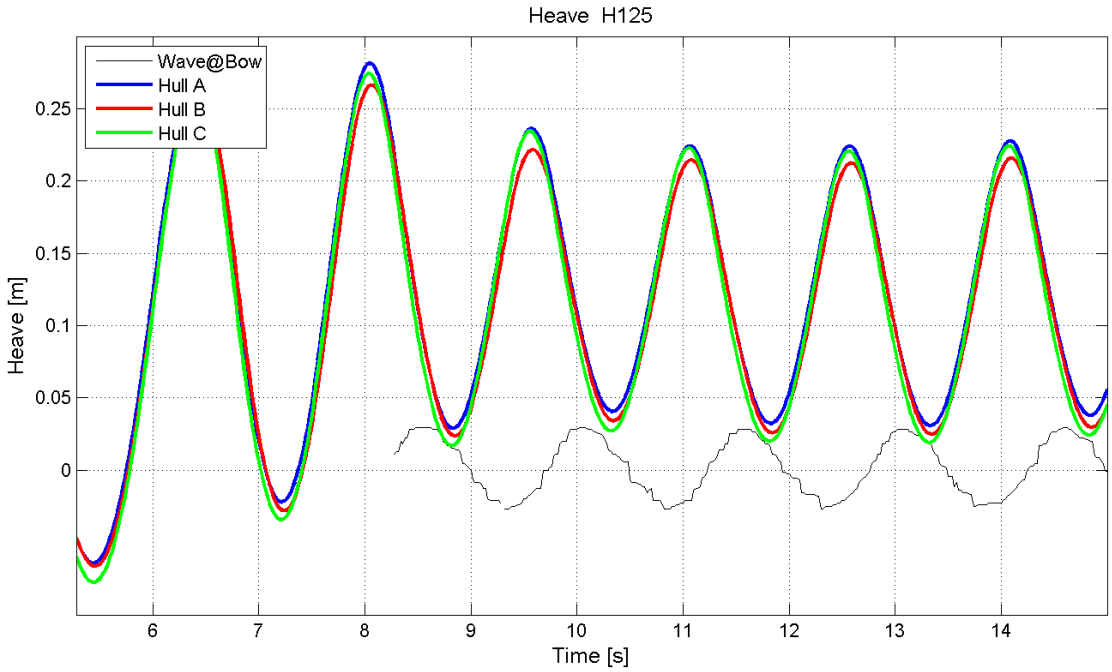

Figure 5-12 Heeled heave 12.5m wavelength

From *Figure 5-11* it is evident that hull C is experiencing higher heave motions, compared to hull A and B. The maximum and minimum heave motions are close to half a second out of phase with the wave height at the bow which means that the yacht has a peak in heave when a wave peak is at mid ship.

As *Figure 5-12* indicates, hull A having the highest heave motions while heeled, with hull C and hull B following. It can however be noted that the heave curves for the heeling cases are at an offset so that hull A and B are having almost the same total heave motion while C is heaving more; as also is seen in the upright case, see *Figure 5-34*.

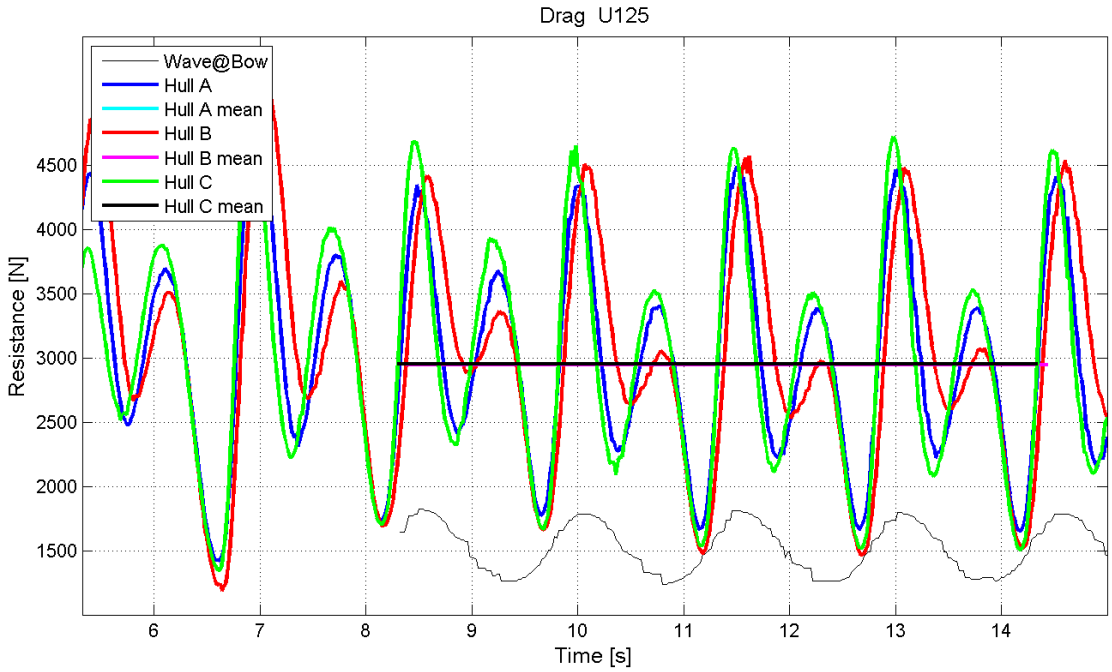

Figure 5-13 Upright drag in 12.5 m wavelength

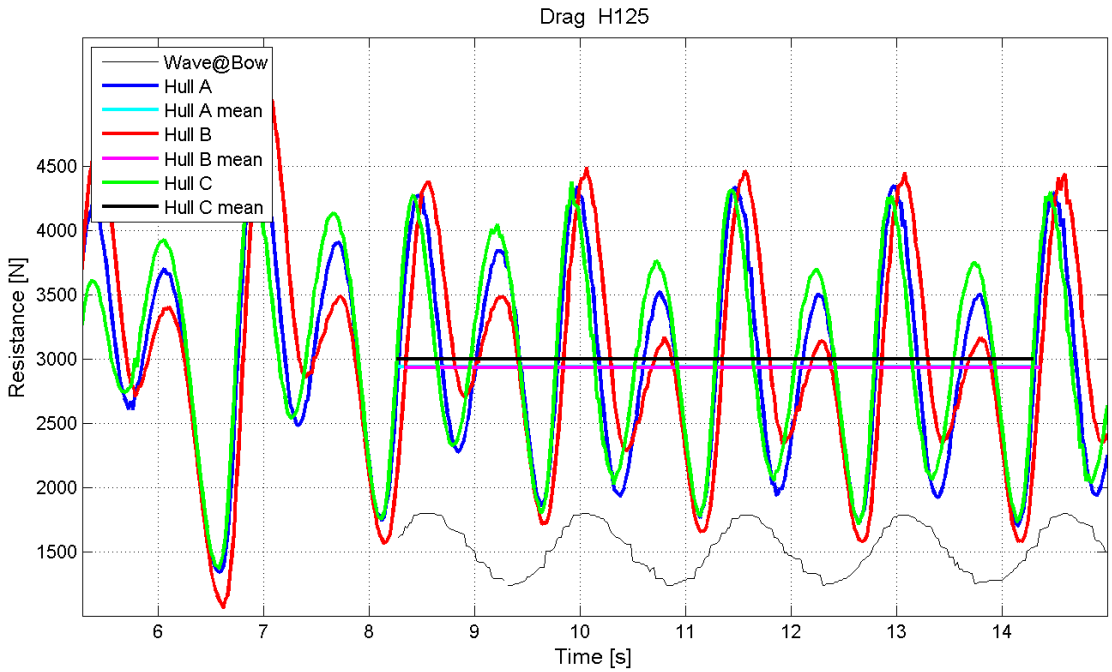

Figure 5-14 Heeled Drag wave length 12.5 m

The average values as seen in *Figure 5-13*, indicate that there is no noticeable difference between the three hulls since the resistance values are indistinguishable. However from the total range of the data for the 12.5m wave, fluctuations between the simulations for the different hulls are visible and one could suggest that hull C has the highest amount of resistance both when the hull dives in and returns from the wave encounter. There is a noticeable decrease in resistance for all hulls just as the wave trough passes the bow and there is a big difference in the secondary resistance crest for the three hulls. The secondary resistance crest, like the ones in starting at 9 and 12 seconds are in phase with the peaks in stern pitch seen in *Figure 5-9*. The secondary

resistance curve is smaller for hull B both in decreased and increased resistance as can be seen in *Figure 5-13* where the curve for hull B around the 12 second line does not stretch so far up or down as the curves for hull A and C. The secondary trough in resistance, as the ones just before 9s in the figure, shows significantly more resistance for hull B.

In *Figure 5-14* the time-series drag for the three hulls are presented for the heeled case in the shortest wave length. From the average values it is evident that hull C has the highest resistance and is followed by hull A and then B which is the best in performance. The average values are close to each other as is seen in *Table 5-2*. There is however a difference in the time series results which is clearly seen particularly in the secondary phase of the wave encounter that shows a much higher peak in resistance for hull C. This behaviour for the secondary drag peak could also be seen for the upright case, see *Figure 5-13*. Pictures from the simulations are in APPENDIX B - Upright condition pictures and APPENDIX C - Heeled condition pictures; figures for the first resistance peaks are *Figure 10-1*, *Figure 10-2* and *Figure 10-3* for the upright case and hull A, B and C respectively. The same pictures for the heeled case are *Figure 11-1*, *Figure 11-2* and *Figure 11-3*. The secondary troughs in resistance are seen in *Figure 10-4*, *Figure 10-5*, *Figure 10-6*, *Figure 11-4*, *Figure 11-5* and *Figure 11-6*; for each boat in upright and heeled condition. The secondary peaks in resistance are seen in *Figure 10-7*, *Figure 10-8*, *Figure 10-9*, *Figure 11-7*, *Figure 11-8* and *Figure 11-9*. Finally the minimum drag are when the boat are in the condition shown in *Figure 10-10*, *Figure 10-11*, *Figure 10-12*, *Figure 11-10*, *Figure 11-11* and *Figure 11-12*.

5.2.2 25 m wavelength

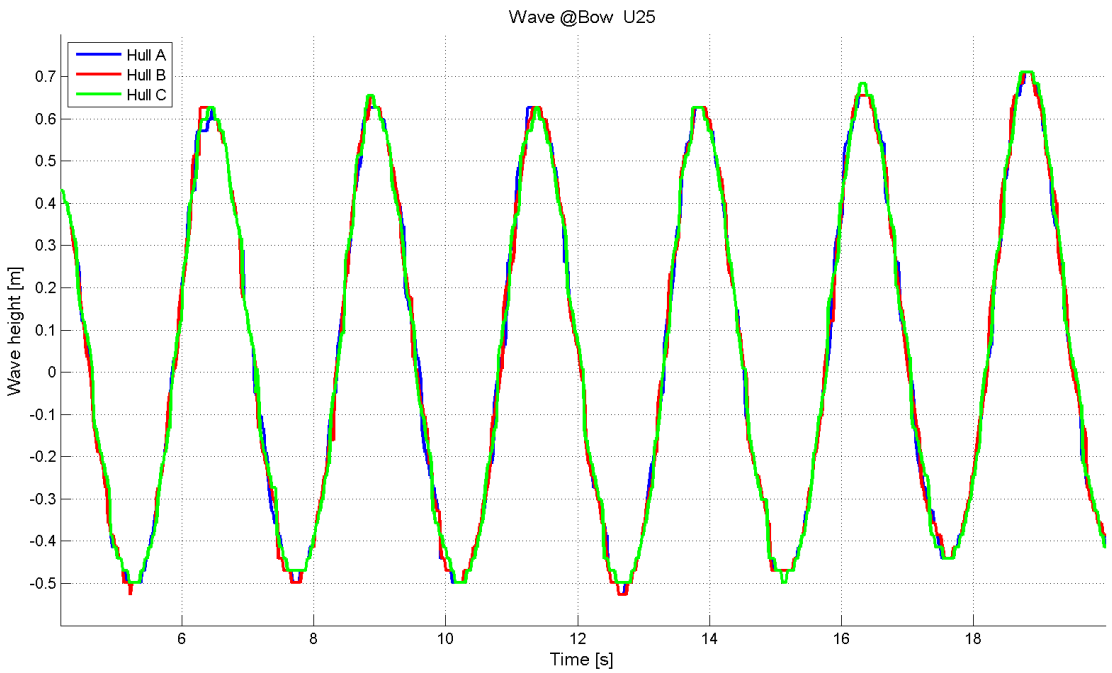

Figure 5-15 Wave of 25m length at bow when yacht is upright.

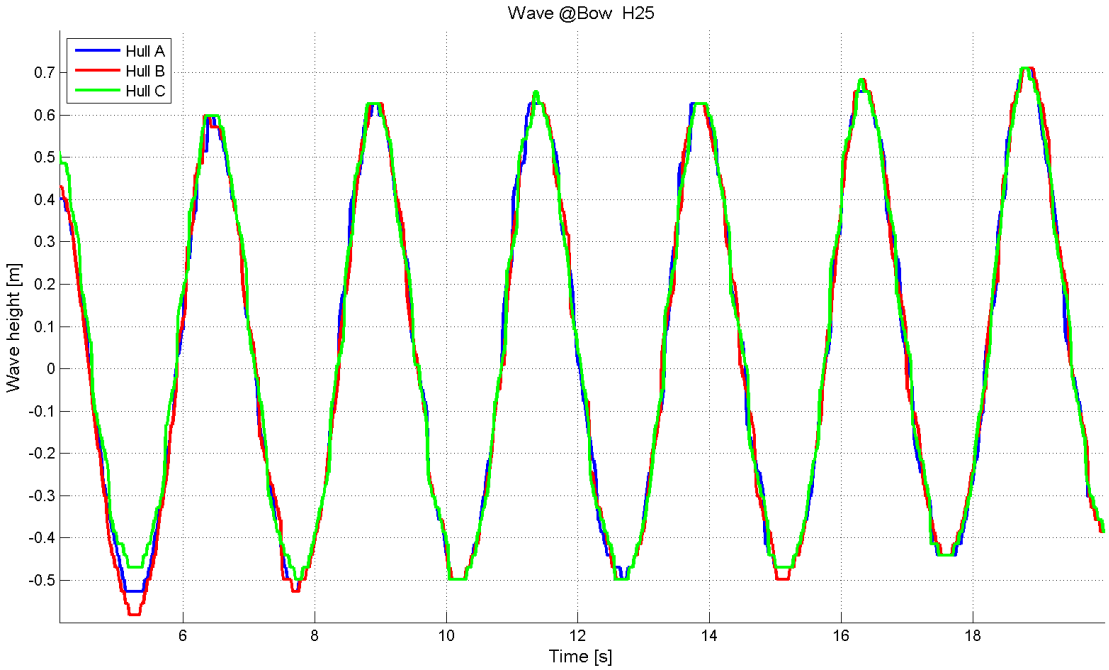

Figure 5-16 Wave of 25m length at bow when yacht is heeled

In *Figure 5-15* and *Figure 5-16* the λ=25 m wave is shown for the upright and heeled case. The wave height is measured on the same places as for *Figure 5-7* and *Figure 5-8*. The wave height used in the calculations of the normalized added resistance in waves is shown in *Table 4-5*. The wave height is measured on the water surface and as can be seen from the figures the wave differs little from the simulations of each boat. The wave height is also very similar the upright and heeled case.

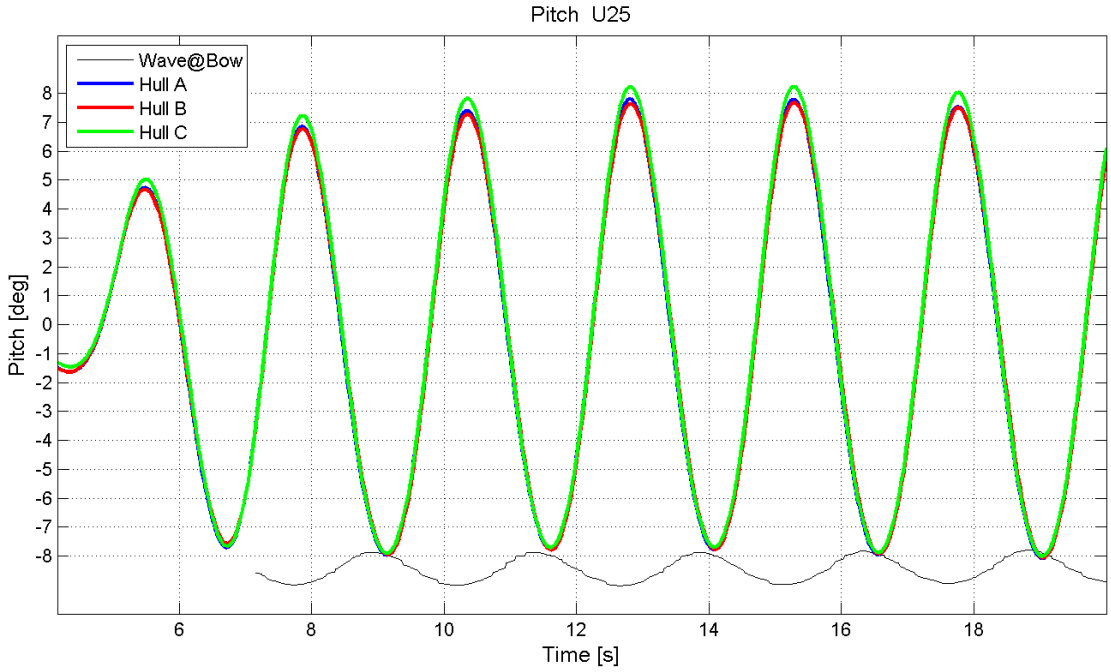

Figure 5-17 Pitch motions for 25m wavelength

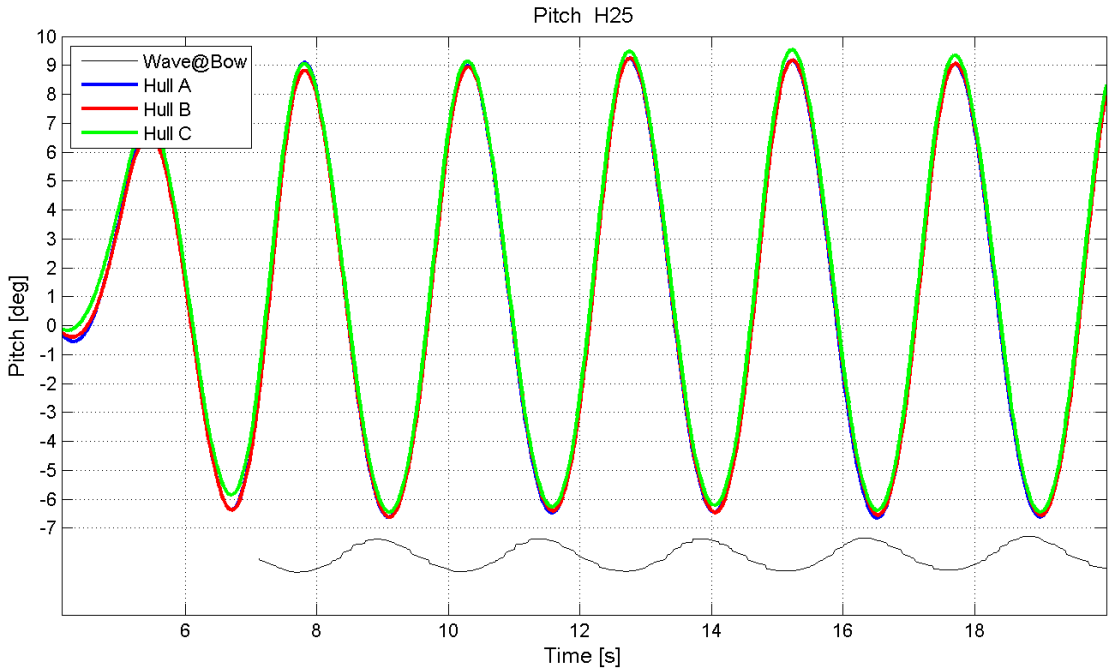

Figure 5-18 Heeled pitch 25 m wavelength

From *Figure 5-17* it is visible that hull C experiences the highest bow pitch angle while hull B has a slightly larger stern pitch and hull A is in between. However, the differences in pitch angle are in the range of less than one degree and hull C is having more forward pitch also in flat water, see *Table 5-1*. When heeled to 20^{o} in a 25m wave, hull C still exhibits the highest peaks for the pitch angle measurements. The boat has the same behaviour for negative pitch angles as for the upright case, see *Figure 5-18*.

For the 25 meter wave the pitch rotation is also in phase with the wave height at the bow; which it is not for the shorter wavelength. This can be seen in *Figure 5-15* and *Figure 5-17* where the largest pitch angle occurs at a wave peak, the same behaviour can also be seen in *Figure 5-18* for the heeled case.

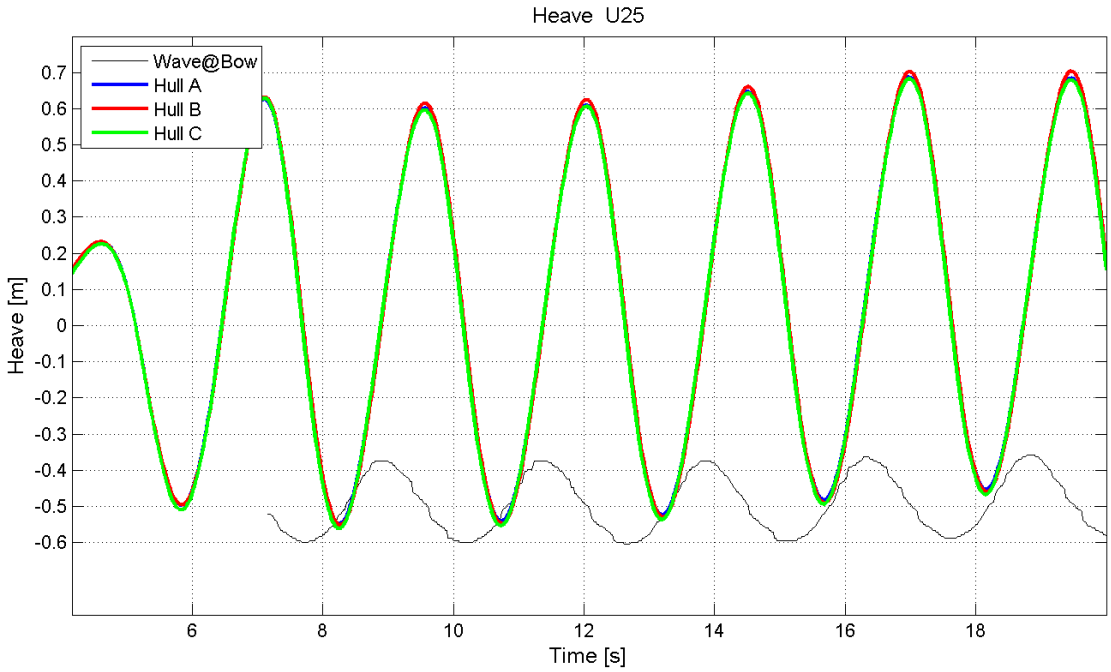

Figure 5-19 Heave motions for the 25m wavelength

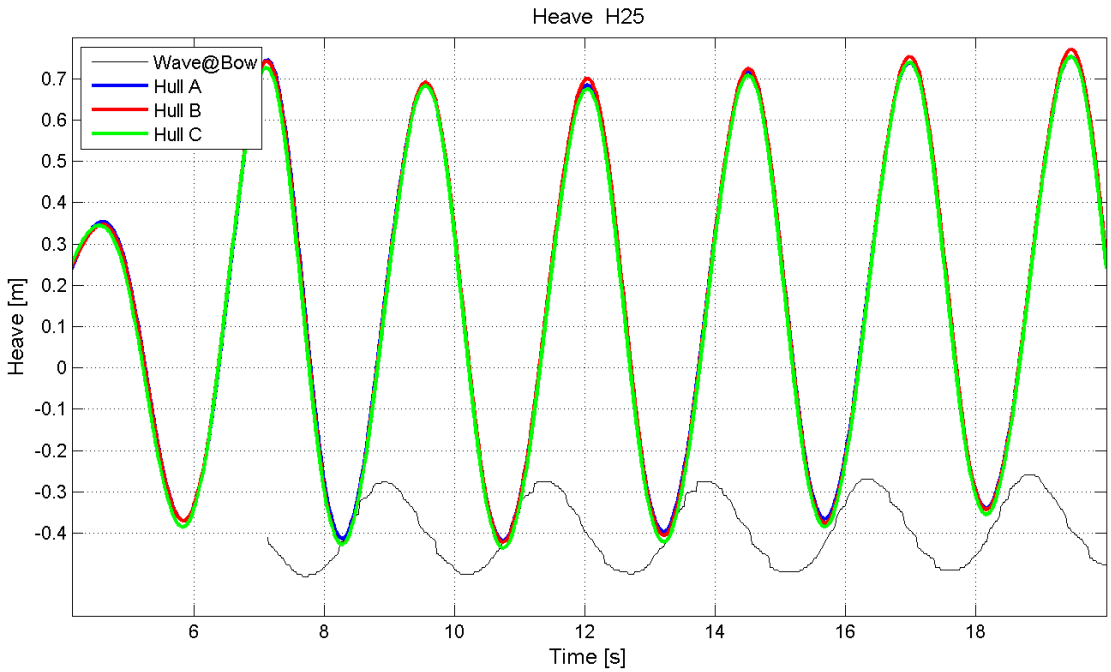

Figure 5-20 Heeled heave at 25m wavelength

As can be seen from *Figure 5-19*, hull B is the one that experience that highest amount of heave motions. The yachts heaves with the waves for this wave length as the peaks and troughs of the waves match with the heave motion of the yachts, both in amplitude and in phase. The values for hulls A and C are however very close. The same behaviour can be seen in the heave plot for the heeled case in *Figure 5-20*.

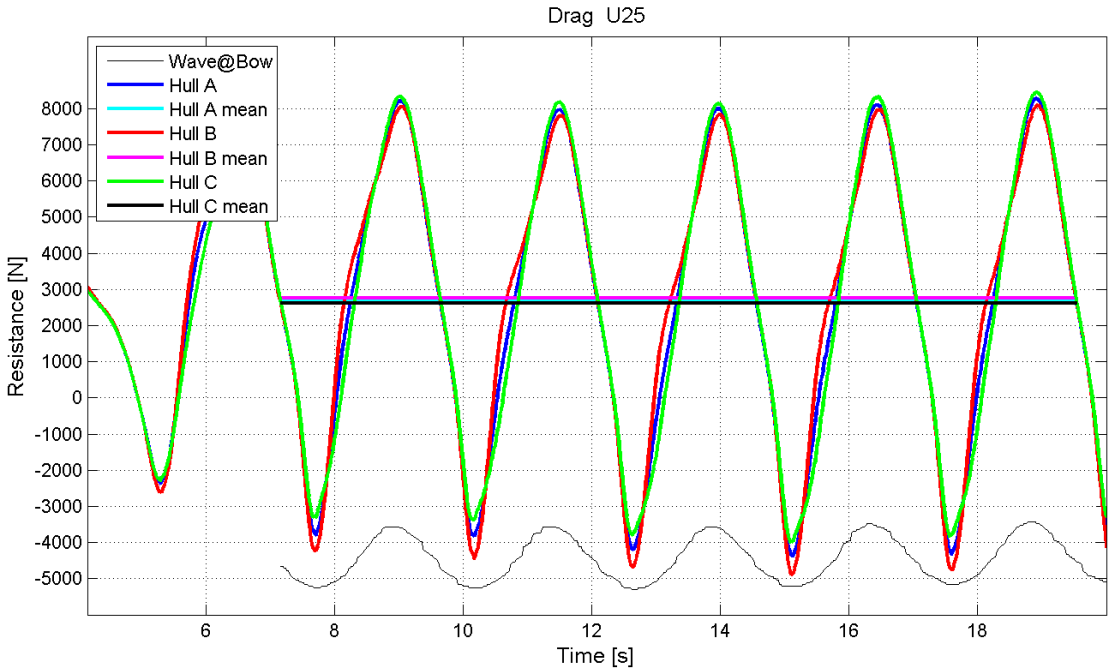

Figure 5-21 Drag in 25 m wavelength

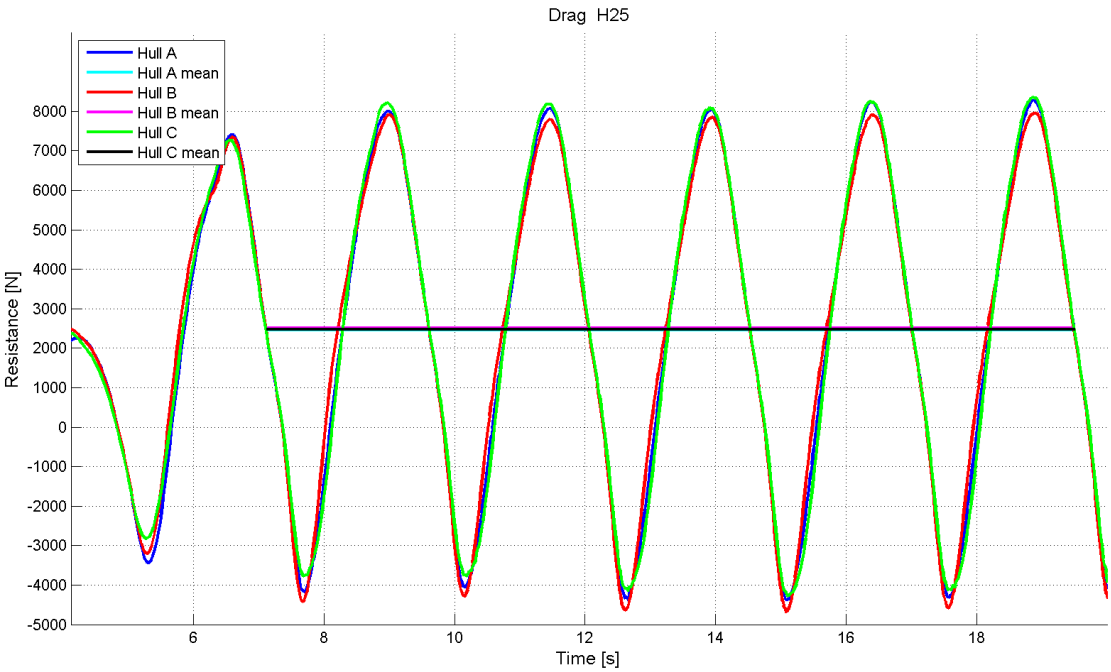

Figure 5-22 Heeled Drag for the 25m wavelength

In the 25m wave the difference between the resistance values of the three hulls is larger when averaged but there is less difference in the time series than for the 12.5m In *Table 5-2* the average values show that hull C has the smallest resistance value and hull A has second most resistance and hull B has the most resistance. However the average values are close even though hull B has the largest forward push, i.e. the largest negative value in *Figure 5-21*, and the smallest resistance peak. This is because the resistance of hull B rises more quickly from the lowest point; as can be seen around 18 s in the figure. This happens even though hull pitches the least to the bow in the wave trough, see *Figure 5-17*. For the heeled case, the yacht hull that has

the smallest resistance from an average set of data points, is hull A, then hull C follows and the highest resistance is experienced by hull B, see *Figure 5-22* and *Table 5-2*. The same behaviour is though present as for the upright case. The peaks in resistance for the upright case and the 25m wavelength are for the condition seen in *Figure 10-13*, *Figure 10-14* and *Figure 10-15* and in *Figure 10-13*, *Figure 10-14* and *Figure 10-15* for the heeled case. The scene for minimum resistance of the yachts are seen in *Figure 10-16*, *Figure 10-17*, *Figure 10-18*, *Figure 11-16*, *Figure 11-17* and *Figure 11-18*.

5.2.3 34.5m wavelength

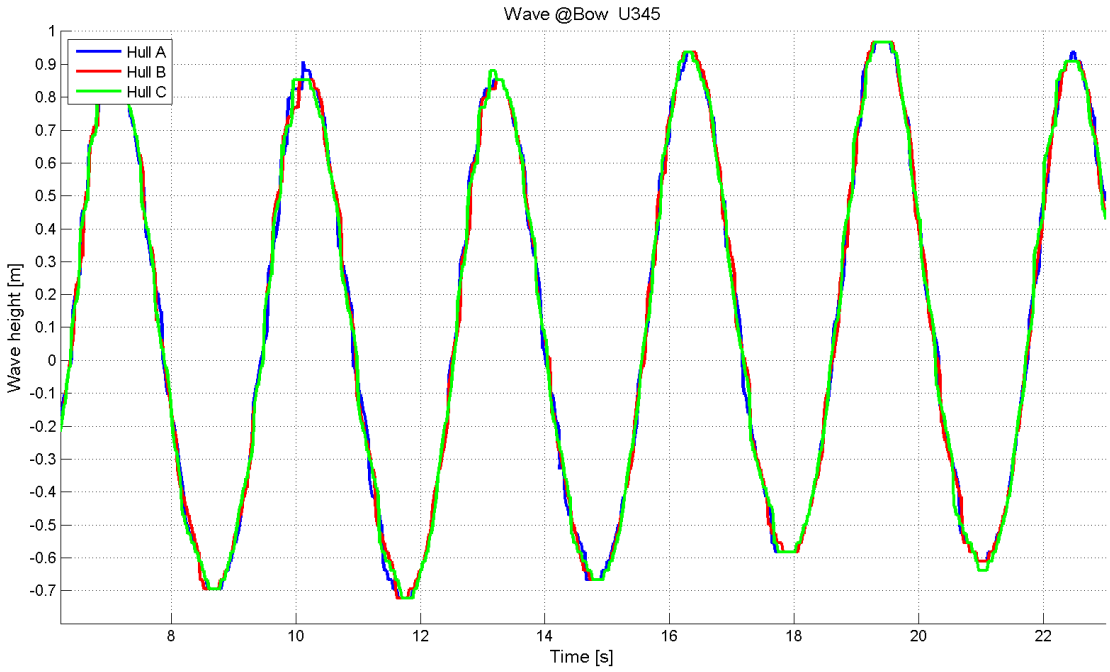

Figure 5-23 Wave of 34.5m length at bow when yacht is upright.

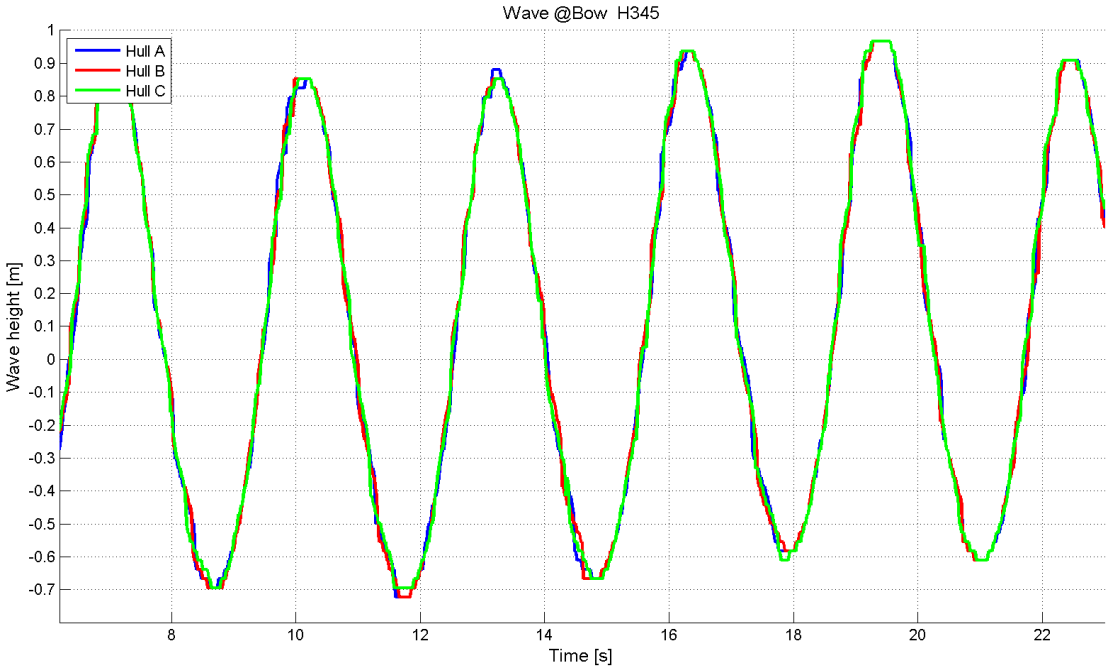

Figure 5-24 Wave of 34.5m length at bow when yacht is heeled

In *Figure 5-23* and *Figure 5-24* the different wave heights and time series of the 34.5m waves is seen.

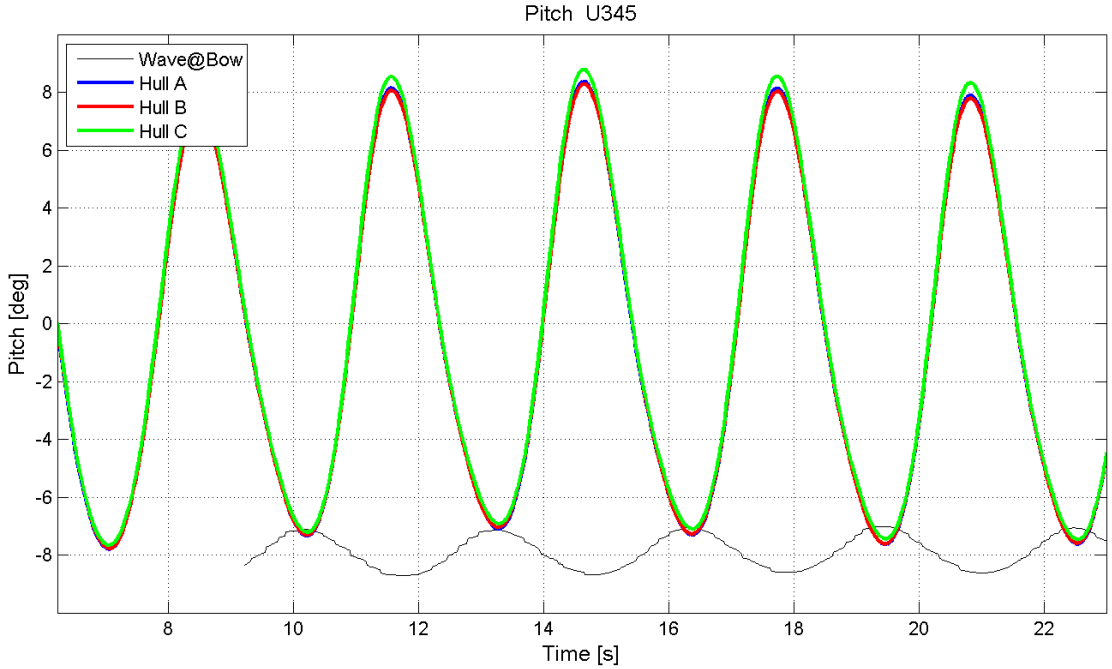

Figure 5-25 Pitch motions in degrees for the 34.5 m wavelength

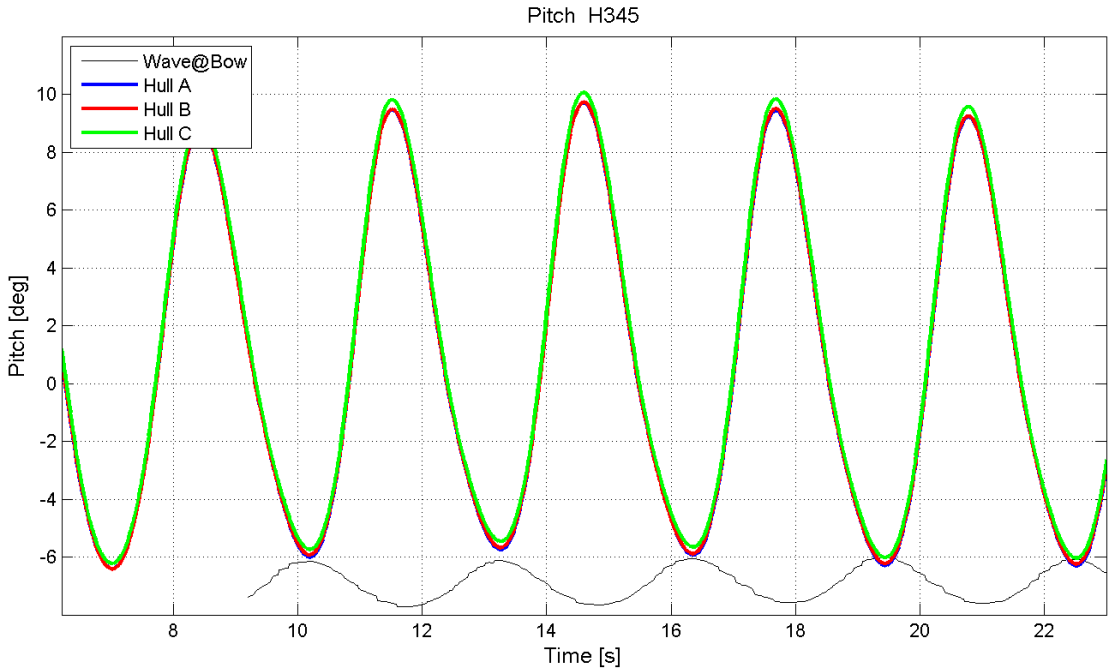

Figure 5-26 Pitch motions for heeled case scenario for a 34.5 wavelength

From *Figure 5-25*, it can be seen that hull C is the yacht that has the largest bow pitch angles also for the 34.5m wave. The stern pitch is however very similar for all the hulls even if hull C is pitching less to the stern. The same result can be seen in *Figure 5-26* for the heeled case. The pitch angle values of all hulls are also within the range of less than one degree.

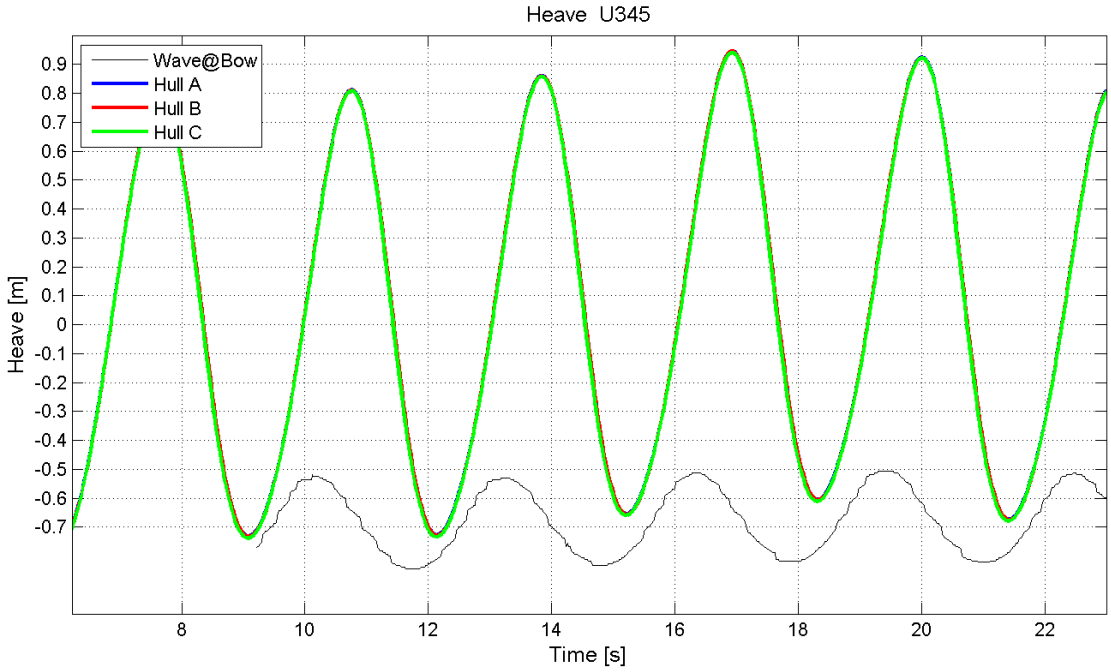

Figure 5-27 Heave motions for upright conditions in a 34.5 wavelength

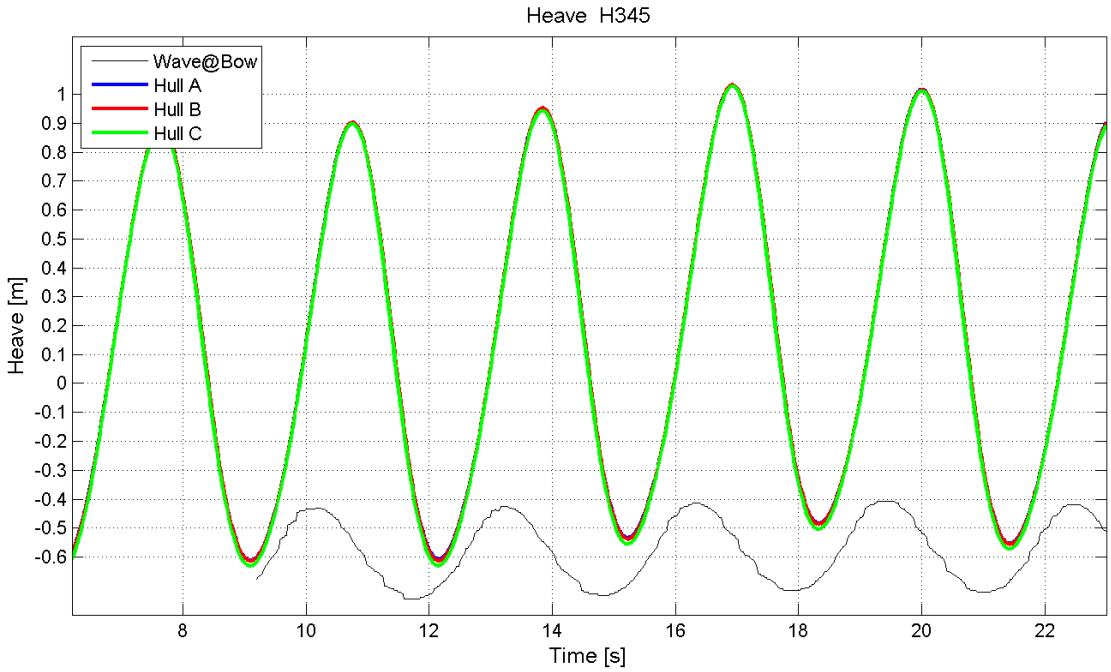

Figure 5-28 Heave motions for heeled case in a 34.5m wave

In *Figure 5-27* the heave motion for the upright case is shown. The yachts are all having heave motion peaks close the wave amplitude when the wave has reached mid ship; the same behaviour is seen in *Figure 5-28* for the heeled case.

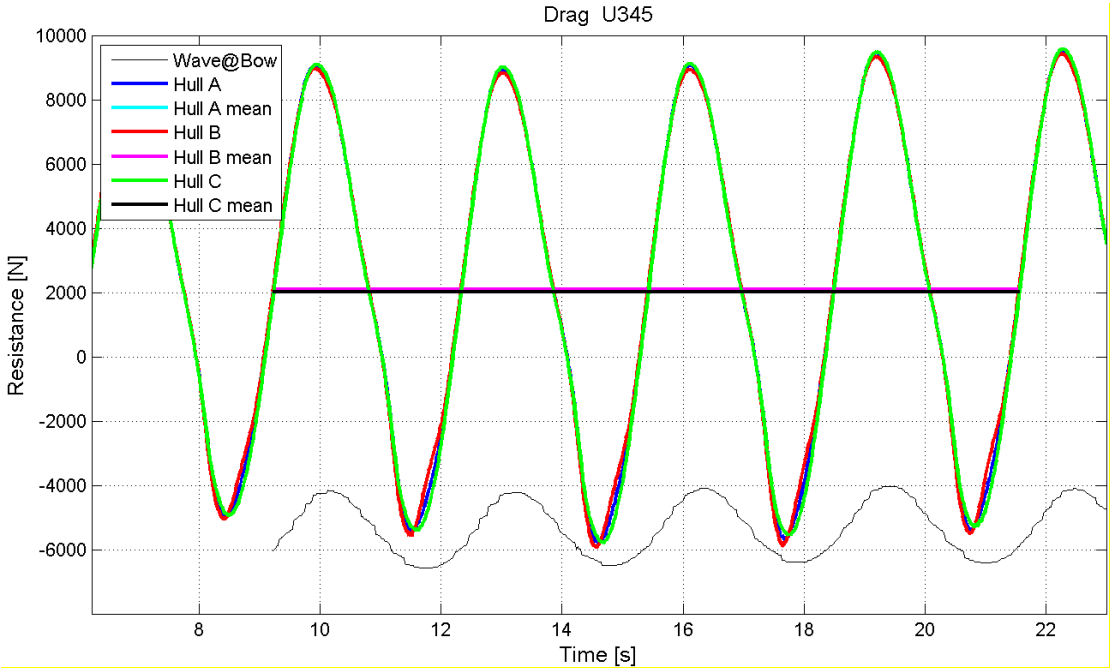

Figure 5-29 Drag in 34.5 m wavelength

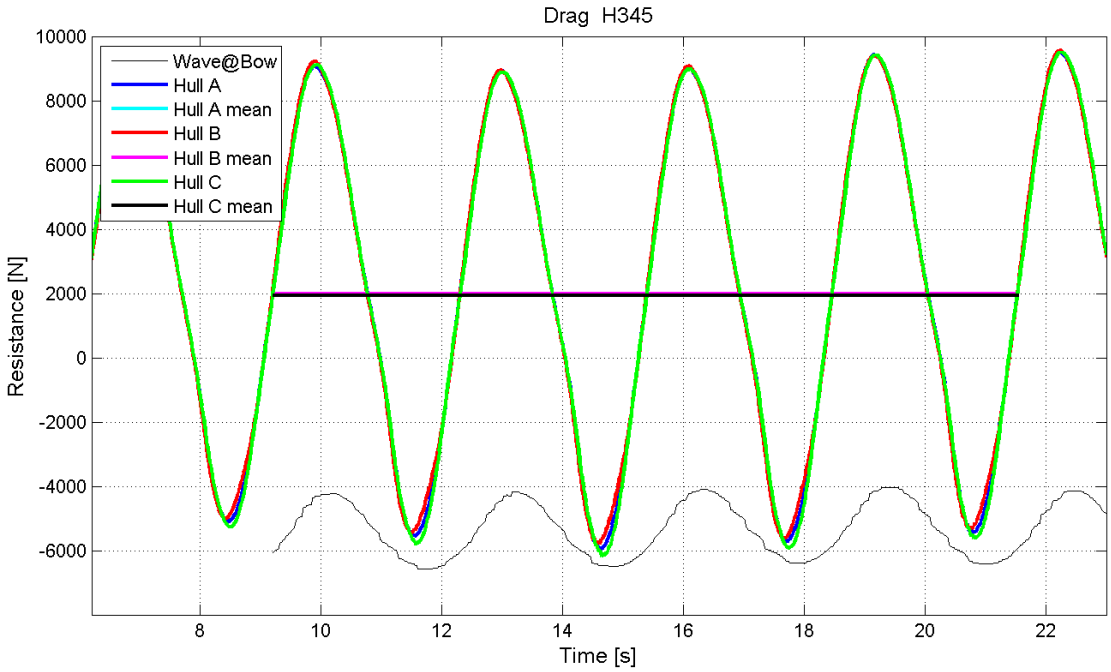

Figure 5-30 Heeled drag 34.5 m wavelength

For the longest wave, in the heeling case, hull B has the highest resistance followed by hull A and last to come hull C with the smallest one. Hull C does however have the smallest resistance in the flat water case. Similar to *Figure 5-21* hull B has both the smallest resistance peak and the most forward push but it still has the largest average resistance, see *Table 5-2*, *Figure 5-29* and *Figure 5-34*. However, for the heeling case hull C has more forward push in this wavelength. The lower part of the resistance curve has the same effect on the average resistance here as it does in the 25m wave case. Further is it worth to notice that as the wave length progresses the simulation data are coming more close to one another without many fluctuations in resistance in comparison with the wave length of 12.5m, where this more evident.

In *Table 5.2* the average drag values and the relation between them can be seen, here hull A in upright condition is the benchmark. In the shortest wave length all values are very close but it is worth noticing that here hull C has more resistance when heeled which is not seen in any other case. Hull B is the best performing in the shortest wavelength, with a small margin, hull C is best in the longest wavelength and there is a tie between hull A and C in the middle wavelength. The values presented in the table is however the average resistance without the deduction of the flat water resistance. The normalized added resistance in waves is shown in *Figure 5-39*.

As for the other wavelengths the environment and position of the boats during resistance peaks and troughs are found in *Figure 10-19*, *Figure 10-20*, *Figure 10-21*, *Figure 10-22*, *Figure 10-23* and *Figure 10-24* for the upright case and in *Figure 11-19*, *Figure 11-20*, *Figure 11-21*, *Figure 11-22*, *Figure 11-23* and *Figure 11-24* for the heeled case. On each page of the appendices the same peak or trough in resistance are shown for each yacht. This is so that a comparison can easily be made between them.

5.2.4 Combined results

Table 5-2 Drag Average Values for the different wave lengths and hulls

Drag [N] with drag percentage of hull A upright in parentheses			
λ=12.5 m	**A**	**B**	**C**
Upright	2951.7 (100%)	2942.7 (99.67%)	2952.8 (100.03%)
Heeled	2935.6 (99.45%)	2928.9 (99.22%)	2996.4 (101.51%)
λ=25 m	**A**	**B**	**C**
Upright	2661.4 (100%)	2752.6 (103.42)	2620.9 (98.47%)
Heeled	2453.2 (92.17%)	2501.2 (93.98%)	2469.1 (92.77%)
λ=34.5 m	**A**	**B**	**C**
Upright	2066.5 (100%)	2090.8 (101.17%)	2006.1 (97.07%)
Heeled	1974.3 (95.53%)	1998.2 (96.69%)	1930.0 (93.394%)

Next a comparison of the drag, pitch and heave for the different wave lengths in upright and heeled cases will follow. For drag and pitch the minimum and maximum values will be presented. The total heave motion is shown in different wave lengths as well as the average drag.

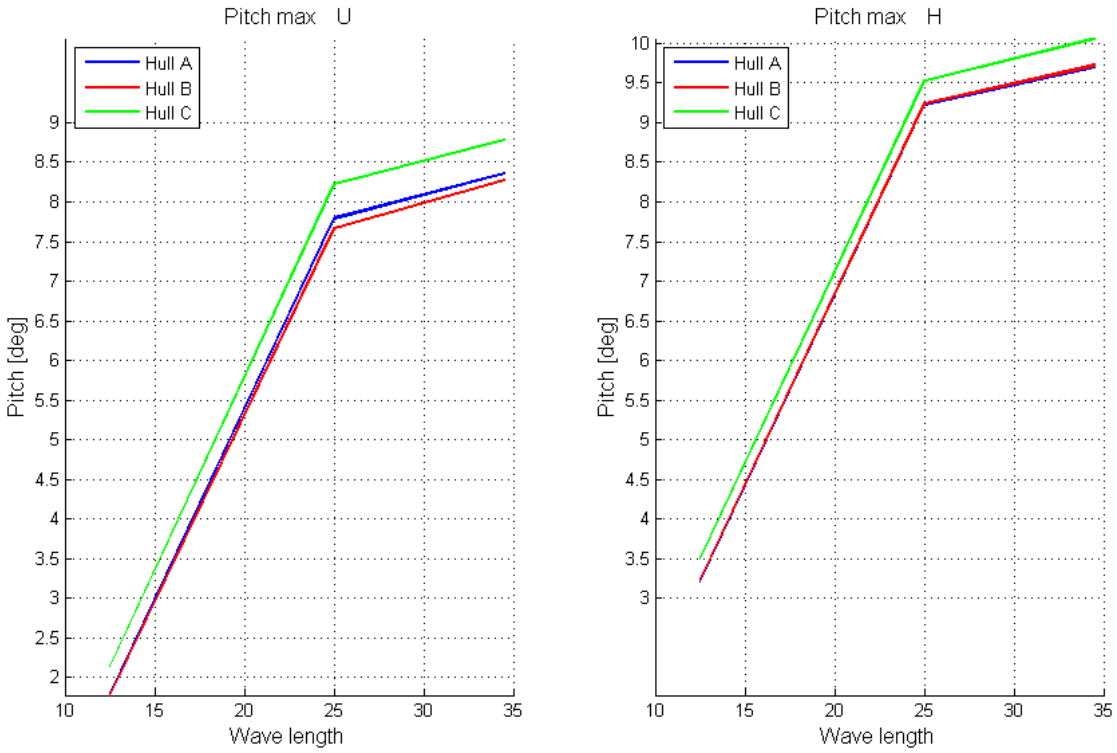

Figure 5-31 Max bow pitch values for the three hulls in upright and heeled condition

In *Figure 5-31* the maximum bow pitch angles are shown for all hulls. Hull C has the most bow pitch in all cases as also seen in the flat water case. All yachts are pitching more to the bow in the heeled condition. Hull A and B has more similar bow pitch angle and the bow pitch follows the progression of the LCF, see *Table 2-1*, where the location of LCF for hull C is most to the stern.

In *Figure 5-32* the stern pitch is visible and from the results, hull A has the largest stern pitch for the longer wavelengths with hull B and hull C following. The difference for the shorter wavelengths in the upright condition is however small and it is only in the 34.5 m wave that hull C is trimming less to the stern. A consequence of the bow pitch being larger for the heeled case is that the stern pitch is less.

The combined pitch rotations are shown in *Figure 5-33*.

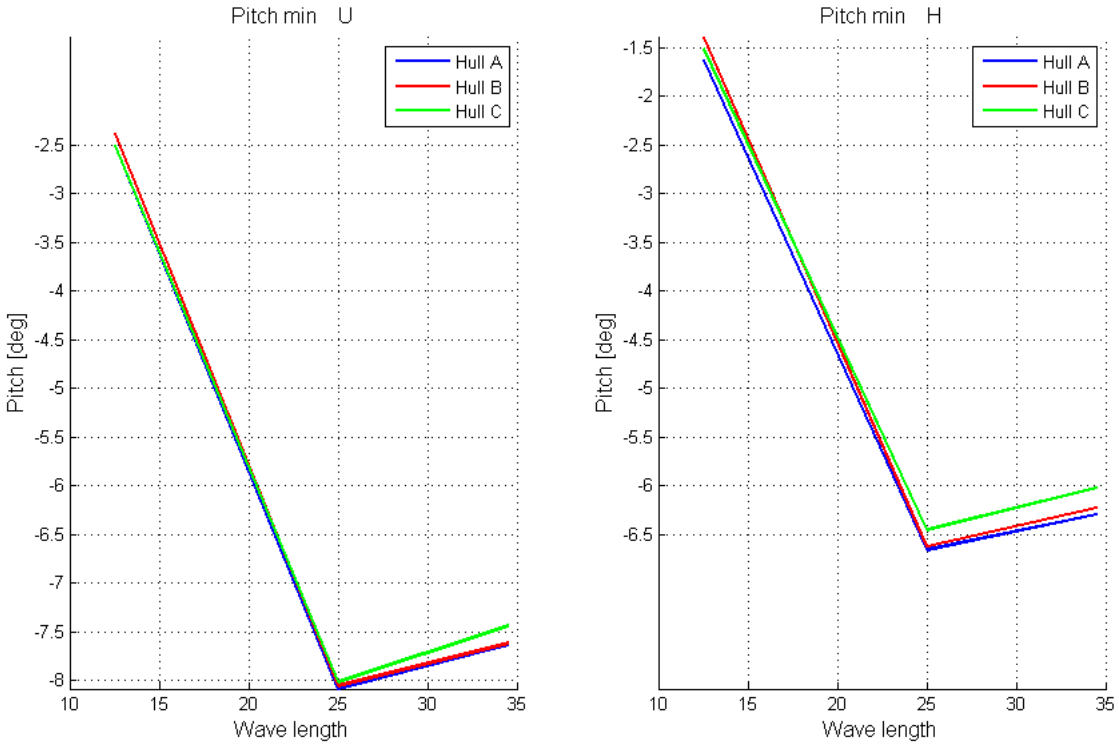

Figure 5-32 Maximum stern pitch values for the three hulls in upright and heeled condition

As can be seen from *Figure 5-33*, pitch travel values for hull C are the largest meaning that it will experience largest pitch motions; bow to stern. The difference in the heeled case is however small.

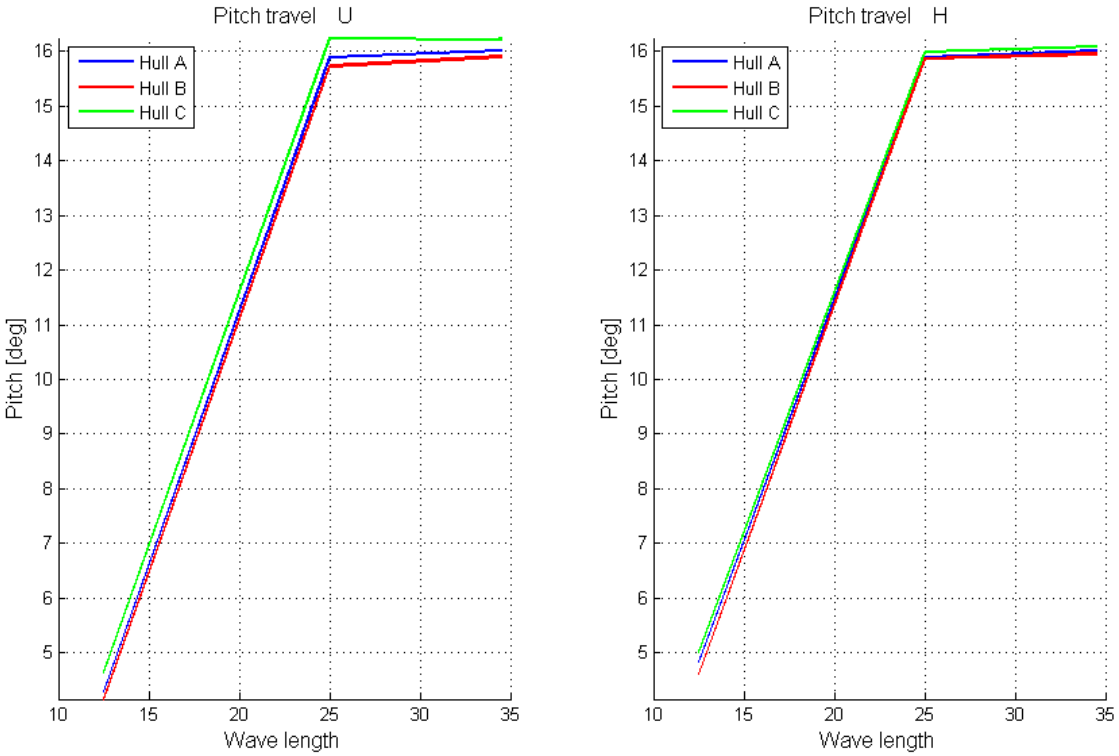

Figure 5-33 Pitch travel values for the three hulls in upright and heeled condition

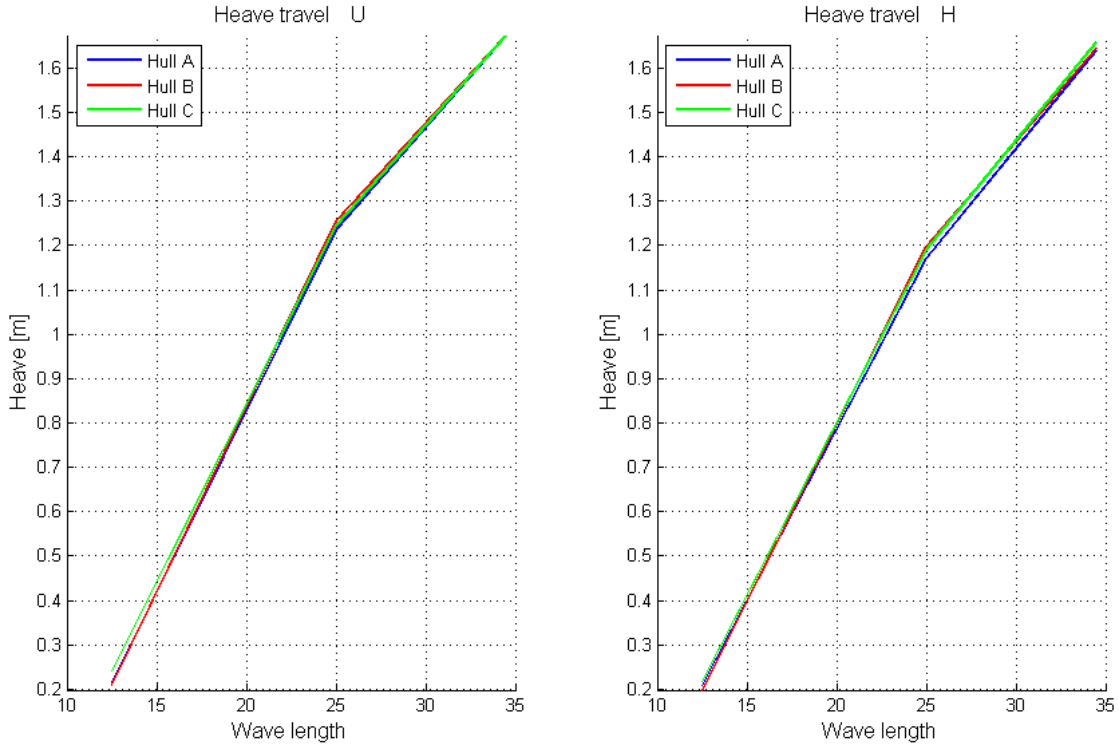

Figure 5-34 Heave travel values for the three hulls in upright and heeled condition

The heave motions shown in *Figure 5-34* are very similar for all three hulls and follow very closely the wave height for the two longer wave lengths. For the 12.5 m wave the boats are heaving significantly less than the wave height.

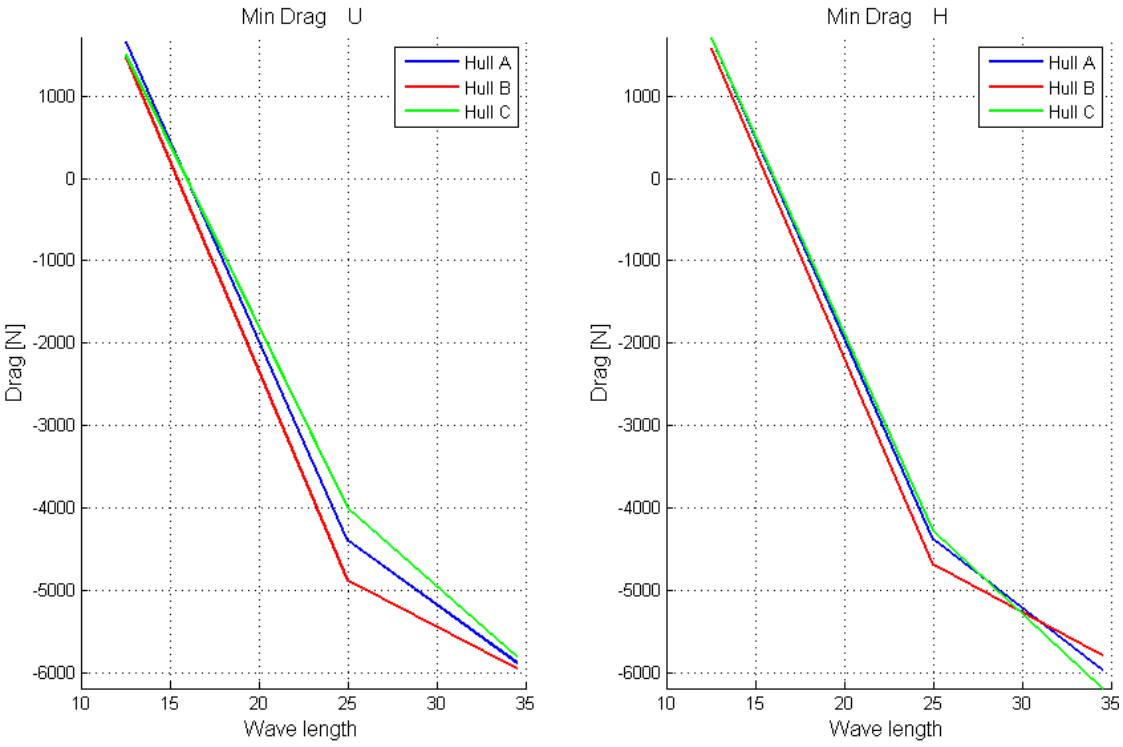

Figure 5-35 Drag minimum values for the three hulls in upright and heeled condition

In *Figure 5-35* the minimum drag values are shown for upright and heeled case. For wave lengths 25m and 34.5m all yachts are having negative drag values which mean that the boats are being pushed forward by the wave. In all but one case, heeled in 34.5m wave length, hull B is having the least resistance and the highest amount of forward push. The difference between hull B and C in the middle wave is close to 1000 N in the upright case.

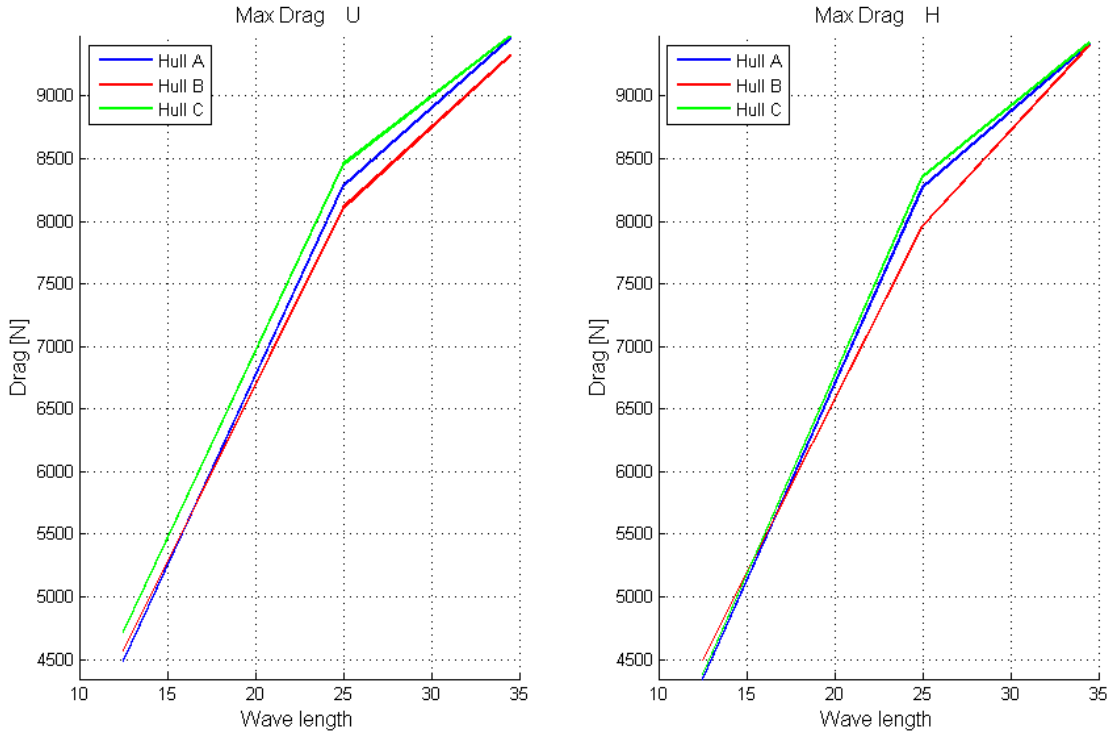

Figure 5-36 Drag maximum values for the three hulls in upright and heeled condition

Figure 5-36 shows that hull C has the highest peak values in resistance for all but one case. The difference in peak resistance is in the range of 500 N for the 25 m long wave. Despite hull B having the lowest peak in resistance and the most forward push it can be seen in *Figure 5-37* that it has the largest average resistance. The average drag follows the progression of bow slenderness in the upright case while in the heeled case all hulls takes the first place in some wave case.

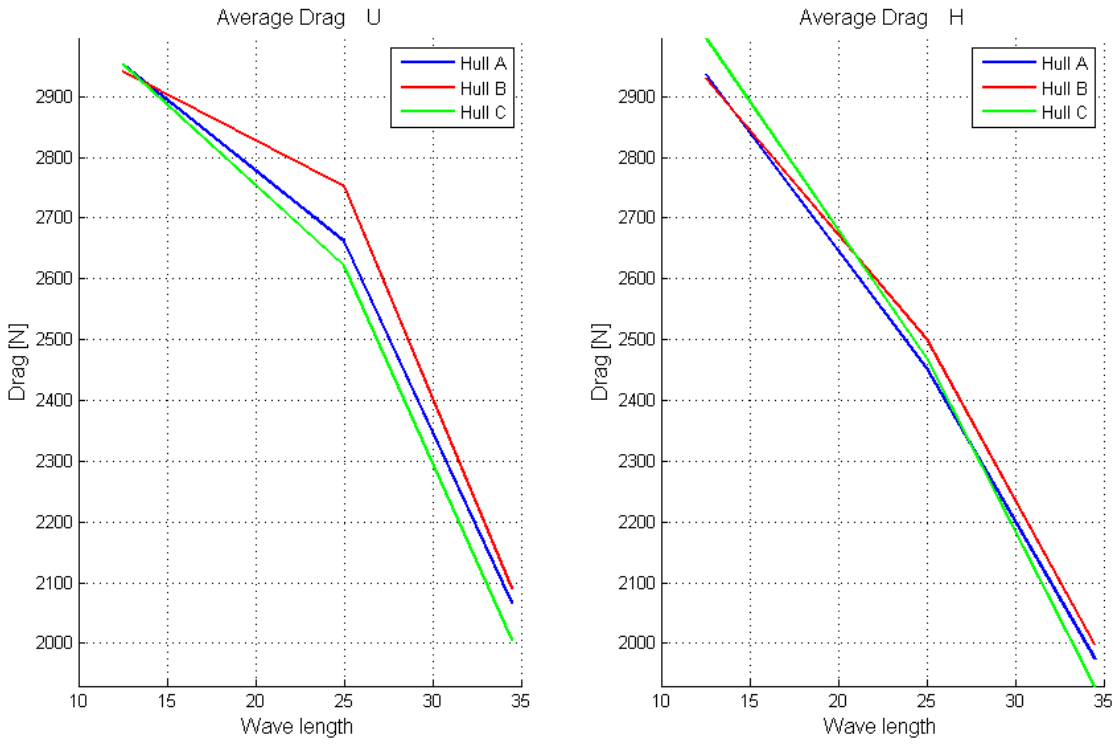

Figure 5-37 Drag average values for the three hulls in upright and heeled condition

The different resistance components, flat water drag, added resistance due to heel and added resistance in waves are shown in as bars in *Figure 5-38*. The added resistance due to heel, in green, is negative for all yachts. The red bars are the added resistance in waves and the blue bars are the flat water resistance. The small difference between the averaged resistances is clear since there is not a very big difference between the bars for each wave case.

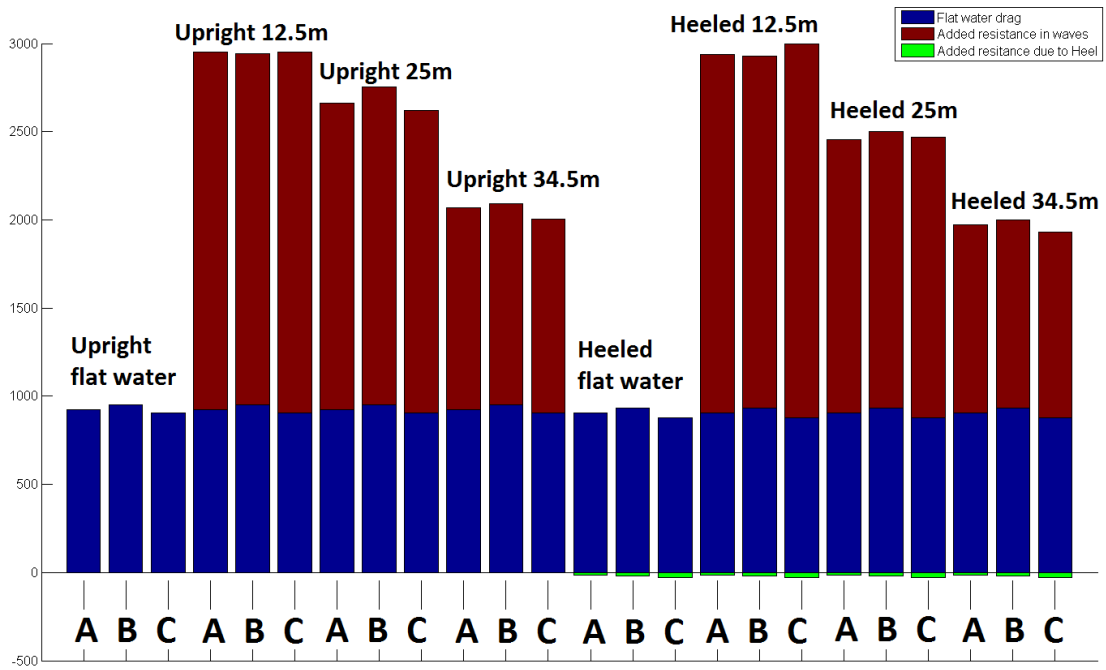

Figure 5-38 Resistance components

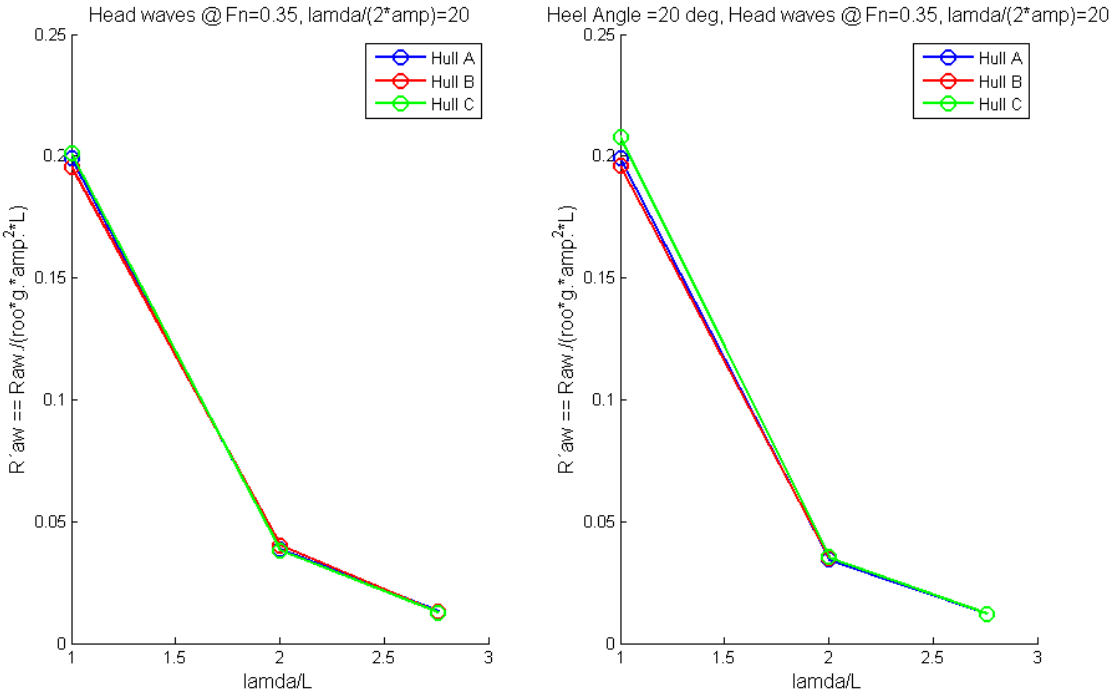

Figure 5-39 Normalized added resistance in waves

The normalized added resistance in wave using *Eq. 5* are shown in *Figure 5-39*. The wave heights used are shown in *Table 4-5*. As can be seen in the figure the added resistance for the different hulls is very similar and the added resistance in waves is also very similar for the upright and the heeled case. The only difference between the hulls can be seen in the shortest wave length where hull C has more added resistance in waves. The added resistance in waves are also significantly smaller for the two longer wave lengths.

6 Discussion

From observing the drag plot in the 12.5m wave case, it is noticeable that the highest peaks in resistance occur when the bow of the yacht meets a wave crest. That is reasonable because the yachts are passing the crest of the wave and the resistance goes up since the wave moves in the opposite direction. The opposite effect is seen when the yacht is travelling down the crest to meet the trough, where the resistance is the smallest. Another important observation, by comparing the pitch plot and the wave plot, is that the yachts are pitching to the bow-up when they meet wave crests and towards the stern for troughs. Moving down the wave the yachts still have a small pitch towards the stern and have so because the inertia and mass of the yachts prevent them from recovering fast enough from the last wave encounter. This behaviour of the yacht and the results are in contrast with the longer wavelengths. When the yacht has a wave crest at the bow, for the 25m and 34.5m wave lengths, pitch towards stern, instead of to bow, exhibits its maximum values but resistance still exhibits its maximum values.

For the 12.5m wave, when the yacht meets a wave trough at the bow, a secondary peak in the resistance curve appears and this occurs when the yacht is pitching to the stern. This happens because the wave crest that has passed the bow has now reached midship and there is now a trough just in front of the bow. The crest now encounters a more blunt geometry in the yacht midship area and for that reason it exhibits a secondary peak with noticeably smaller values in drag than at the first peak. The smallest value appears for hull B, which dives the least into the wave. The least resistance is when the boats have pitch angles close to zero. From the overall results hull C has the largest resistance and it also experiences the largest bow pitch. For this wave length, hull B is the best hull because it has the smallest values for first and second resistance peaks. Its resistance peak has the smallest value when the trough is at the bow but the highest value when the wave trough has reached midship, the secondary resistance trough. The secondary resistance trough occurs when the bow is passing through the wave. Hull B can therefore be named the least beneficial design for punching through waves. Hull B however has the smallest resistance for the largest resistance trough.

For the 25m and 34.5m long waves the resistance of the yachts follows the frequency of crests and troughs of the waves. Increases in resistance are seen when the yachts are going up the wave slope and the wave pushes the boat forward when it is going down the waves. The boats are also pitching in phase with the waves; this is because the encounter frequency is equal or less than the natural pitch frequency of the yachts. Maximum pitch rotations, bow to stern, are almost equal for the two longer wavelengths which, if compared to the wave amplitude, gives larger motions for the wave that matches the natural frequency. When hull B is entering a wave it has less resistance because it does not dive as much into the wave. However it has more resistance when going out of the wave because of the fuller sections far down. This is evident when comparing hulls B and C when they are going out of the wave; this is also seen for the short wavelength.

Hull C has more resistance when diving in to a wave because it travels further into the water but this effect is compensated by the narrow bow that does not slow it down when going out of the wave. The results of hull A are often in between results of the

two extreme hulls as was expected from the intermediate design. From this study it is proven that the effect of returning from a wave encounter with ease is more important than having low resistance while entering a wave.

There is a paradox that both the peak in resistance and peak in forward push do not seem to have any effect on the average resistance. This is true in most cases as hull B has both the minimum resistance peak and the maximum forward push but is still the boat with most average resistance. Instead it is the amount of resistance measured integrated between the maxima and minima values that makes hull C better. This result comes into agreement with one of the thoughts that troubled Yacht designer Gabriel Heyman, which are mentioned in Section 1.1, that a yacht with sharp entry angle may be able to pierce the wave without a high increase in resistance, while a hull with volume in the lower bow will experience an increase in resistance. But, contradictory to this thought, the hull with the lowest peak in resistance is hull B with its chunky low sections.

Furthermore, when calculating the added resistance in waves, the hulls are also showing very similar results and thus hull C is best because it has the least resistance in flat water. This indicates that normal flat water resistance tests might be sufficient to evaluate the characteristics of yachts.

The sharp entry angle of hull C proved to be very efficient in both flat water and most of the wave cases. Hull C is, however, performing worse than the other hulls when water reaches high up the sides of the bow, as for the shortest wave length and the 25 m wave when the yachts are heeled. This indicates that a flared top, with high increase in volume high up, is not effective and that it is the sharp bottom part of the forebody that gives the advantage. The behaviour of hull B supports this theory as it is effective, compared to the others, when water reaches the slim tumble home top. Therefore it is reasonable to suggest that a combination hull of hull B and hull C, with sharp entry and tumble home top, would be the most effective. With no reserve volume, the motions of this hull would however be even more extreme than hull C which is a disadvantage in itself.

How the different forebodies perform in following waves is an interesting topic that is not covered in this thesis. The result in following waves may have been very different since many modern racing mono-hulls are made mainly for downwind sailing and often have a more voluminous bow.

7 Conclusions

The best shape, when running against waves, is a very slim and sharp bow. This shape does however create the biggest peak in resistance and the smallest troughs. Hull B with more volume around the waterline and thus a more blunt entry angle show the smallest peaks in resistance but the biggest resistance overall. The peaks and troughs in resistance do not have a big influence on the average drag because they last only fractions of a second. Instead it is the resistance between the peaks that gives a boat an advantage. The resistance between the peaks follows the trends from flat water resistance where hull C is the best.

A more pointed bow creates more pitch rotation and also more trim in flat water. The shape of the bow does not have a big influence on heave as the heave motions of all yachts are very similar in all waves. The pitch angles affect how large the resistance peaks and trough are as hull C is pitching more and has the largest peaks in resistance. Hull B is pitching the least and has the largest troughs in resistance. If the resistances are averaged over time it is instead hull C, which is pitching the most, that has the least overall resistance. This is however due to the sharp bow and not because of the large pitching angles.

In the simulation of heel without any appendages all hulls have decreased resistance; this is most likely due to the deceased wetted area and not the changes in geometry. In the heeled case the resistances of the boats are even more similar and it is only in the shortest wavelength that hull C gets a distinct disadvantage when being heeled. The changes in pitch from the upright case are visible but cannot be directly coupled to the changes in resistance. Hull C is pitching the most also for the heeled case but a distinction of which hull is the best cannot be made since all boats have the least resistance in one of the tested cases.

More volume at the waterline, as for hull B, is an advantage in short wavelengths. This decreases the pitching movements and prevents the bow from going deep into a wave. For longer wavelengths where the yachts have time to pitch with the waves a shaper pointed bow, as for hull C, is better.

If the speed of the yachts had not been kept constant but rather the propulsion force had been kept constant or made as a function of the surge-motion the result may have been very different since the big peaks in resistance of hull C may make a larger difference. More wavelengths need to be tested, in between 12.5m and 25m, in order to see what other waves that create the secondary resistance peak and trough as seen in the 12.5m wave. As hull C is better in longer wavelengths, and hull B in shorter, another short wavelength might also be in favor of hull B.

Hull A is the best by a small margin in the heeled 25m wavelength case but has in all other cases intermediate values of pitch and resistance. The fact that hull A has intermediate performance values goes well with the fact that it is the intermediate design.

8 References

Davidson, L. (2015). Fluid mechanics, turbulent flow and turbulence modeling. Fluid mechanics, turbulent flow and turbulence modeling.Department of Applied Mechanics, Division of Fluid Dynamics p.182-182.

Keuning J.A, R. O., Damman A (2000). The Influence of the Bowshape on the performance of the Sailing Yacht. Amsterdam, Delft University of Technology.

Eça, L. and M. Hoekstra (2014). "A procedure for the estimation of the numerical uncertainty of CFD calculations based on grid refinement studies." *Journal of Computational Physics*" **262**(0): 104-130.

Keuning J.A,Vermeulen K. J., H.P ten Have. *An Approximation Method for the Added resistance in Waves of a Sailing yacht*. 2nd International Symposium on Design and Production of motor and Sailing Yachts MDY '06,Madrid,Spain,2006

Larsson L., Eliasson R. E., Orych M.(2014). Camden,Maine,Principles of Yacht Design ed.IV., International Marine Publishing.

Larsson, L. R., Hoyte . (2010). Principles of Naval Architecture Series - Ship Resistance and Flow, Society of Naval Architects and Marine Engineers (SNAME).

Lewis, E. V. (1989). Motion in Waves and Controlability. Society of Naval Architects and Marine Engineers (SNAME), NJ.

LLoyd, A. R. J. M. (1998). SEAKEEPING: Ship behaviour in rough weather. 26 Spithead Avenue, Ellis Horwood Limited.

Roache, P. J. (1998). Verification and Validation in Computational Science and Engineering. Albuquerque,New Mexico, USA.

Schlichting, H. (1979) *Boundary-Layer Theory* McGraw Hill, New York, U.S.A

Söderberg, P. (1987). The Swedish Coastal Wave Climate, SSPA.

White F. M. (2015). Fluid Mechanics, 7th Ed., McGraw-Hill.

Larsson L.,Zou Lu, (2014). *CFD Verification and Validation in Practice - A Study Based on Resistance Submissions to the Gothenburg 2010 Workshop on Numerical Ship Hydrodynamics*. 30th Symposium on Naval Hydrodynamics. Hobart,Tasmania, Australia**.**

9 Appendix A

Table 9-1 Summary of values with heeled in parenthesis

Yacht	A	B	C
Wavelength	**12.5 m**		
Max resistance [kN]	4.4890, (4.3425)	4.5688, (4.4905)	4.7188, (4.3748)
Min resistance [kN]	1.6506, (1.6994)	1.4676, (1.5757)	1.5014, (1.7115)
Average resistance [kN]	2.9517, (2.9356)	2.9427, (2.9289)	2.9528, (2.9964)
Total Pitch [deg]	4.2931, (4.8344)	4.1586, (4.6132)	4.6483, (5.0145)
Total Heave [m]	0.2146, (0.2072)	0.2093, (0.1980)	0.2417, (0.2175)
Wavelength	**25 m**		
Max resistance [kN]	8.2855, (8.2735)	8.1089, (7.9614)	8.4555, (8.3589)
Min resistance [kN]	-4.3962, (-4.3809)	-4.8783, (-4.6869)	-3.9996, (-4.2740)
Average resistance [kN]	2.6614, (2.4532)	2.7526, (2.5012)	2.6209, (2.4691)
Total Pitch [deg]	15.8841, (15.8908)	15.7275, (15.8657)	16.2374, (15.9807)
Total Heave [m]	1.2348, (1.1707)	1.2546, (1.1972)	1.2439, (1.1894)
Wavelength	**34.5 m**		
Max resistance [kN]	9.4579, (9.4182)	9.3227, (9.4041)	9.4829, (9.4245)
Min resistance [kN]	-5.8679, (-5.9563)	-5.9371, (-5.7767)	-5.7969, (-6.1811)
Average resistance [kN]	2.0665, (1.9743)	2.0908, (1.9982)	2.0061, (1.9300)
Total Pitch [deg]	16.0036, (15.9968)	15.9001, (15.9505)	16.2249, (16.0800)
Total Heave [m]	1.6727, (1.6392)	1.6737, (1.6445)	1.6738, (1.6577)

10 APPENDIX B - Upright condition pictures

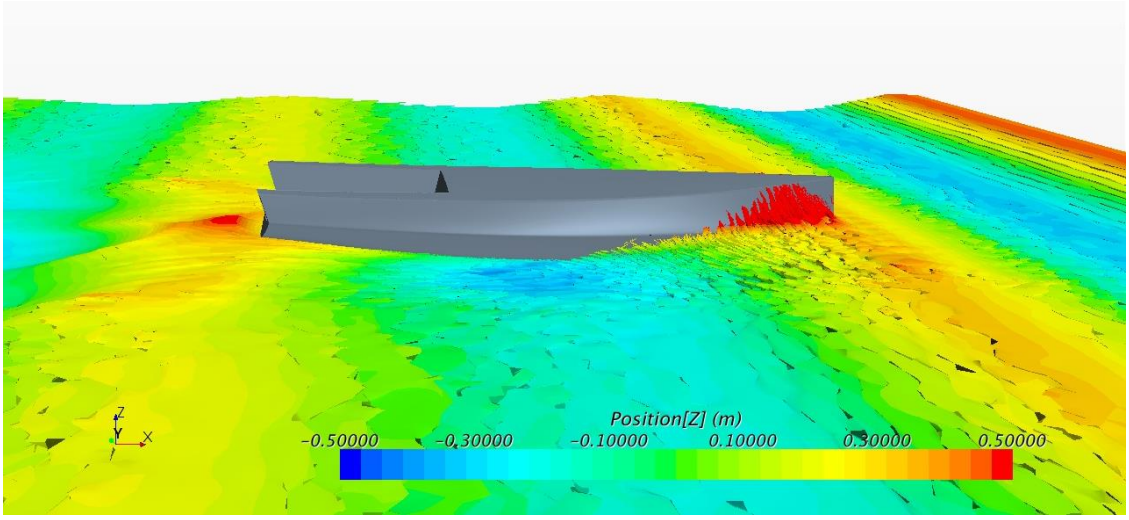

Figure 10-1 Hull A peak resistance in 12.5 m wave, upright, at 8.5s

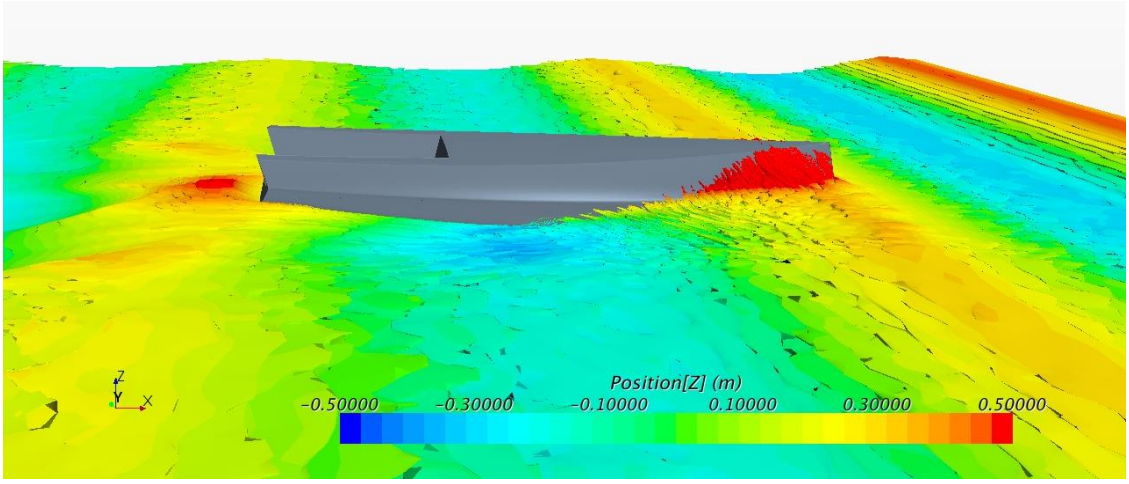

Figure 10-2 Hull B peak resistance in 12.5 m wave, upright, at 8.5s

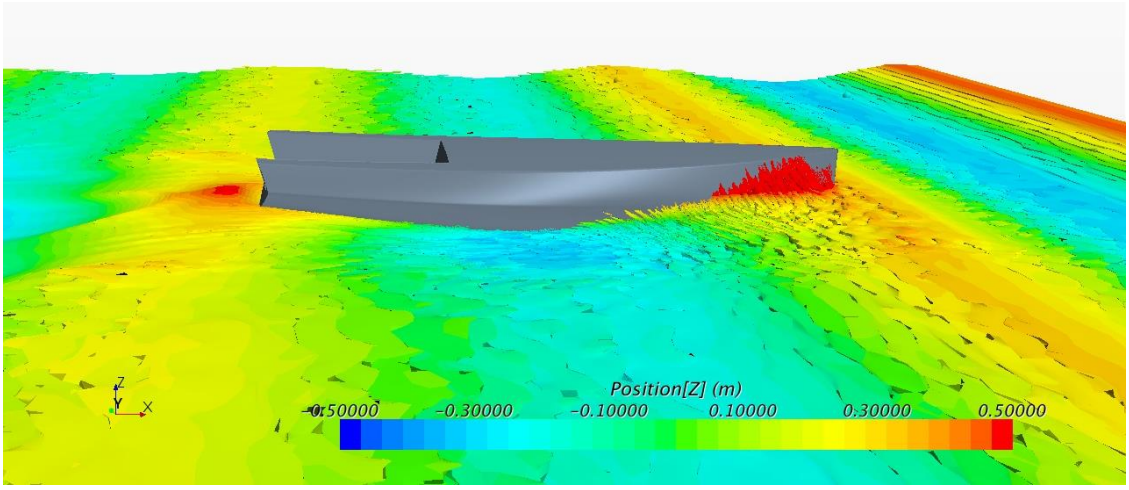

Figure 10-3 Hull C peak resistance in 12.5 m wave, upright, at 8.5s

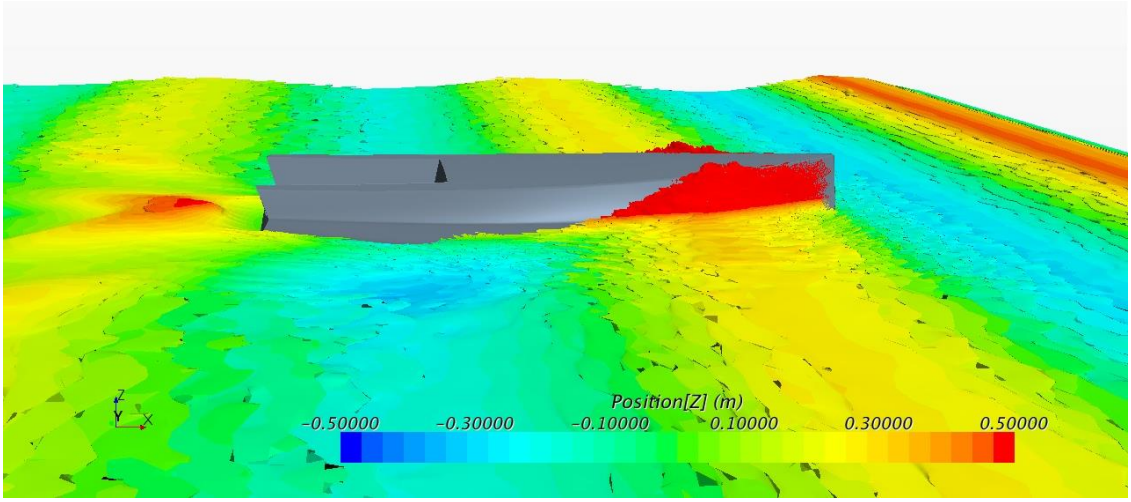

Figure 10-4 Hull A secondary resistance trough in 12.5 m wave, upright, at 8.9s

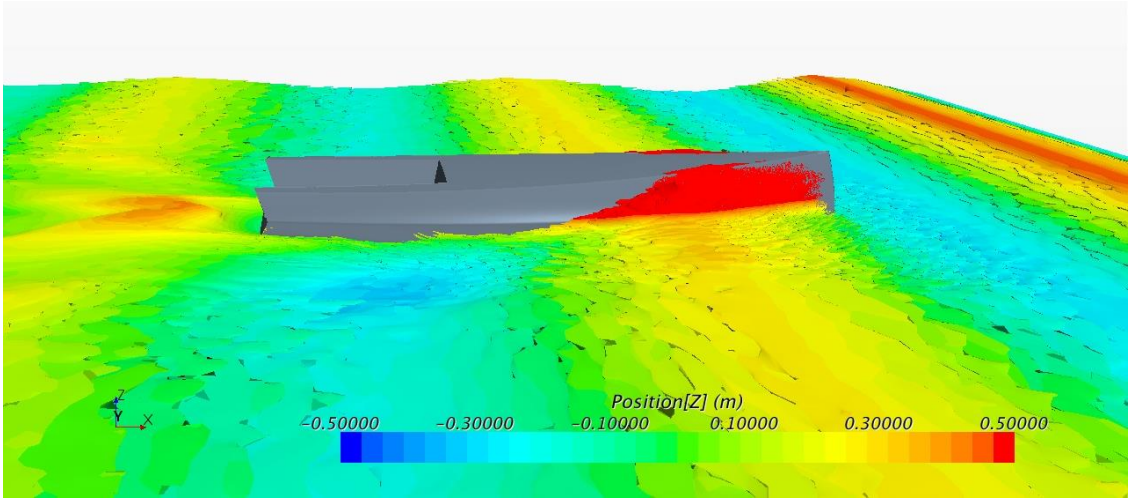

Figure 10-5 Hull B secondary resistance trough in 12.5 m wave, upright, at 8.9s

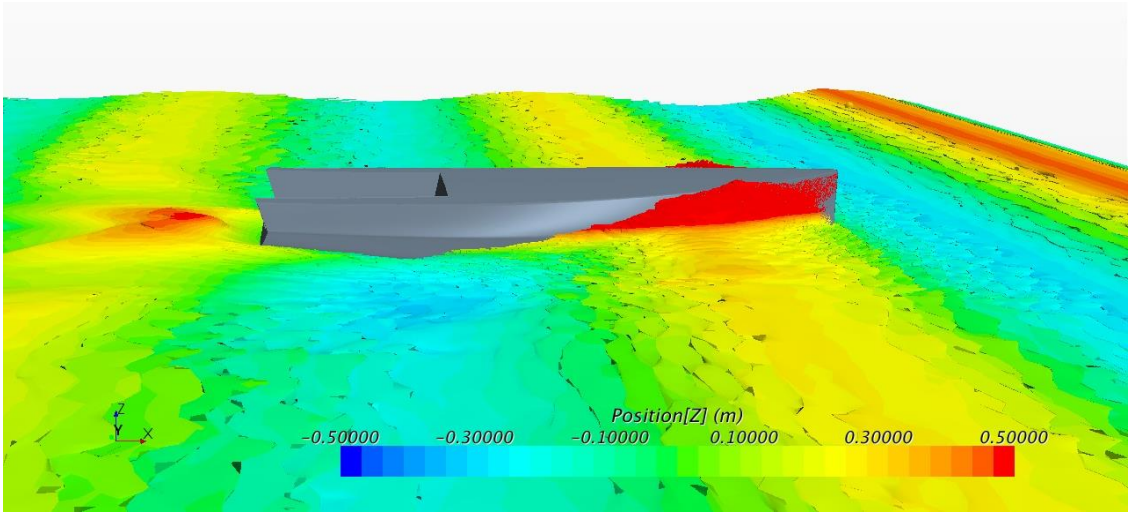

Figure 10-6 Hull C secondary resistance trough in 12.5 m wave, upright, at 8.9s

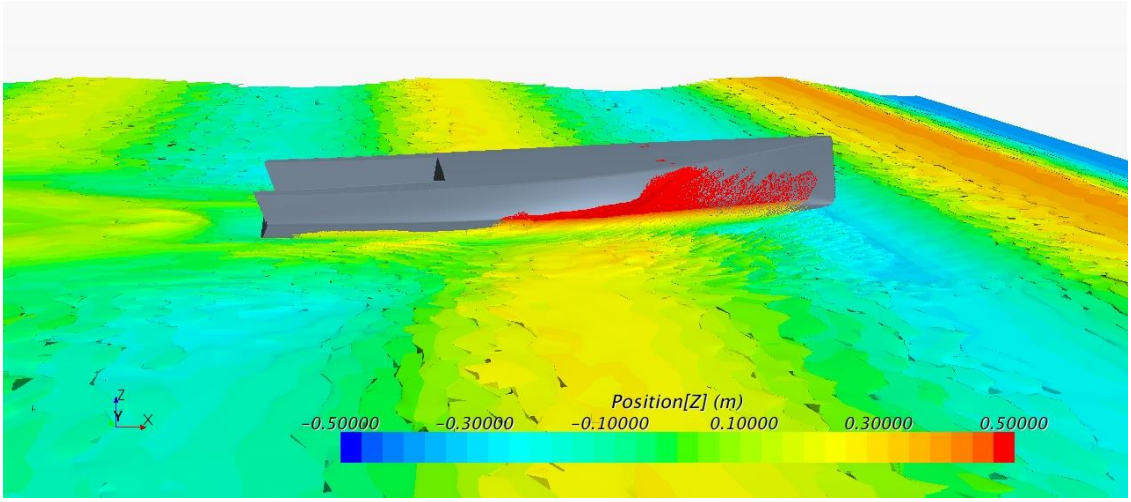

Figure 10-7 Hull A secondary resistance peak in 12.5 m wave, upright, at 9.2s

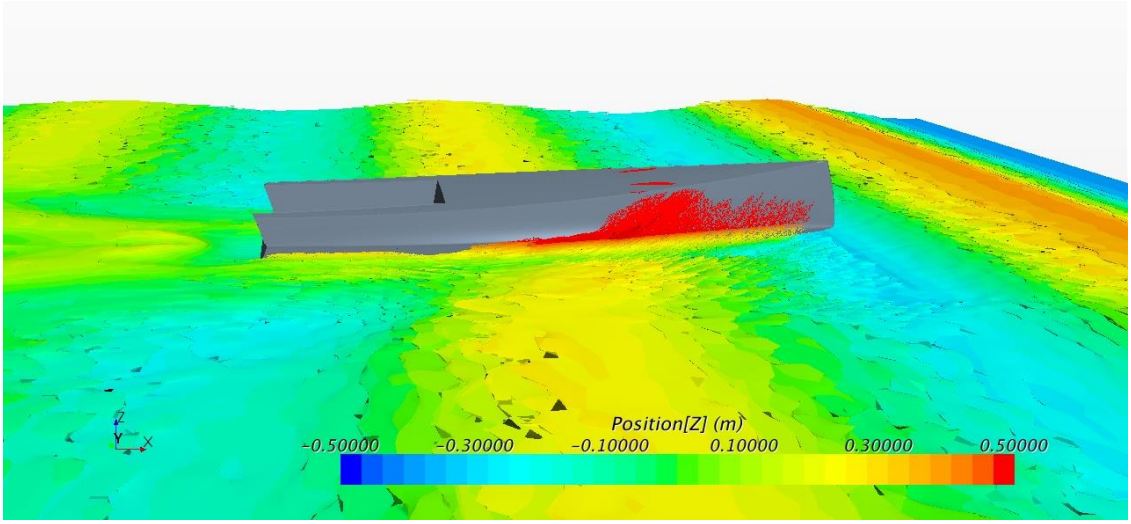

Figure 10-8 Hull B secondary resistance peak in 12.5 m wave, upright, at 9.2s

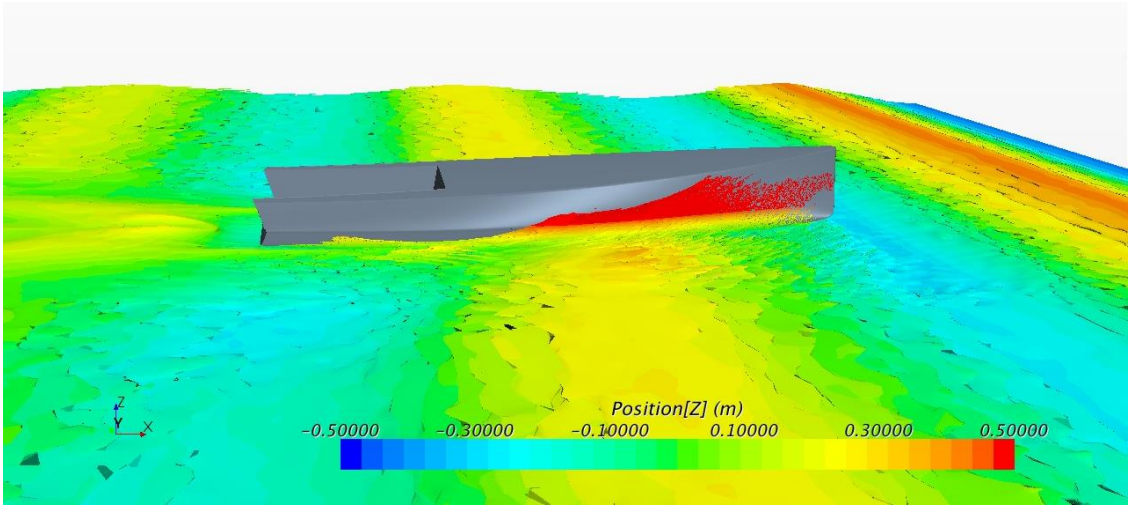

Figure 10-9 Hull C secondary resistance peak in 12.5 m wave, upright, at 9.2s

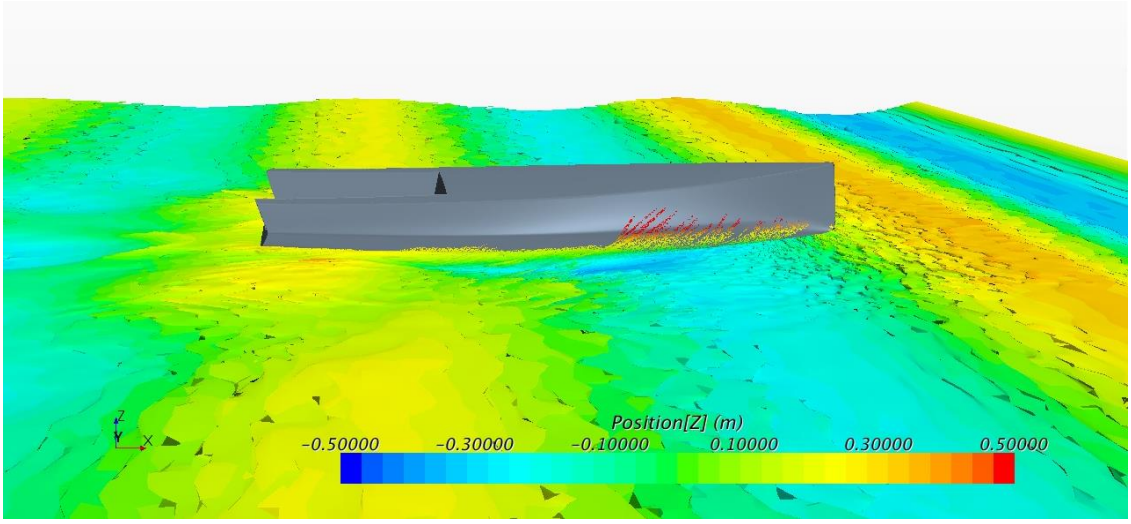

Figure 10-10 Hull A minimum resistance in 12.5 m wave, upright, at 9.7s

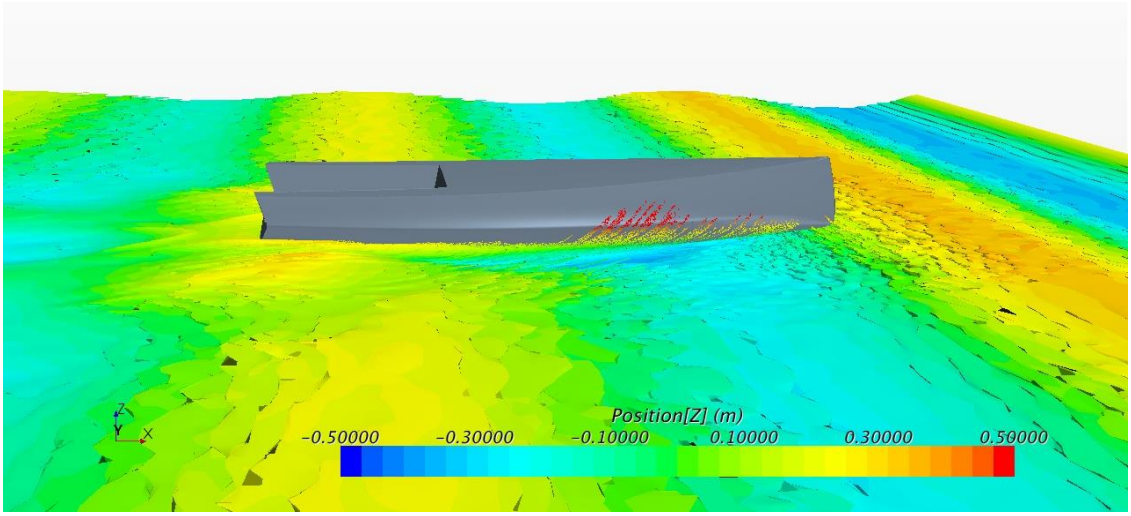

Figure 10-11 Hull B minimum resistance in 12.5 m wave, upright, at 9.7s

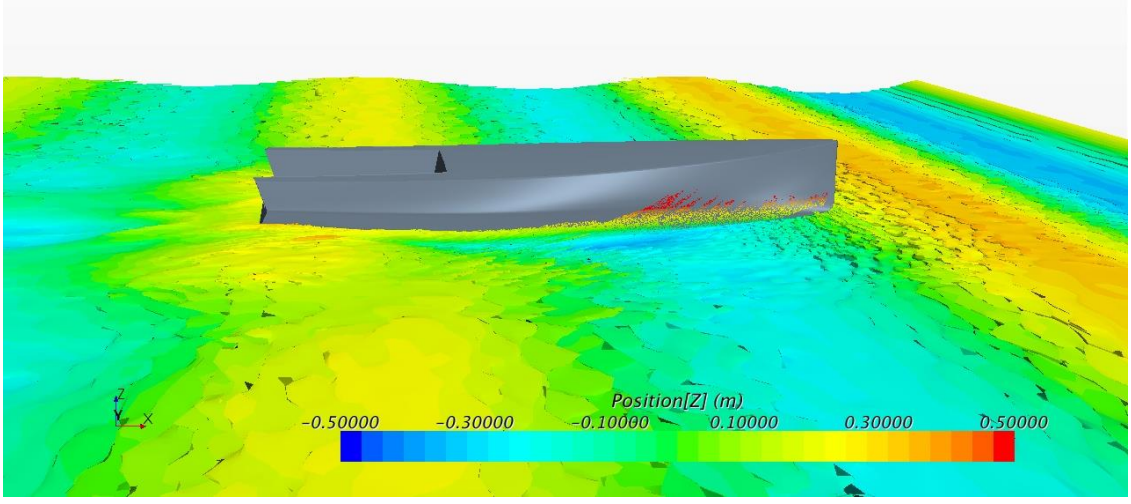

Figure 10-12 Hull C minimum resistance in 12.5 m wave, upright, at 9.7s

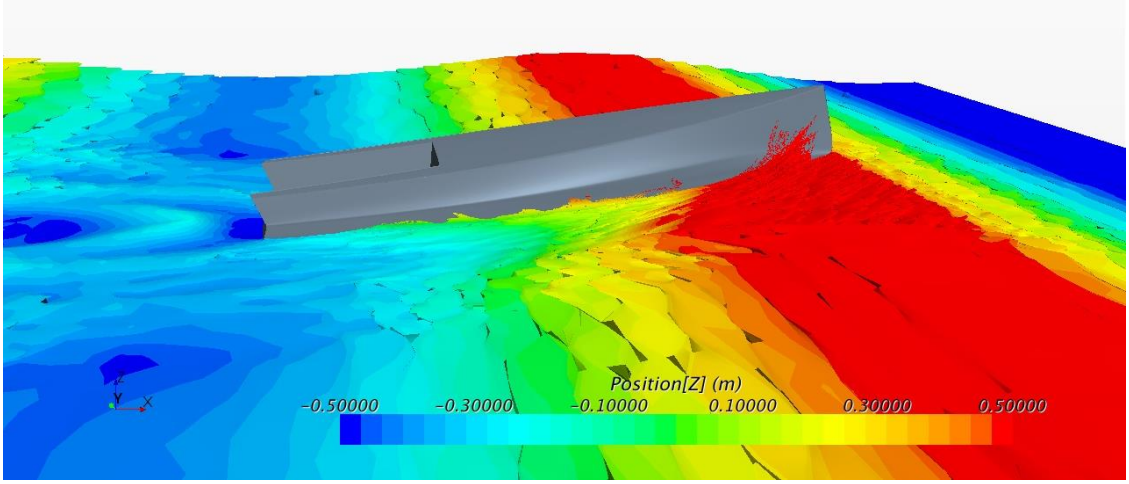

Figure 10-13 Hull A peak resistance in 25m wave, upright, at 9s

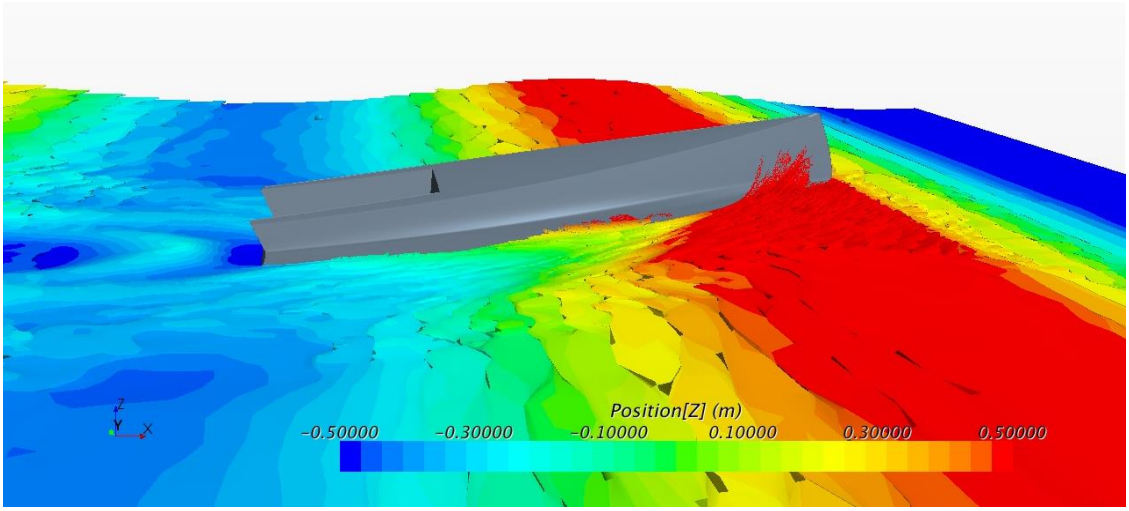

Figure 10-14 Hull B peak resistance in 25m wave, upright, at 9s

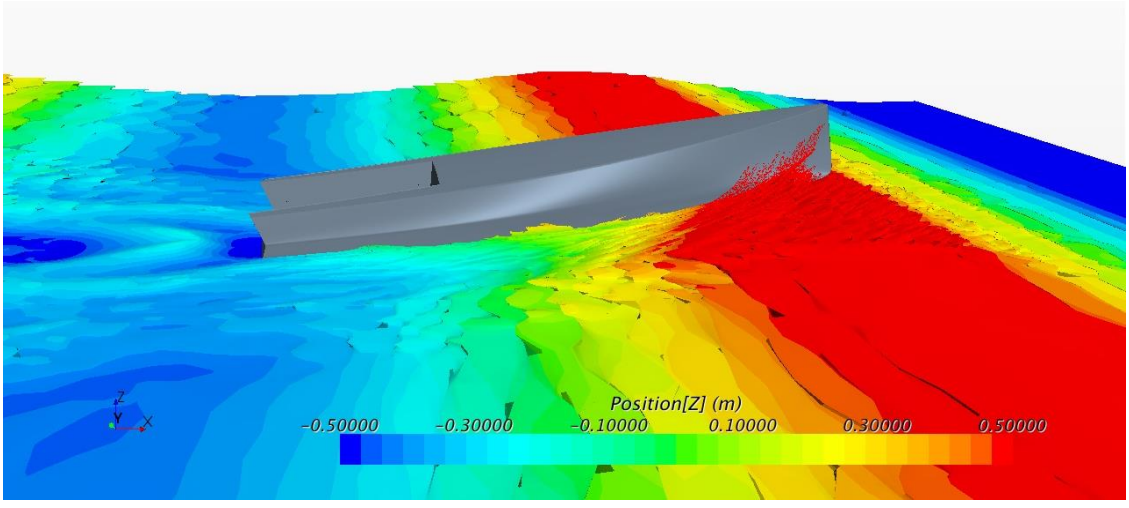

Figure 10-15 Hull C peak resistance in 25m wave, upright, at 9s

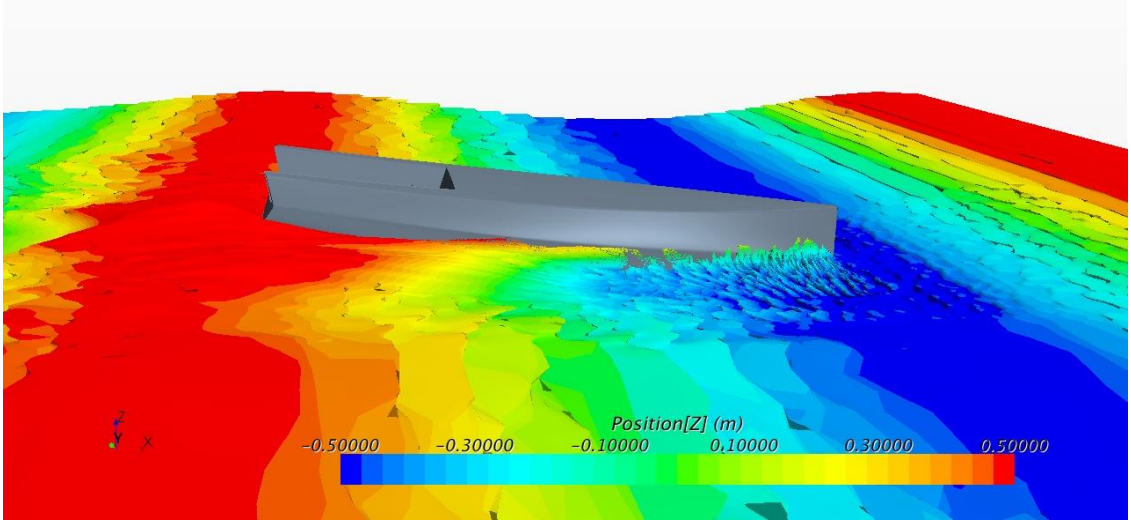

Figure 10-16 Hull A minimum resistance in 25m wave, upright, at 10.2s

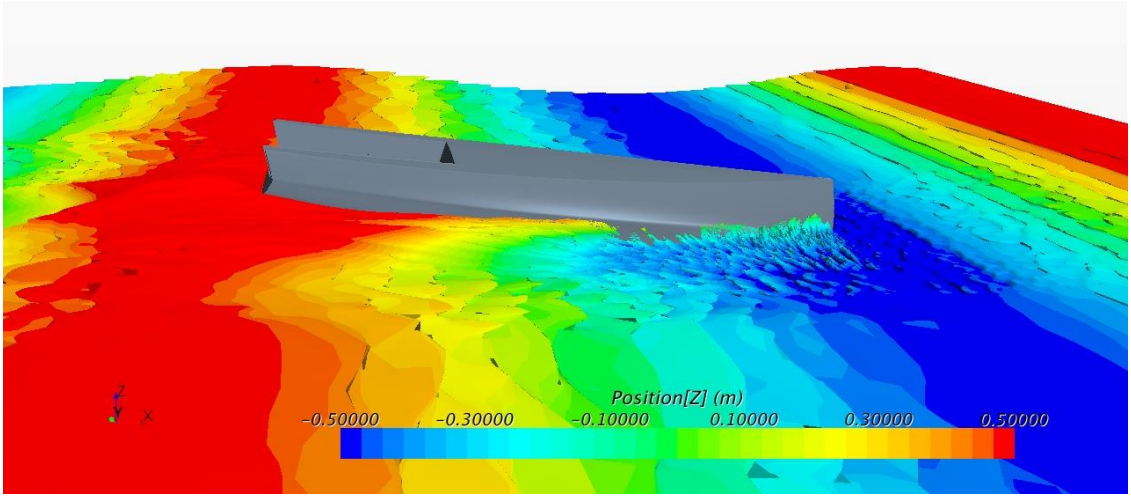

Figure 10-17 Hull B minimum resistance in 25m wave, upright, at 10.2s

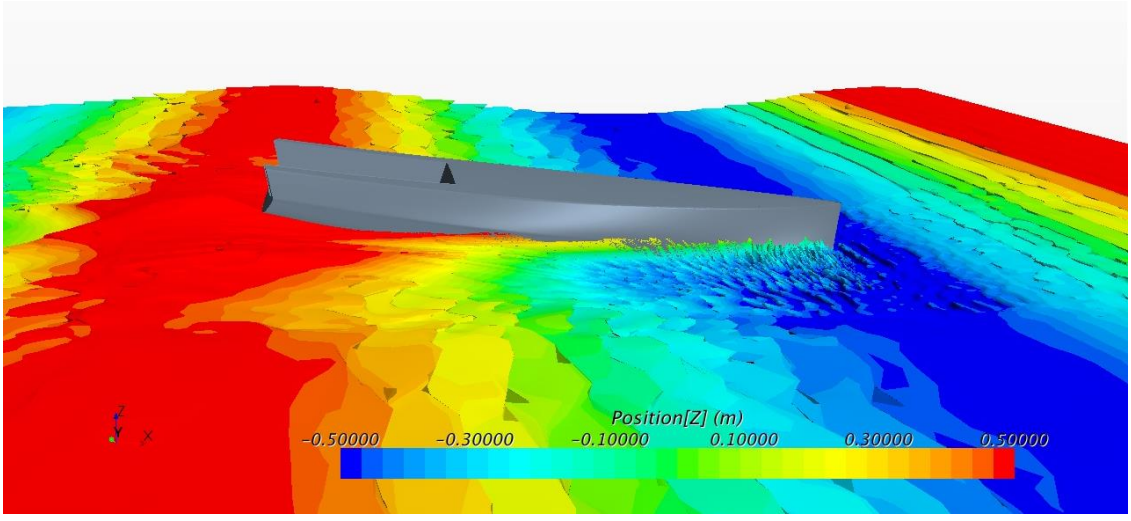

Figure 10-18 Hull C minimum resistance in 25m wave, upright, at 10.2s

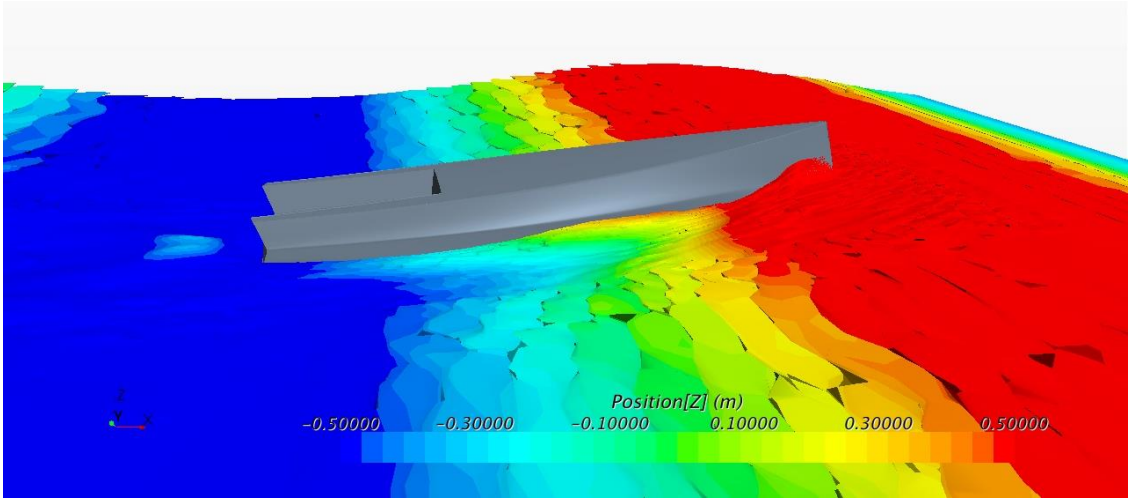

Figure 10-19 Hull A peak resistance in 34.5m wave, upright, at 9.9s

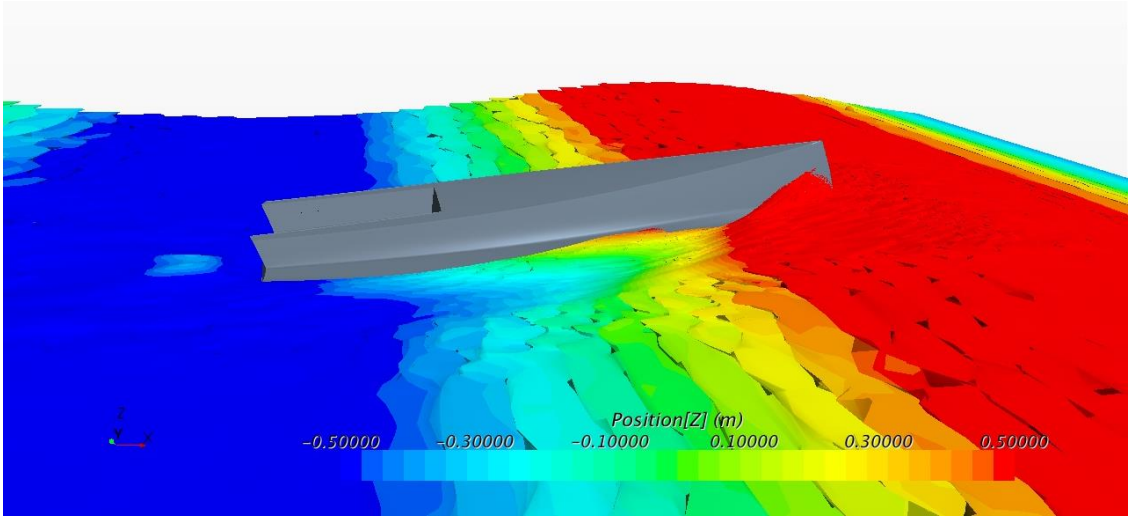

Figure 10-20 Hull B peak resistance in 34.5m wave, upright, at 9.9s

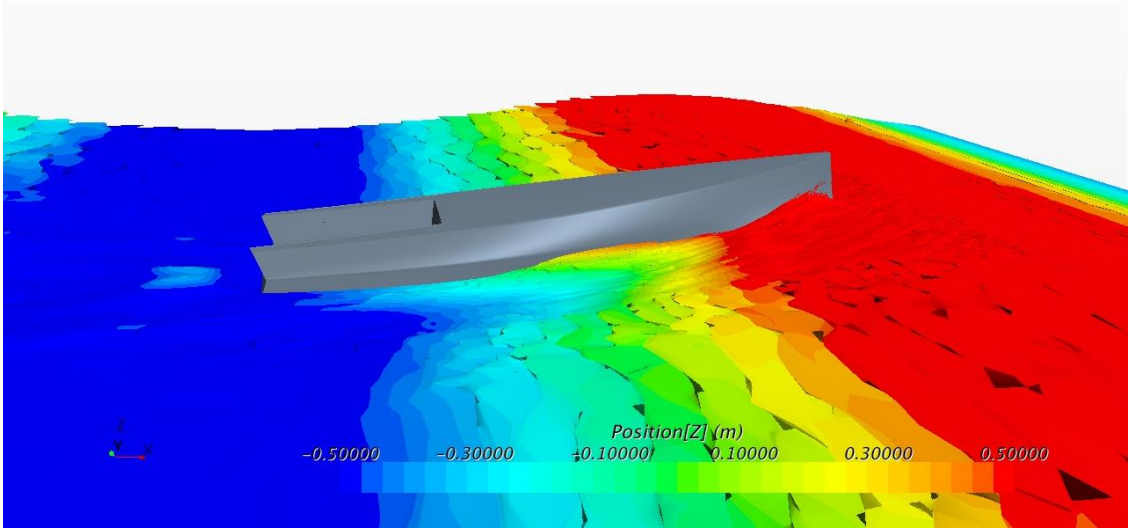

Figure 10-21 Hull C peak resistance in 34.5m wave, upright, at 9.9s

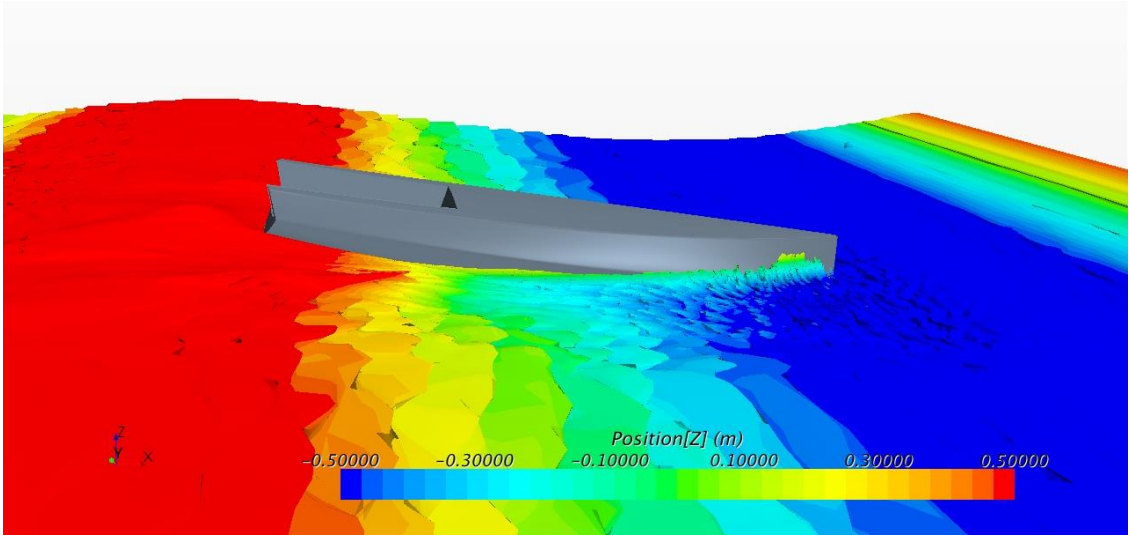

Figure 10-22 Hull A minimum resistance in 34.5m wave, upright, at 11.5s

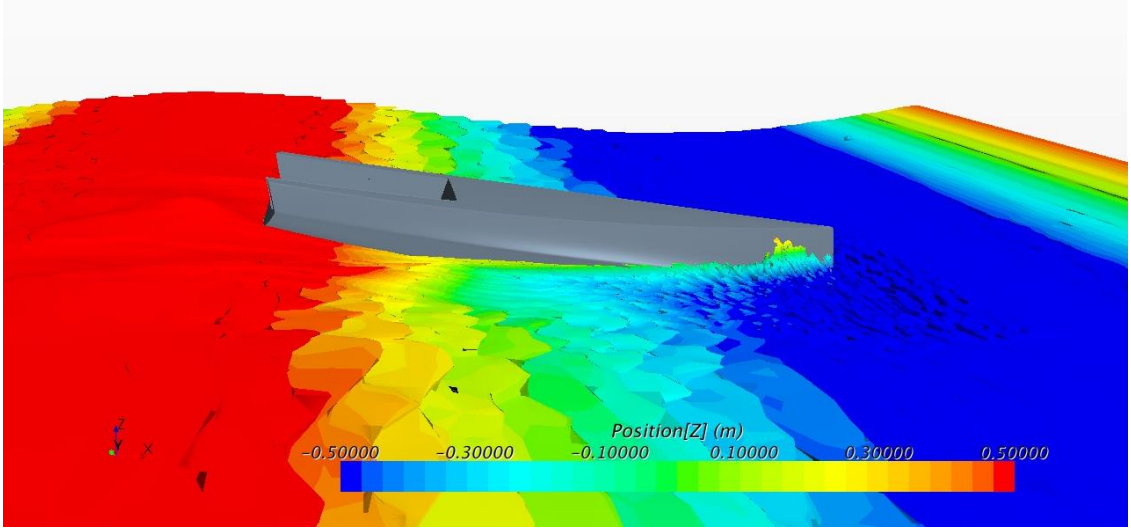

Figure 10-23 Hull B minimum resistance in 34.5m wave, upright, at 11.5s

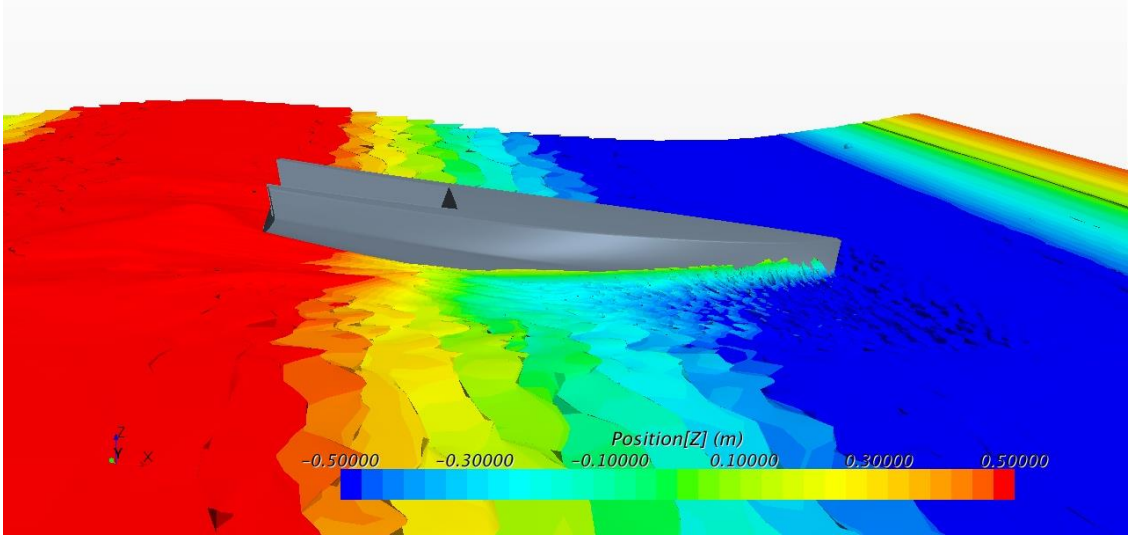

Figure 10-24 Hull C minimum resistance in 34.5m wave, upright, at 11.5s

11 APPENDIX C - Heeled condition pictures

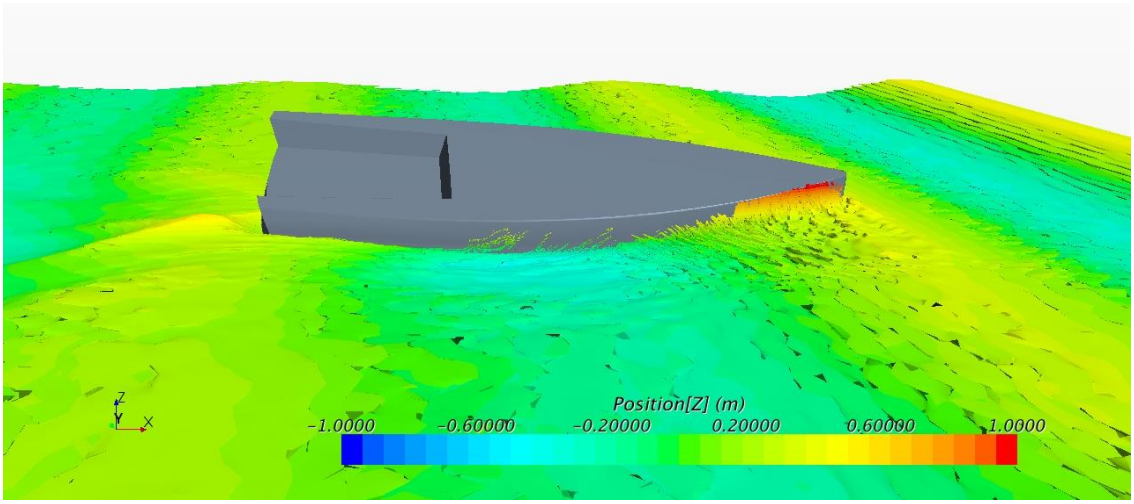

Figure 11-1 Hull A peak resistance in 12.5 m wave, heeled, at 8.5s

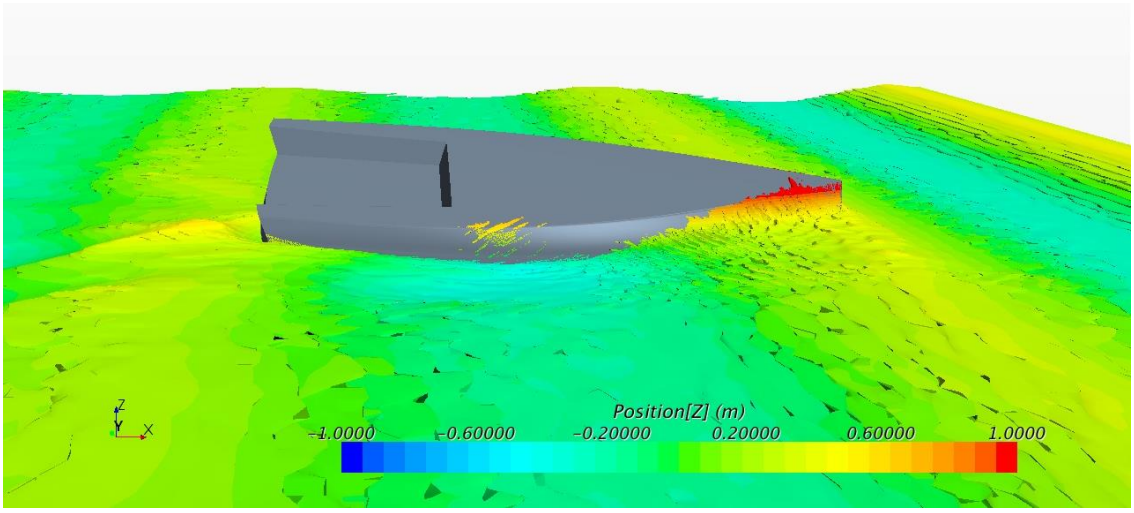

Figure 11-2 Hull B peak resistance in 12.5 m wave, heeled, at 8.5s

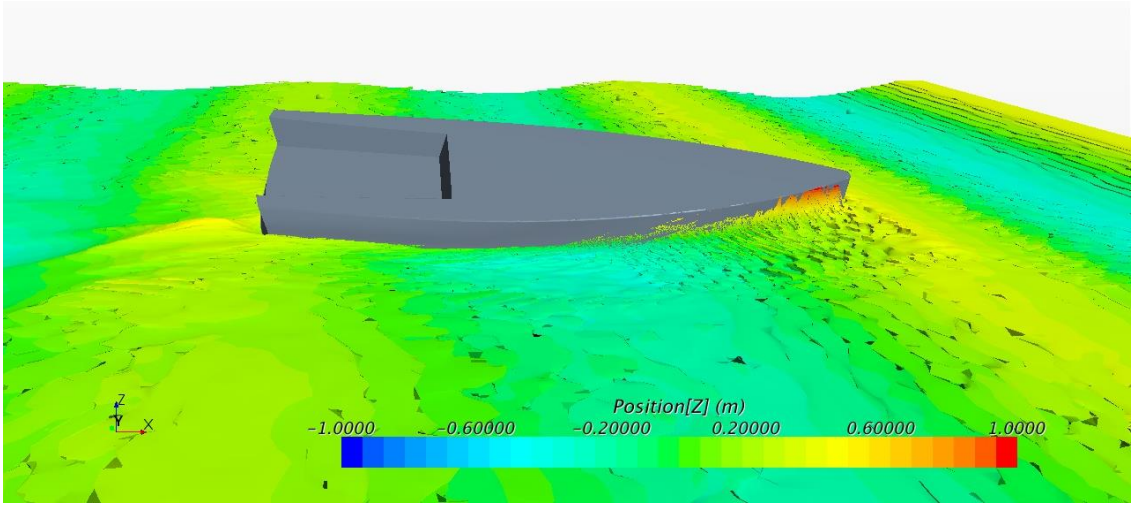

Figure 11-3 Hull C peak resistance in 12.5 m wave, heeled, at 8.5s

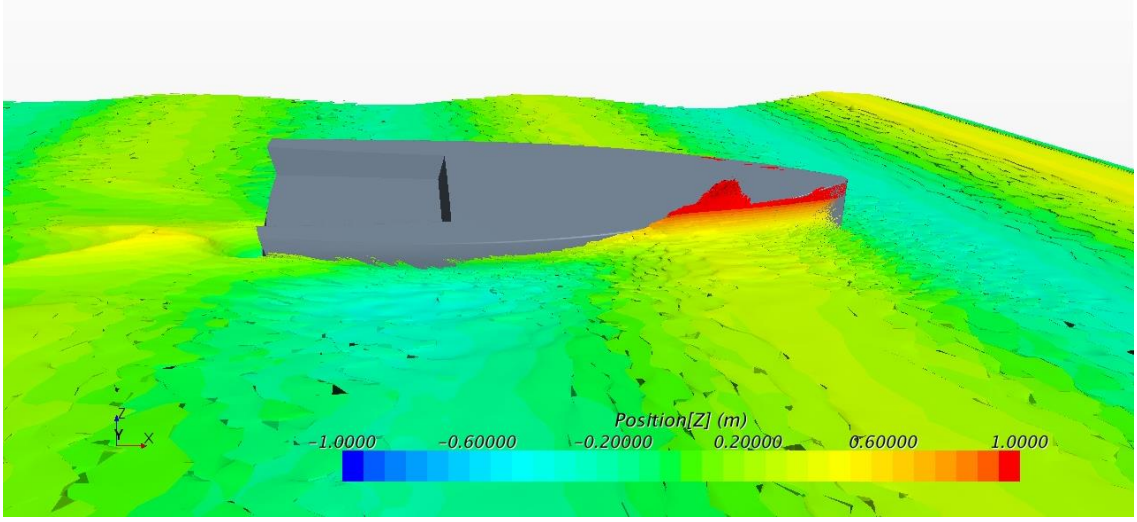

Figure 11-4 Hull A secondary resistance trough in 12.5 m wave, heeled, at 7.4s

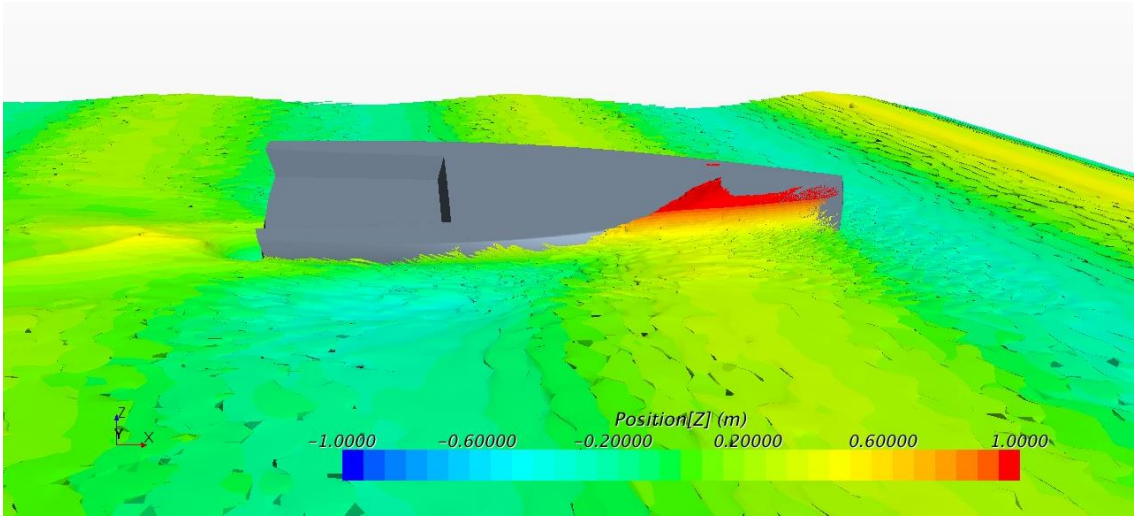

Figure 11-5 Hull B secondary resistance trough in 12.5 m wave, heeled, at 7.4s

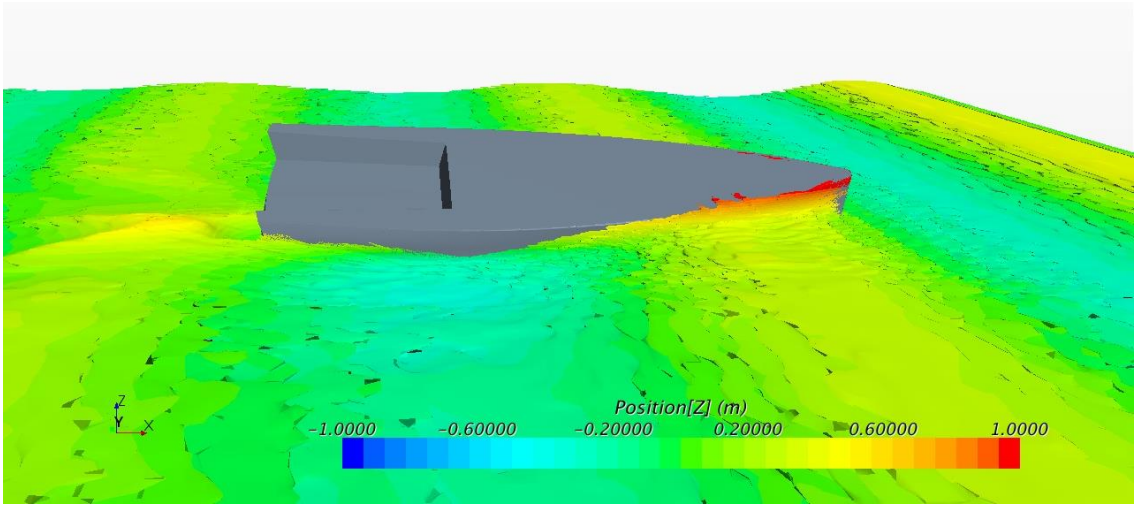

Figure 11-6 Hull C secondary resistance trough in 12.5 m wave, heeled, at 7.4s

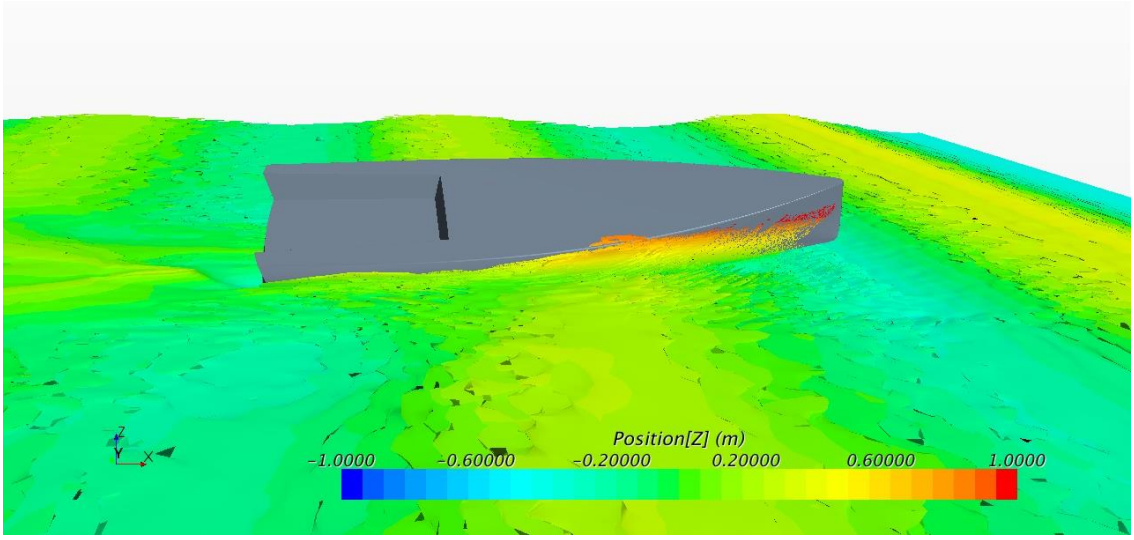

Figure 11-7 Hull A secondary resistance peak in 12.5 m wave, heeled, 7.7s

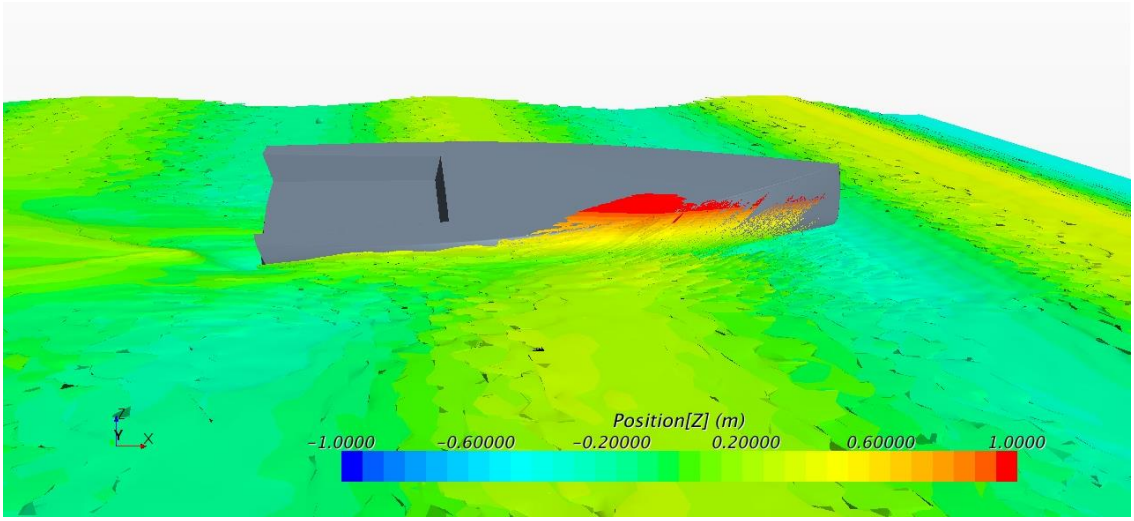

Figure 11-8 Hull B secondary resistance peak in 12.5 m wave, heeled, 7.7s

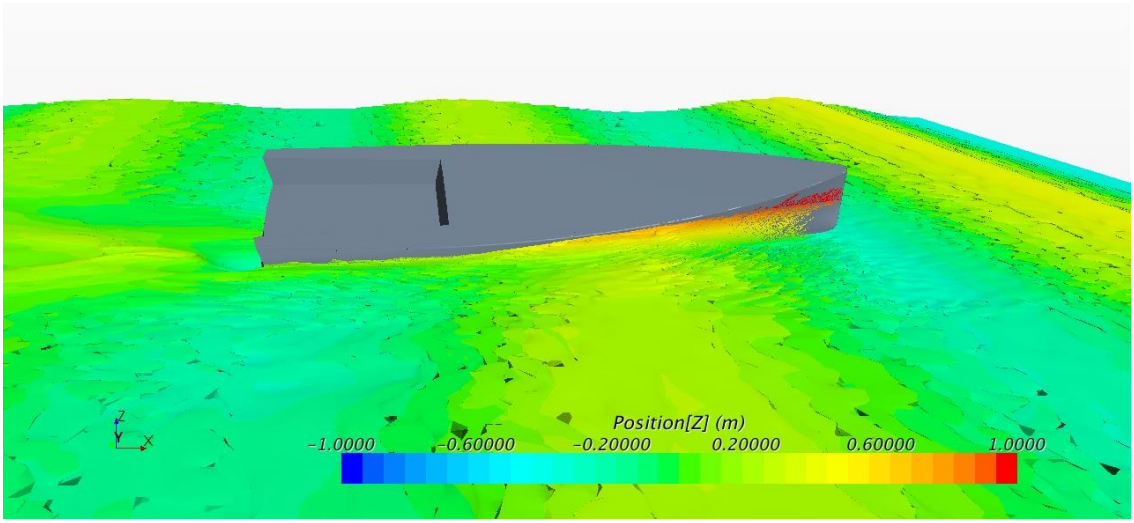

Figure 11-9 Hull C secondary resistance peak in 12.5 m wave, heeled, 7.7s

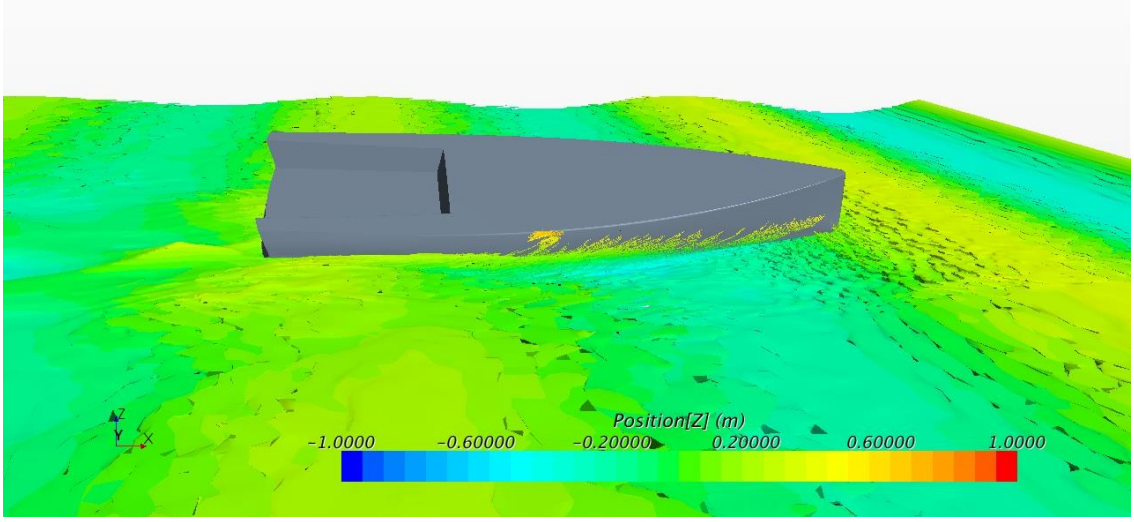

Figure 11-10 Hull A minimum resistance in 12.5 m wave, heeled, at 8.1s

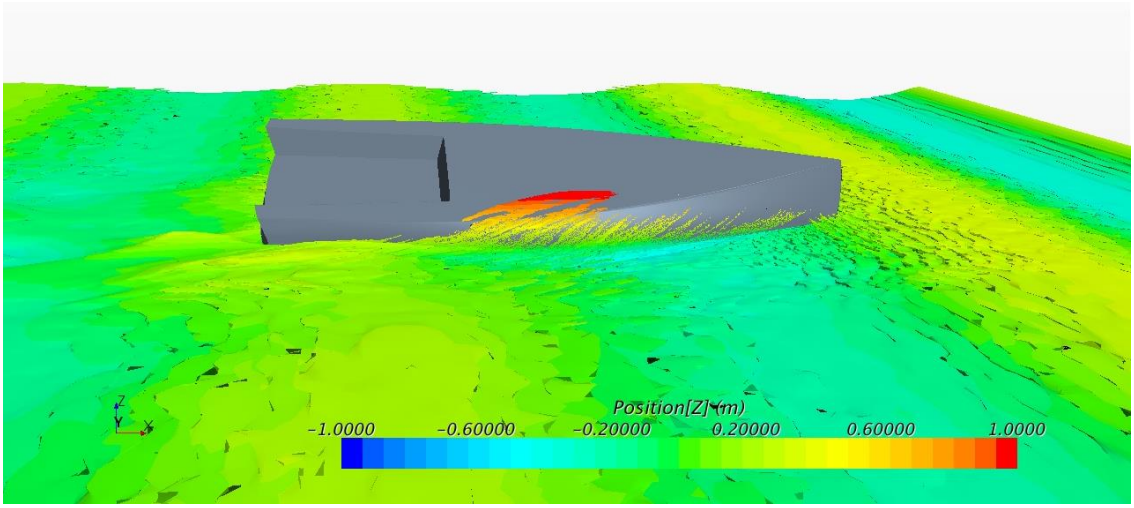

Figure 11-11 Hull B minimum resistance in 12.5 m wave, heeled, at 8.1s

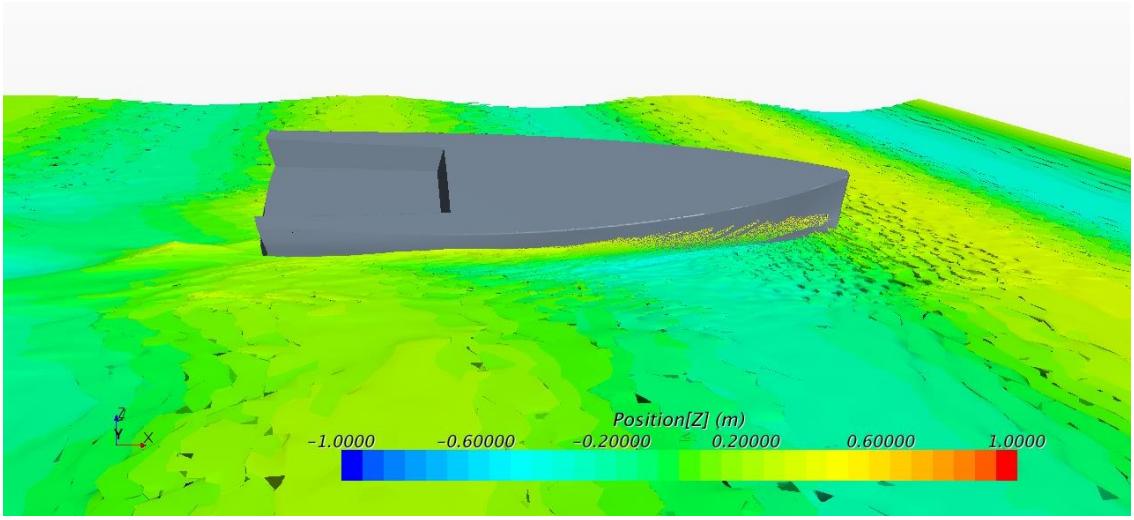

Figure 11-12 Hull C minimum resistance in 12.5 m wave, heeled, at 8.1s

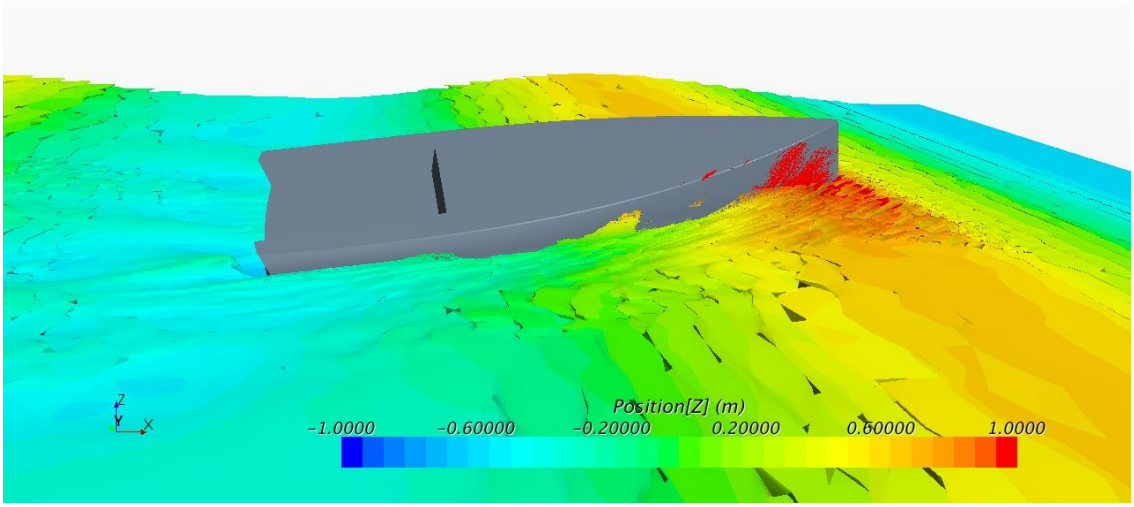

Figure 11-13 Hull A peak resistance in 25m wave, heeled, at 9s

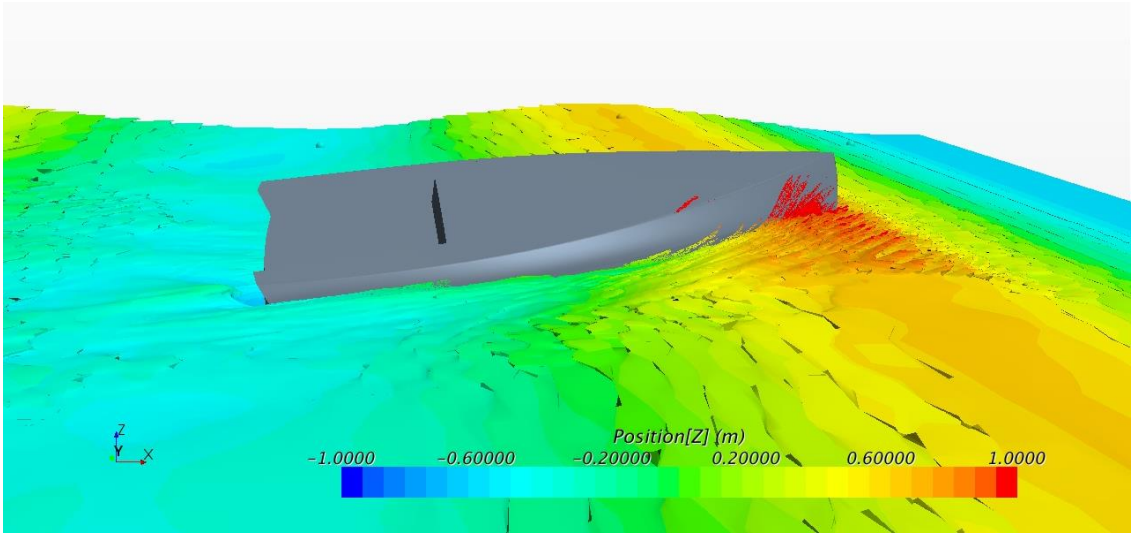

Figure 11-14 Hull B peak resistance in 25m wave, heeled, at 9s

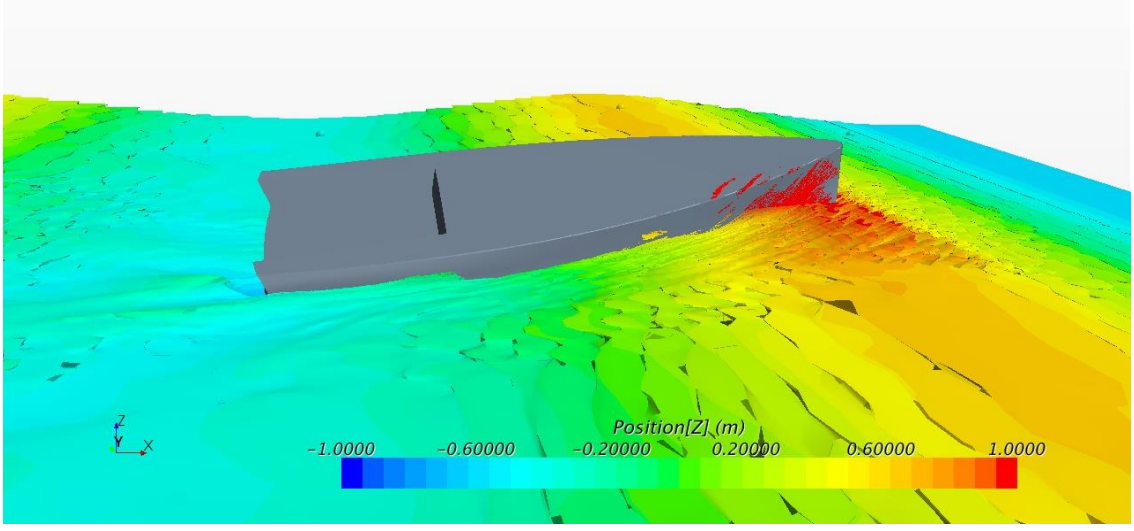

Figure 11-15 Hull C peak resistance in 25m wave, heeled, at 9s

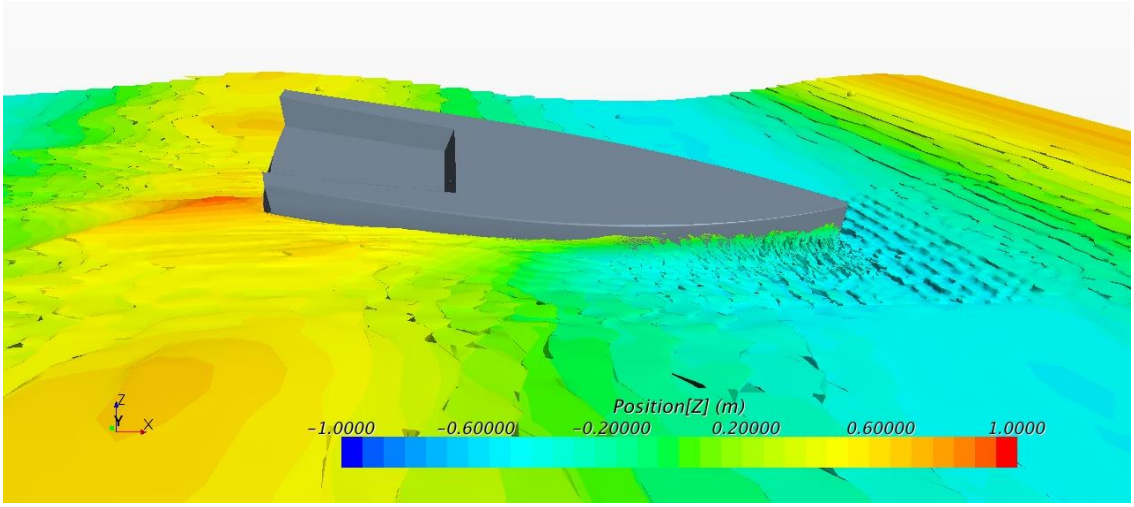

Figure 11-16 Hull A minimum resistance in 25m wave, heeled, at 10.2s

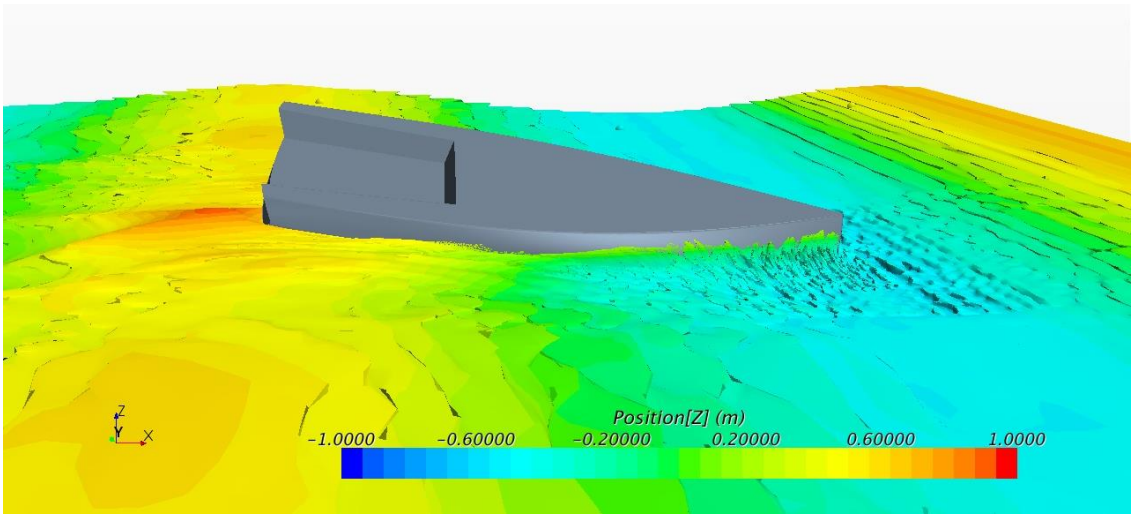

Figure 11-17 Hull B minimum resistance in 25m wave, heeled, at 10.2s

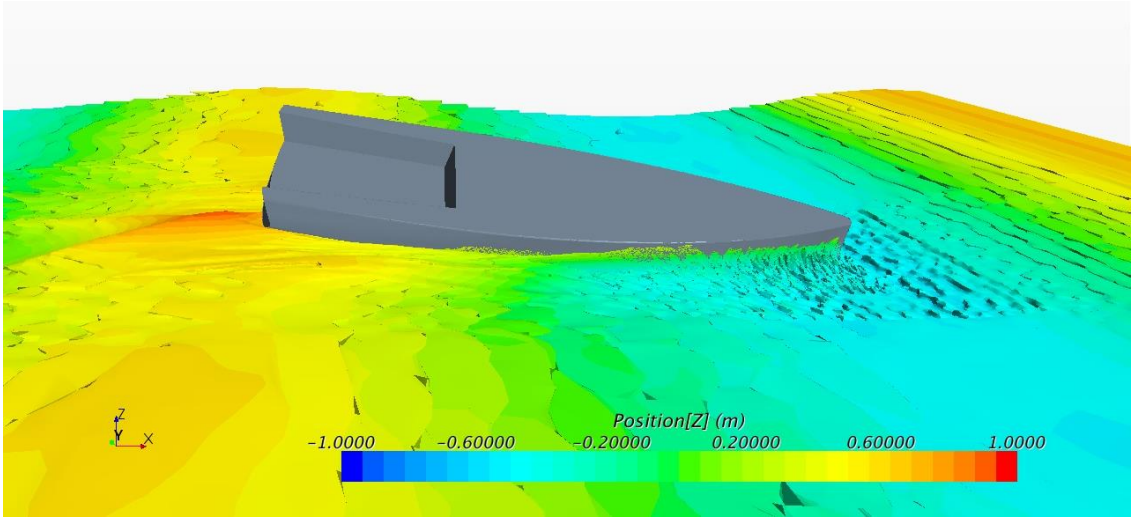

Figure 11-18 Hull C minimum resistance in 25m wave, heeled, at 10.2s

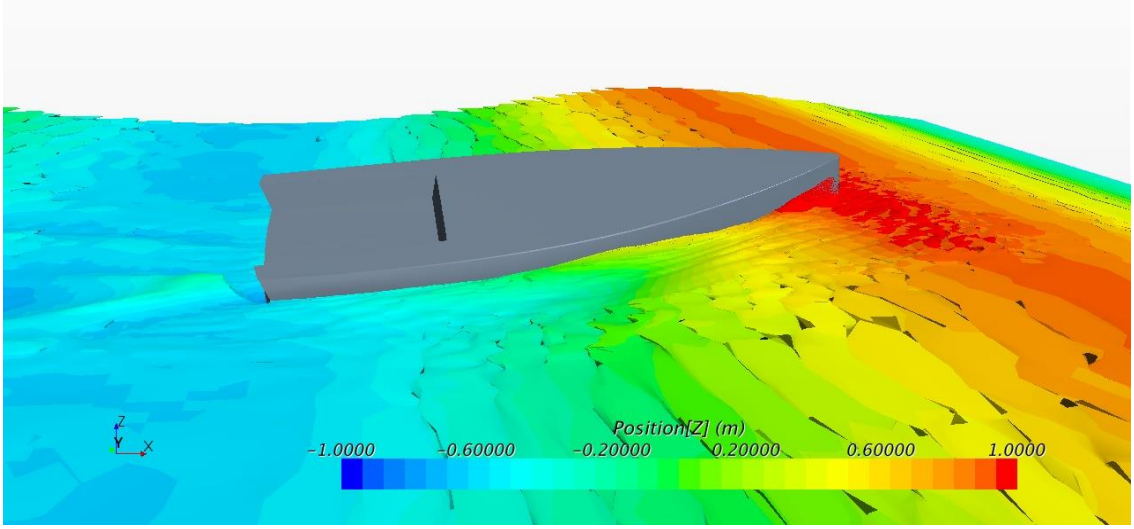

Figure 11-19 Hull A peak resistance in 34.5m wave, heeled, at 9.9s

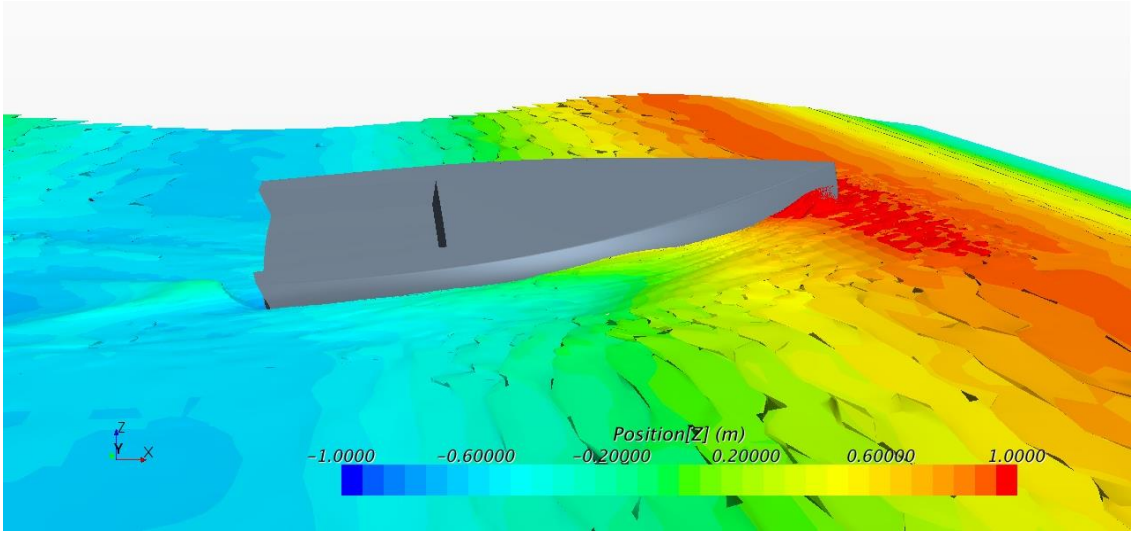

Figure 11-20 Hull B peak resistance in 34.5m wave, heeled, at 9.9s

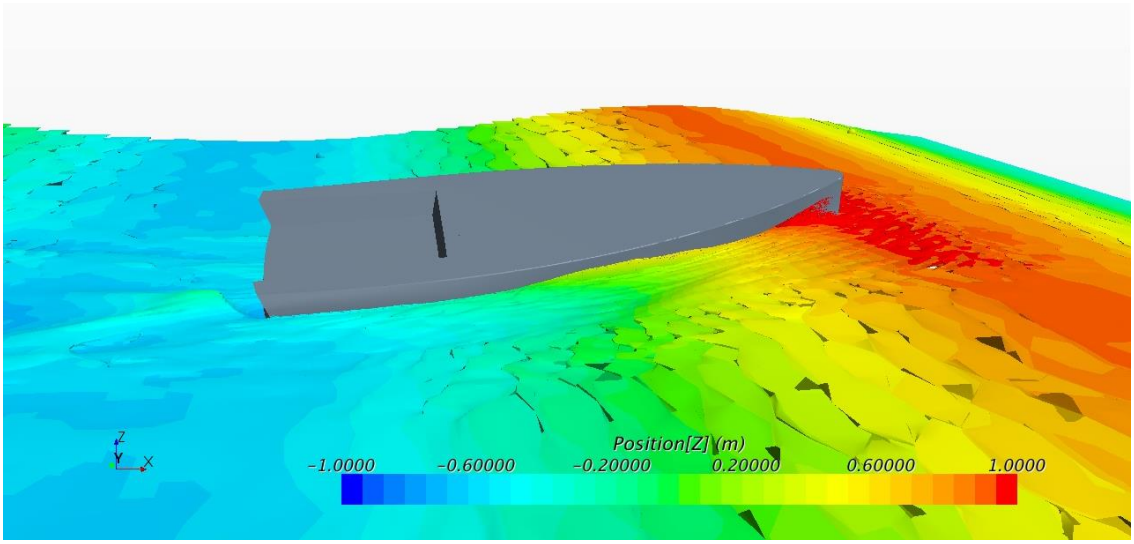

Figure 11-21 Hull C peak resistance in 34.5m wave, heeled, at 9.9s

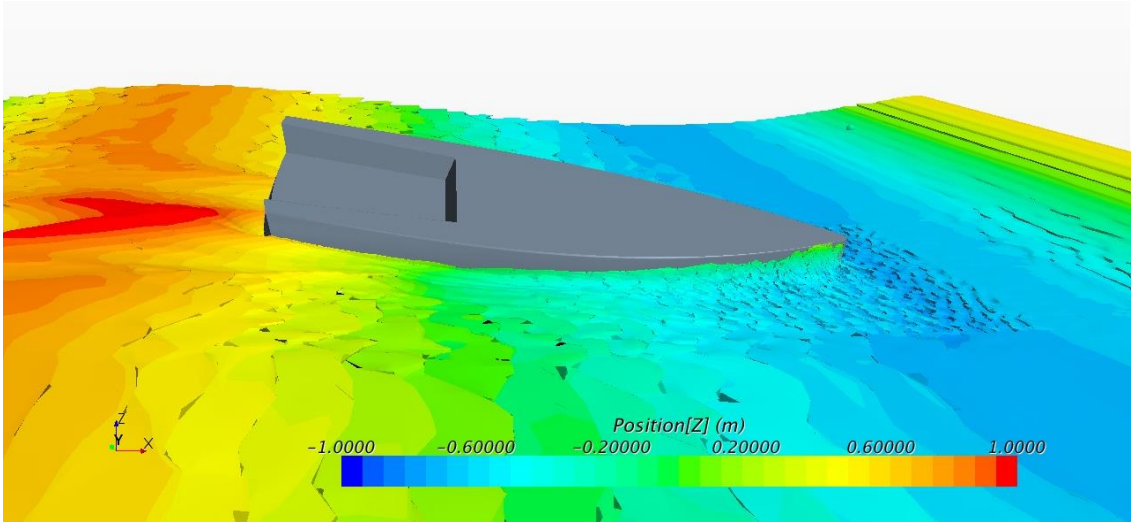

Figure 11-22 Hull A minimum resistance in 34.5m wave, heeled, at 11.5s

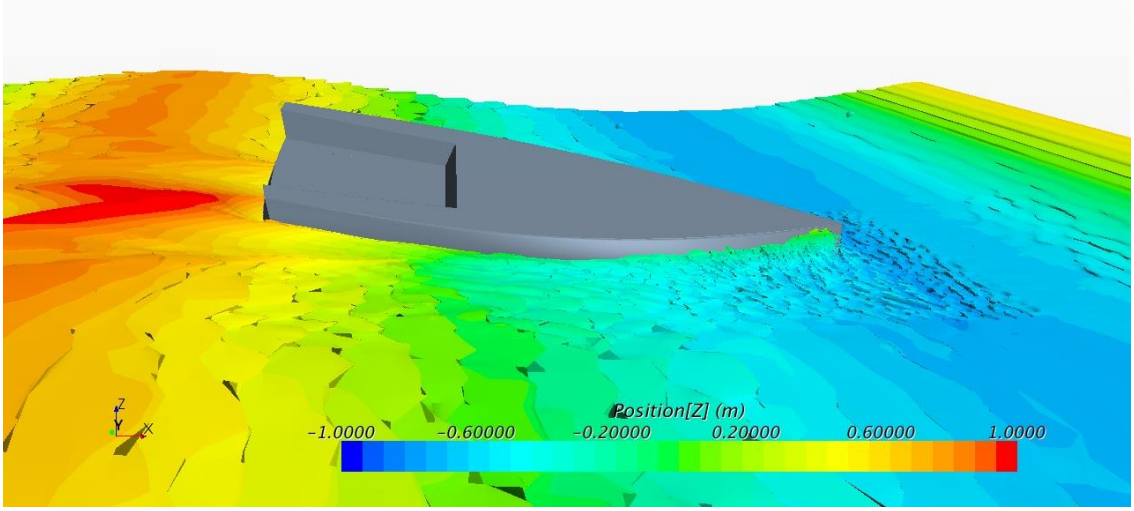

Figure 11-23 Hull B minimum resistance in 34.5m wave, heeled, at 11.5s

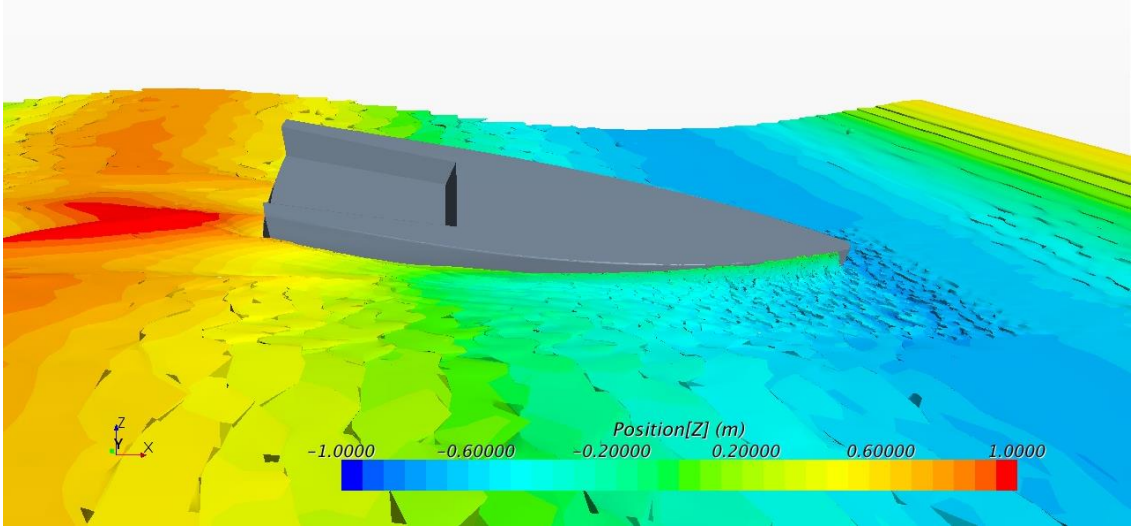

Figure 11-24 Hull C minimum resistance in 34.5m wave, heeled, at 11.5s